



Near-Field Baseband Communication System For Use In Biomedical Implants

Sandeep Manjunath

A THESIS SUBMITTED TO THE FACULTY OF ENGINEERING AT THE
UNIVERSITY OF GLASGOW FOR THE DEGREE OF DOCTOR OF PHILOSOPHY

June 2009

Copyright © Sandeep Manjunath 2009
All Rights Reserved

ABSTRACT

This thesis introduces the reader to the near-field baseband pulse radio communication for biomedical implants. It details the design and implementation of the complete communication system with a particular emphasis on the antenna structure and waveform coding that is compatible with this particular technology. The wireless communication system has great employability in small pill-sized biomedical diagnostic devices offering the advantages of low power consumption and easy integration with SoC and lab-in-a-pill technologies.

The greatest challenge was the choice of antenna that had to be made to effectively transmit the pulses. A systematic approach has been carried out in arriving at the most suitable antenna for efficient emanation of pulses and the fields around it are analysed electromagnetically using a commercially available software. A magnetic antenna can be used to transmit the information from inside a human body to the outside world. The performance of the above antenna was evaluated in a salt solution of different concentrations which is similar to a highly conductive lossy medium like a human body.

Near-field baseband pulse transmission is a waveform transmission scheme wherein the pulse shape is crucial for decoding information at the receiver. This demands a new approach to the antenna design, both at the transmitter and the receiver. The antenna had to be analysed in the time-domain to know its effects on the pulse and an expression for the antenna bandwidth has been proposed in this thesis. The receiving antenna should be able to detect very short pulses

and while doing so has to also maintain the pulse shape with minimal distortion. Different loading configurations were explored to determine the most feasible one for receiving very short pulses.

Return-to-zero (RZ), Non-return-zero (NRZ) and manchester coded pulse waveforms were tested for their compatibility and performance with the near-field baseband pulse radio communication. It was concluded that manchester coded waveform are perfectly suited for this particular near-field communication technology. Pulse interval modulation was also investigated and the findings suggested that it was easier to implement and had a high throughput rate too. A simple receiver algorithm has been suggested and practically tested on a digital signal processor. There is further scope for research to develop complex signal processing algorithms at the receiver.



For Pappa and Amma



*Vidyaa Dadaathi Vinayam, Vinaaya Dyaati Paatralhaam
Paatralhaathi Dhanamaapnothi, Dhanaathi Dharmam Tathah Sukham*

ACKNOWLEDGEMENTS

This thesis and the work presented herein, could not have been possible without the support of many different people. First and foremost, I would like to thank my academic supervisor, David Cumming, for providing me with an excellent opportunity to work on this project and also for his undeniable support and confidence in my work. He has been a reservoir of knowledge providing valuable guidance and helping me find a direction for research. I was lucky enough to have an ORSAS award and Faculty of Engineering graduate scholarship to pursue my research studies and I am deeply indebted to both these funding bodies.

Thanks to Stuart Fairbairn and the team of the Electronics workshop for making innumerable PCBs. Thanks to Shona for placing orders to buy components from external suppliers. I was very fortunate to be a part of the Microsystem Technology group which was very friendly and welcoming, that helped me settle down quickly during my early days. I would like to thank all the present and past members of the group like Ata Khalid, Alison Cleary, Mark Milgrew, Kevin Chai, Sonia Paluchowski Caldwell, John Wallace, Tim Drysdale, Edward Walsby, Gabriel Conte, Anna Sheridan, Feng Hong, Li Chong, Touqeer Azam and everyone else. Special thanks to Ata and Alison for keeping up my spirits and instilling confidence, especially when the chips were down. I would like to make a special mention of Mark and Kevin for being great friends. Thanks to John for reminding me to take some time off the research work to watch the blockbuster movies. Sonia has been very kind and helpful in providing insights

into the Scottish culture, so much so, that I am beginning to like it very much.

Beyond University, I am extremely grateful to my parents who have been the pillars of support throughout my education. I am very fortunate to have such loving parents who were always confident of my abilities and believed that one day I will reach the pinnacle of education ie., PhD. I hope that I will make my parents proud and keep them always happy. I also extend my gratitude to my brother for looking after my parents in my absence and help me keep focused on the reseach work. I feel short of words to extend my thankfulness to my dearest friend Pradeep who has been a patient listener and an excellent pal, who is true to the phrase, "A friend in need is a friend indeed". Thanks to my cousin Ravi, and his wife Sindhu, for making me feel at home and cooking my favourite dishes.

Sandeep Manjunath

June 2009

PUBLICATIONS

1. S. Manjunath and D. R. S. Cumming, “Magnetic antenna for pulse radio communication”, *Proceedings of the 5th IEEE EMBS UK and Republic of Ireland Postgraduate Conference on Biomedical Engineering and Medical Physics*, to be published July 2009.
2. S. Manjunath and D. R. S. Cumming, “Application of near-field ultra wide-band to wireless sensors”, *University of Glasgow, Department of Electronics and Electrical Engineering, Postgraduate Research Conference*, Glasgow, United Kingdom, Apr. 2007.
3. S. Manjunath and D. R. S. Cumming, “Pulse radio communication for implantable biomedical systems”, *submitted to IEEE trans. on biomedical circuits and systems*.

GLOSSARY

AC	Alternating Current
ADC	Analog-to-Digital Converter
ADC	Analogue-Digital Converter
ADS	Advanced Design System simulator
AM	Amplitude-modulate
ASK	Amplitude Shift Keying
BER	Bit error rate
BiCMOS	Bipolar Complementary Metal-Oxide Semiconductor
CMOS	Complementary Metal-Oxide Semiconductor
CW	Continuous Wave
DSP	Digital Signal Processor
DSP	Digital signal processor
EKG	Electrocardiograph
ERS	Endoradiosonde

FDTD	Finite Difference Time Domain
FFT	Fast Fourier Transform
FM	Frequency-modulate
FM/AM	frequency modulated subcarrier/amplitude modulated carrier
FOM	Figure of Merit
GI	Gastrointestinal
HF	High Frequency
IC	Integrated Circuit
ICNIRP	International Commission on Non-Ionizing Radiation Protection
IDE	Integrated development environment
IDEAS	Integrated Diagnostics for Environmental and Analytical Systems
IR	Infrared
ISI	Intersymbol Interference
LIAP	Lab-in-a-pill
MICS	Medical Implant Communications Service
OOK	On-off keying
PAM	Pulse Amplitude Modulation
PCB	Printed Circuit Board
PCM	Pulse Code Modulation
PDM	Pulse Duration Modulation
PIM	Pulse Interval Modulation
PIM	Pulse interval modulation

PN	Pseudo random Noise
PPM	Pulse Position Modulation
PWM	Pulse Width Modulation
RF	Radio frequency
RFID	Radio Frequency Identification Device
RFID	Radio Frequency Identification
SNR	Signal-to-Noise Ratio
SoC	System-on-Chip
TV	Television
UHF	Ultra High Frequency
UWB	Ultra-wide band
VHF	Very High Frequency
VSWR	Voltage Standing Wave Ratio

CONTENTS

Abstract	i
Dedication	iii
Dedication	iv
Acknowledgements	v
Publications	vii
Glossary	viii
1 Introduction	2
1.1 Introduction	3
1.2 Motivation	3
1.3 Aim and Objectives	5
1.4 Thesis Outline	6
1.5 Summary	7
2 Literature Review	8
2.1 Introduction	9
2.2 Implantable Microsystems	9
2.2.1 Wireless Biotelemetry	10

2.3	Endoradiosondes	12
2.3.1	Principle	14
2.3.1.1	Transmitter	14
2.3.2	Modulation	15
2.3.3	Wavelength	15
2.3.4	Transmitting Range	16
2.3.5	Active and Passive Systems	16
2.4	Implanted Transmitters	16
2.4.1	Wireless Transmission Schemes	19
2.5	Impulse radio	32
2.6	Antennas	35
2.6.1	Antenna Design	36
2.7	Summary	38
3	System Design	39
3.1	Introduction	41
3.2	Implantable Microsystem	41
3.3	Communication Transceivers	42
3.3.1	Near-field electromagnetic wireless communication	43
3.3.2	Far-field electromagnetic wireless communication	43
3.4	Baseband wireless communication	43
3.5	Pulse Shaping Mechanism	45
3.5.1	Filter Response	48
3.5.2	Input Impedance	50
3.5.3	Radiation Power Density	53
3.6	Wave Propagation	54
3.6.1	Tissue Properties	55
3.7	Antenna	58
3.7.1	Dipole or Linear-wire Antenna	58
3.7.2	Loop Antenna	61
3.8	Lumped Element Equivalent Circuit-Dipole Antenna	62
3.8.1	The Three-Element Equivalent Circuit	62
3.8.2	The Four-Element Equivalent Circuit	64

3.9	Results and Discussion	66
3.10	Summary	68
4	Loop Antenna Design for Pulse Radio	69
4.1	Introduction	70
4.2	Coil Properties	70
4.2.1	External Inductance	71
4.2.2	Internal Impedance	71
4.2.2.1	Skin Effect	72
4.2.2.2	Proximity Effect	73
4.3	Simulation Results and Verification	76
4.3.1	External and Internal Inductance	76
4.4	Pulse Shaping Filter	79
4.4.1	Filter Design	80
4.4.1.1	Filter Analysis	82
4.4.1.2	Pulse Characterisation	89
4.5	Antenna Bandwidth	90
4.6	Summary	92
5	HFSS and Antenna Modelling	94
5.1	Introduction	95
5.2	Antenna	95
5.2.1	Printed Loop Antenna	97
5.2.2	Solenoidal Loop Antenna	99
5.2.3	Result Interpretation	102
5.3	Experimental Results	104
5.4	Summary	108
6	Pulse Radio Communication	110
6.1	Introduction	111
6.2	Digital Communication	111
6.2.1	PCM Waveforms	112
6.2.2	Pulse Interval Modulation	116
6.3	Receiver Design	120

6.3.1	Digital Filter	120
6.3.2	Filter Design	122
6.4	Summary	128
7	Antenna in Receiving Mode	129
7.1	Introduction	130
7.2	Near-Field Magnetic Communication	130
7.3	Loop Antenna Equivalent Circuit	131
7.3.1	Near-field Transmission Model	134
7.3.2	System Design	139
7.3.3	Simulation Parameters	141
7.4	Experimental Results	146
7.4.1	Salt Water Experiment	149
7.5	Summary	151
8	Conclusion	152
8.1	Introduction	153
8.2	Final Analysis	153
8.2.1	Low-Frequency Magnetic Fields	153
8.2.2	Overdamped Circuit Configuration	155
8.2.3	Magnetic Antenna	157
8.2.4	Coding Schemes-Amplitude Modulation	158
8.2.5	Receiving Antenna Design	159
8.3	Future Work	160
8.3.1	Pulse Shape Analysis	160
8.3.2	UWB Antennas	162
8.4	Summary	162
	Appendix A	163
	Appendix B	168
	Appendix C	174
	References	179

LIST OF FIGURES

2.1	Block Diagram of a Biotelemetry System [1].	18
2.2	FM/AM Telemetry System [2].	21
2.3	Transmitter and the Sensing Unit [2].	22
2.4	Skin Tunnel Transformer.	24
2.5	Power and Telemetry System of a Skin Tunnel Transformer [3].	24
2.6	Block Diagram showing the use of a single RF frequency for energy transfer and signal transmission [4].	25
2.7	Circuit used to cause a periodic frequency keying of the remote unit L-C circuit [5].	27
2.8	Overall system block diagram for the multichannel microstimulator [6].	28
2.9	On-chip transmitter circuit design [6].	29
2.10	Spread spectrum transmitter.	34
2.11	FCC spectral mask for indoor unlicensed UWB transmission.	35
3.1	Generic Biomedical Device- A Conceptual Diagram [7].	41
3.2	A Block Diagram of the Near-Field Communication System.	45
3.3	Antenna Field Regions [8].	49
3.4	Antenna in transmitting mode.	50
3.5	Thevenin equivalent circuit of an antenna.	51

3.6	The variations in RMS electric and magnetic fields when a plane wave travelling in the positive z direction impinges upon a simple 1D phantom [9].	57
3.7	Electrical field strength dependence on fat layer thickness [9].	57
3.8	Electrical field strength dependence on fat layer thickness [9].	58
3.9	Three-element equivalent circuit of a dipole.	63
3.10	Four-element equivalent circuit of a dipole.	64
3.11	New four-element equivalent circuit of a dipole.	65
3.12	Simulated voltage waveforms:(a)Electric energy waveform; and (b)Magnetic energy waveform	67
4.1	Equivalent Circuit of a Loop Antenna.	70
4.2	(a)Skin Effect in a Single Conductor; and (b)Proximity Effect and Skin Effect in Adjacent Conductors.	72
4.3	Variations of external and internal inductances of a single coil.	77
4.4	Smith's proximity effect theory for a four turn coil of radius 5 mm with a wire radius of 0.355 mm.	78
4.5	Smith's proximity effect theory for an eight turn coil of radius 5 mm with a wire radius of 0.355 mm.	78
4.6	Smith's proximity effect theory for a four turn coil of radius 10 mm with a wire radius of 1 mm.	79
4.7	Smith's proximity effect theory for an eight turn coil of radius 10 mm with a wire radius of 1 mm.	79
4.8	Input Square Pulse of Amplitude 0.5 V.	82
4.9	Output at the Antenna Terminals.	83
4.10	(a)Series <i>RLC</i> Circuit; and (b)Parallel <i>RLC</i> Circuit.	84
4.11	Phasor Diagrams:(a)Series <i>RLC</i> Circuit; and (b)Parallel <i>RLC</i> Circuit.	85
4.12	Amplitude and phase characteristics of (a)Series RLC and (b)Parallel RLC circuits for varying values of ζ . $ H $ is the magnitude and $\angle H$ is the phase of the transfer function, with subscripts s and p denoting either a series or parallel RLC circuit respectively.	87

4.13	Time Domain Response of a Parallel RLC Circuit:(a) $\zeta=0.05$; (b) $\zeta=0.05$; (c) $\zeta=0.2$ and (d) $\zeta=18.5$. In all the cases except (b), $L=0.3 \mu\text{H}$, $R=10 \Omega$ and in (b), $L=20 \text{ nH}$. C was different in all cases.	88
4.14	Normalised Magnitude Spectrum of the Pulse and Pulse-Shaping Filter.	91
5.1	Square Planar Inductor.	97
5.2	Printed Loop Antenna.	99
5.3	Inductance vs Frequency.	100
5.4	Simulated Gain Patterns of the Planar Square Loop Antenna:(a)Elevation Plane ($\phi = 90^\circ$) and (b)Azimuthal Plane ($\theta = 90^\circ$).	100
5.5	Solenoidal Loop Antenna.	101
5.6	Inductance vs Frequency.	102
5.7	Simulated Gain Patterns of the Solenoidal Loop Antenna:(a)Elevation Plane ($\phi = 90^\circ$) and (b)Azimuthal Plane ($\theta = 90^\circ$).	102
5.8	Gain vs Distance for Antennas:(a)Planar Square Loop and (b)Solenoidal Loop.	103
5.9	Magneto-concentration effect in a ferromagnetic bar. When a high permeability bar is placed in a homogeneous magnetic field parallel with the plate, the magnetic flux tends to concentrate in the bar [10].	105
5.10	Measured time domain input signal and its spectrum in the frequency domain. Hanning window with 200 MSa/s sample rate was used to capture the input signal.	106
5.11	Measured time domain transmitted signal and its spectrum in the frequency domain. Hanning window with 200 MSa/s sample rate was used to capture the input signal.	106
5.12	Measured relative signal strength as a function of distance for an (a) Air core solenoidal coil of 15 turns and (b) Square Planar Loop Antenna of 6 turns, with a receive antenna, which is a coil of 15 turns and radius 5 mm.	107

5.13	Schematic illustrating the experimental setup of the transmitting and receiving coil for measuring the received relative signal strength of the loop antenna in the elevation and azimuth plane. (a) Measured relative signal strength as a function of elevation angle θ and fixed azimuth angle ϕ . (b) Measured relative signal strength as a function of azimuth angle ϕ and fixed elevation angle θ . Measurements were taken at axial distances of 5 cm and 10 cm in both the cases.	108
6.1	Binary Digit Waveform Representation:(a)PCM Sequence; (b)Pulse Representation of the PCM Word and (c)Pulse-Waveform.	112
6.2	Binary Digit Waveform Representation of 10110001.	114
6.3	Binary Digit Waveform Representation of 10110001:(a)NRZ, (b)RZ and (c)Manchester Code.	115
6.4	Pulse Interval Modulation.	117
6.5	Flow Chart for implementing Pulse Interval Modulation.	118
6.6	Pulse Interval Modulated Data Pattern: 0x03, 0x04, 0x05 and 0x06.	119
6.7	Pole Zero Plot of the Digital Filter used to reconstruct the transmitted pulse.	124
6.8	Magnitude and phase response of the digital filter, with two poles at 1; zeroes at -0.11 and -0.99	125
6.9	Impulse response of the digital filter.	126
6.10	Step response of the digital filter.	126
6.11	(a)Waveform received by the loop antenna that acts as input to the digital filter; and (b)Reconstructed waveform at the output of the digital filter.	127
7.1	Electrical Equivalent Circuit of a Loop Antenna.	132
7.2	π equivalent circuit of the distributed stray capacitance of the solenoid air-core inductor.	133
7.3	Near-Field Transmission Model.	134
7.4	Air-Core Transformer [11].	136
7.5	Two coils of radii a and A separated by an axial distance of ρ . The various distances that are calculated are also shown [12].	137

7.6	Calculated Stray Capacitances of a Solenoidal Coil as a function of the number of turns.	140
7.7	Calculated Stray Capacitances of a Spiral Coil as a function of the number of turns.	140
7.8	Calculated Stray Capacitances of a 10-Turn Solenoidal Coil as a function of the Coil Radius.	141
7.9	Calculated Stray Capacitances of a 10-Turn Spiral Coil as a function of the Average Coil Radius.	141
7.10	Simulation Results of an Inductor.	143
7.11	Simulation Results of an Inductor with different loading configurations.	145
7.12	Transmitted information bits.	146
7.13	Captured waveform by a 10-turn solenoidal loop antenna at a distance of about 9 cm. The rising and falling edges are clearly visible that makes identification of the bits transmitted.	147
7.14	Captured waveform by a 7-turn spiral loop antenna at a distance of about 15 cm. Although the rising and falling edges are clearly visible, the antenna is liable to ringing taking more time for transients to attain a steady-state. The bits can still be efficiently detected.	148
7.15	SNR against distance for the solenoidal and spiral loop antenna.	148
7.16	Captured waveform by a 7-turn spiral loop antenna at a distance of about 15 cm. The rising and falling edges are clearly visible that makes identification of the bits transmitted. The transmitter was inside a beaker containing salt solution.	150

LIST OF TABLES

2.1	Recent prototype pill specifications.	13
3.1	Tissue Parameters at 10 MHz.	55
3.2	Tissue Parameters at 100 MHz.	56
3.3	Tissue Parameters at 400 MHz.	56
3.4	Tissue Parameters at 403.5 MHz.	56
3.5	Lumped Element Values.	66
4.1	Normalised additional ohmic resistance per unit length due to the proximity effect R_p/R_o [13].	75
4.2	Minimum wire radius for Smith's proximity effect analysis to be valid for various near-field frequencies.	76
5.1	Coefficients for Current Sheet Expansion.	98
5.2	Physical and Electrical characteristics of the loop antenna	104
7.1	Mutual inductance for two equal solenoidal loop antennas with increasing distance between their axes.	139
7.2	Mutual inductance for two equal solenoidal loop antennas with increasing distance between the centers of the antennas at a fixed distance between them ($\rho=2$ cm).	139
7.3	Simulation parameters.	142

7.4	Various Concentrations of Salt Solution and its respective Conductivity.	149
8.1	Pulse Shape Metrics.	161

CHAPTER 1

INTRODUCTION

Contents

1.1 Introduction	3
1.2 Motivation	3
1.3 Aim and Objectives	5
1.4 Thesis Outline	6
1.5 Summary	7

1.1 Introduction

This chapter illustrates the motivation for the research in terms of its relevance to a biomedical implant communication system. The aim and key objectives are discussed and a summary of the thesis is given.

1.2 Motivation

Biomedical implants are instrumental in providing data that is otherwise difficult to obtain [14]. The subject can be allowed to remain in a relatively normal physiological and psychological state by ensuring minimal interference to their normal pattern of activities. A radio transmitter can be swallowed and the physiological data can be transmitted wirelessly. An example will be a telemetry sensor designed as a pill to monitor the gastrointestinal tract [15]. The microsystem has three important blocks namely, sensors, signal conditioning circuitry and the wireless telemetry platform. The sensors can sense a variety of physiological variables like temperature, oxygen, pH, etc., The signal conditioning circuits has sub-blocks like analog-to-digital converter (ADC), operational amplifiers, etc., to prepare the signal for wireless transmission. In its infancy, biomedical implants used a simple but effective circuit like a Hartley oscillator to send data over an inductive link. Traditional forms of communication schemes like amplitude modulation (AM) and frequency modulation (FM) have been extensively used in recent times. In these modulation schemes, the physiological signal, obtained by transducers, is amplified and processed to generate the modulation signals for transmission. The receiver consists of an antenna tuned to select the transmitted frequency and a demodulator to separate the signal from the carrier wave.

The physiological information is impressed upon a sinusoidal signal of high frequency. This process is called modulation and the sinusoid is the carrier wave. This is done for the efficient radiation of the information signal from an antenna. The antenna has to be a certain fraction of the wavelength to radiate effectively. In an amplitude-modulated system, the amplitude of the carrier wave is varied with the information signal. In a frequency-modulated system, the frequency of the carrier is varied with the modulating or information bearing signal. In mixed

signal system designs, the information signal is encoded in the form of pulses. If the amplitude of the pulses is used to represent the transmitted information, this method is called pulse amplitude modulation (PAM). If the width of the pulse is varied to represent the information, pulse width modulation (PWM) results. In pulse position modulation (PPM), the timing of a very narrow pulse is varied with respect to a reference pulse. All the above are digital modulation schemes by which digital symbols are transformed into waveforms that take the form of shaped pulses. These pulses undergo bandpass modulation like amplitude shift keying (ASK), phase shift keying (PSK) and frequency shift keying (FSK). The outcome is a sinusoid of very high frequency.

Implantable systems that utilize the architecture relevant to conventional communication systems suffer from the problems of integration with system-on-chip (SoC) technology, high power consumption and switching noise effects. From an application perspective, SoC helps to include complete functionality within a single chip. However as systems become more complex they are increasingly challenging to design. The driving force behind the SoC technology is the integration of more transistors on a single chip, short lead time to market, high performance and flexibility. The SoC has a few issues to be addressed that include power consumption, memory latency and transistor variability [16]. Integration does not only mean placing the analog and digital components spatially together on a single chip. Analog and digital intellectual property blocks have to coexist with effective test and verification strategies deployed to ensure the complete working of the system according to the design specifications. Therefore the reduction of the complexity of any portion of the chip eg., communication circuits, reduces the burden on the SoC design team.

In this work, it is attempted to develop a baseband communication system that operates in the near-field of an antenna. The design is aimed at reducing the power hungry blocks and communicate via digital pulses. The digital pulses are emanated directly from an antenna thereby eliminating the need for modulation. A thorough investigation is carried out in characterising such a pulse based communication system, with an emphasis on the antenna design. Modulation is generally carried out to produce an output signal that is at a higher frequency than the input signal for transmission into space. The modulators generally con-

sist of a DAC, an analog filter and analog mixer. Power consumption increases with the signal bandwidth for a constant dynamic range. A FSK modulator used as a part of the RF transmission circuit of an implantable system consumed 5 mW, or 35 % of the total power budget for the chip to provide a data rate of 5 kbps [15].

1.3 Aim and Objectives

The overall aim of this thesis is to develop a near-field baseband communication system for biomedical implants. The design involves an unconventional approach in which the traditional blocks of a communication system namely, oscillators, mixers and power amplifiers, are discarded and instead the information bearing pulses are directly emanated from an antenna.

The primary objective is to make an antenna choice that should be possible to radiate pulses directly. Each pulse is made up of several harmonic frequency components, thus the need for a wideband antenna to make this baseband communication a viable solution. Antennas can be either electric or magnetic in nature. The suitability of these antenna types has to be determined and an appropriate antenna, for use in near-field baseband pulse communication, has to be selected.

The secondary objective is to analyse the antenna response to a pulse excitation. A pulse invariably undergoes distortion at the terminals of an antenna. A novel design methodology is thus required to describe the antenna parameters that will help a wideband pulse transmission. A study of the time and frequency domain responses of an antenna will form the basis of this research work that will finally help achieve an intelligible pulse transmission scheme for use in ingestible biomedical devices. Various pulse coding schemes will be studied to find their applicability in the near-field baseband pulse transmission system.

The third objective will be to focus on the electromagnetic design of the antenna and decide a suitable radiating structure that has the potential of being able to be integrated with a system-on-chip (SOC) or lab-in-a-pill (LIAP) technology. The antenna has to be omnidirectional and also fulfill the criterion of achieving communication over a reasonable range of operation.

The fourth objective is to design a suitable pulse receiving antenna. The pulse information is incorporated in its shape as well as its time of arrival. Therefore the antenna has to be able to receive pulses with minimum distortion and aid in the demodulation of received pulses. Different antenna loading configurations will be studied to aid in the understanding of the effects of loading on a pulse in the time domain. An optimal design principle for antennas intended for use in pulse receiving communication schemes will be suggested.

The research aims to provide a very simple and attractive wireless communication scheme for use in biomedical implants. Using this technique the transmitter can transmit the data without the need for a dedicated wireless transmitter. In this new design the radio elements are reduced to three single passive elements: an inductor, capacitor and resistor. The requirement for traditional components including mixers, frequency synthesisers and power amplifiers is removed. The novelty of the research work is in providing a methodology for selecting an appropriate resistance and capacitance to make the most effective use of a given implantable loop antenna. Note that the antenna is determined by the pill size and shape. Usually solenoidal shape is preferred over printed loop antennas for its better range of operation. The traditional method of achieving resonance with an inductance and capacitance in the transmitter circuit to make communication possible is not followed here but the digital data pulses are directly emanated by a loop antenna. The values of the capacitance and resistance are optimised to achieve a waveform transmission thereby eliminating the use of modulators and mixers. This is the first detailed study of such a direct communication scheme for biomedical implantable telemetry.

1.4 Thesis Outline

The remainder of this thesis is divided into seven chapters and a brief description of the contents of each chapter is provided to help the reader in gaining an understanding of the core of the substance included in every chapter.

Chapter 2 presents a review of the literature relevant to the development of a near-field baseband communication system.

Chapter 3 discusses the design relevant to pulse based transmission systems,

especially the type of antennas that will be suitable for transmitting pulses.

Chapter 4 provides a new design principle that makes loop antennas a perfect choice for system integration and attempts to characterise the bandwidths required by such wideband magnetic antennas.

Chapter 5 discusses the electromagnetic design of loop antennas and suggests an optimal radiating structure.

Chapter 6 describes different pulse coding schemes that are relevant to the system proposed in this thesis. A hardware realisation of these schemes along with the implementation of a filtering algorithm on a digital signal processor (DSP) at the receiver is included in the discussion.

Chapter 7 describes how to receive the pulses transmitted by a loop antenna with very little distortion thus maintaining the integrity of a pulse at the receiver.

Chapter 8 summarises the salient features of this research study and provides some suggestions for future work.

1.5 Summary

In this chapter, the motivation for developing a communication system to find use in implantable medical systems was presented. This included the description of the research problem along with the advantages provided by such a system. Besides, the aim and objectives of the research work were established and a sketch of the thesis was given. The next chapter will review the literature pertinent to the research work.

CHAPTER 2

LITERATURE REVIEW

Contents

2.1	Introduction	9
2.2	Implantable Microsystems	9
2.2.1	Wireless Biotelemetry	10
2.3	Endoradiosondes	12
2.3.1	Principle	14
2.3.1.1	Transmitter	14
2.3.2	Modulation	15
2.3.3	Wavelength	15
2.3.4	Transmitting Range	16
2.3.5	Active and Passive Systems	16
2.4	Implanted Transmitters	16
2.4.1	Wireless Transmission Schemes	19
2.5	Impulse radio	32
2.6	Antennas	35
2.6.1	Antenna Design	36
2.7	Summary	38

2.1 Introduction

The previous chapter discussed the motivation for the research work, along with aims and objectives. This chapter presents a review of communication schemes developed for implantable systems. It begins with an introduction to pill shaped microsystems and the ways in which the sensed information was sent to the outside world. The chapter then moves on to explain how micromachining technologies benefitted miniaturisation of traditional blocks such as oscillators, mixers, etc., in a communication system and also use of digital modulation schemes to increase data rates. The antenna design techniques for such implants employed by designers and relevant literature discussing the performance of different antenna types is revisited. A new wideband signalling technique called ultra wideband radio is explained and its potential in future, to emerge as a form of implant communication is explained with references to recent findings in the literature.

2.2 Implantable Microsystems

Biomedical Engineering has been around for centuries now with the first reference to Leonardo da Vinci (1415 – 1519). He uniquely combined the mechanics and anatomy of the flight of birds by drawing the pictures of the skeleton and its musculature. Traditional disciplines such as biology and physics were much relied on and utilised by biomedical engineering in its infancy. But it has now become an unrelated and important discipline. A particular sub-field, implantable biotelemetry systems has come forth and with elapse in time gained much momentum [17]. A plethora of biomedical implants has been proposed to improve medical diagnosis and treatment, ever since the implantable pacemaker in the 1950's.

Micromachining technologies and CMOS microelectronics have significantly transformed the field of biomedical, microelectronic implants by providing an excellent platform for the development and implementation of new generations of implantable devices [18]. Miniature size, low power consumption, high reliability, low cost and superior functionality are the significant features of such implantable systems. These implantable systems are used to address various medical prob-

lems, for instance, chronic pain therapy [19], for neural prosthesis [20], for bladder control [21] etc. Temperature, pH and blood glucose concentration, and various other physiological parameters can be measured from within the human body. The above implementations are marked by the ability of the implants to accept commands from an external host system and/or transmit physiological data outwards, as measured from inside the body. Information exchange is often achieved through a wireless interface between the transmission and reception antennas of the systems involved. Sensors on the part of the implants acquire the physiological data whereas intrusion to the human body is usually accomplished through actuators.

2.2.1 Wireless Biotelemetry

Wireless Biotelemetry is defined as transmitting biological or physiological data from a remote location to a location that has the capability of interpreting the data and affect decision making. Biomedical telemetry is a special field of biomedical instrumentation that often permits transmission of biological information from an inaccessible location to a remote monitoring site. This plays a very significant role to obtain a wide spectrum of environmental, physiological and behavioural data [22]. Measurements and monitoring techniques can be applied to human beings and animals with minimum hindrance. The transmitted data can be reproduced. The state of being restrained in animals and human beings as well as the stress of immobilisation can cause alterations of measured variables. Accordingly, the advantage of biotelemetry is the measurement of physiological variables in conscious, unrestrained environment. Wireless, inhibition-free, simultaneous, long-term data gathering are the characteristics of biotelemetry [23, 24, 25].

Any measurable quantity is flexible with biotelemetry. Measurements that can be biotelemetered are determined in two categories:

- Bioelectrical variables such as ECG, EMG and EEG.
- Physiological variables that require transducers, such as blood pressure, gastrointestinal pressure, blood flow and temperature. Suitable transducers

can be employed for the measurement of a wide variety of physiological variables [26].

Biotelemetry began as a laboratory inquisitiveness but evolved into a useful, reliable tool for data acquisition. The pioneer in this field was Einthoven, who in 1903 used telephone lines to transmit electrocardiograms from a hospital to his laboratory. The telephone lines were just conductors to allow current to pass through them and connect the immersion electrodes with a remote galvanometer. In 1921, Winters eliminated the wires and transmitted heart sounds over a marine radio link. Small transmitters were evolved which owed their development to the electronic methods of making external transmitters. In the early 1950's researchers considered the possibility of placing the physiological monitoring transmitters within an animal. The problem was that the unavailability of junction transistors. Thus passive methods were conceived in which there would be neither active elements nor internal power sources. Bob V. Markevitch, an undergraduate made passive circuits which was later studied by Franklin Battat. The transmission of signals from within a subject evolved slowly. The invention of the transistor opened up new avenues. Endoradiosonde was one of the earliest biotelemetry units developed by Mackay and Jacobson. Since the invention of integrated circuit technology in 1958, contributions of microelectronics to biomedicine and health care have been enormous. Many advanced diagnostic, therapeutic and rehabilitative devices and systems would not have been possible without these contributions. Biotelemetry design revolves around the concepts of miniature and micropower. Evolution of semiconductor and microcircuit technologies have been effective in the parallel improvements of these areas.

Since the development of implantable pacemakers in 1958 and 1959 by Wilson Greatbatch and William M. Chardack, abundance of biomedical implants has been proposed and designed to solve various medical problems to improve health care. Some sort of communication scheme is always incorporated in the system to allow the exchange of data between the implanted part and the external part.

A completely programmable implantable pain controller has been reported by Mouine et.al [19]. A small patient unit and a desktop computer form the external part. A microstimulator device is the implantable part. It is a passive system wherein the power and data (stimulation commands) to the implant are

transmitted wirelessly via the inductive link on a 20 MHz carrier. Amplitude modulation and Manchester encoding is employed to serially transmit the data which is picked up by the internal coil; an AC/DC converter is used as a rectifier to power the implant and an AM demodulator to procure the command information from the envelope. Enokawa *et al.* [27] have proposed an implantable, passive telemetry system for sympathetic nerve activity and ECG measurement. Communication between the implant and the external host is achieved hierarchically. The computer transmits commands to the backpack over an infrared (IR) beam. The backpack processes the information and sends the commands to the implant over an inductive link. The sinusoidal carrier is modulated by on-off keying of the commands. The receiving end uses a full-wave rectifier and a DC/DC converter which supplies power to the implant. The implant then applies 21 bit pulse train to a parallel resonant circuit which is received by the tuned amplifier as amplitude variations on its carrier voltage. This technique is referred to as impedance-reflection modulation. The tuned amplifier finally delivers the data to the computer with an FM transmitter. A fully integrated, monolithic, implantable device is proposed for multichannel neural stimulation [28]. The implant receives data, power and clock signal over an inductive link. It is uni-directional and the wireless communication scheme consists of pulse-width encoded pulses at 8.3 kbits/sec, amplitude modulated on a 4 MHz carrier. Error detection is carried out by the implanted chip and the stimulation is aborted if any error is detected. An overview of these systems is necessary to identify the communication schemes that have been in use over the years.

2.3 Endoradiosondes

Endoradiosondes (ERS) are small radio transmitters that are used for wireless radio transmission from closed cavities or inaccessible places. Such transmitters were developed to telemeter data where it is undesirable or impossible to connect a sensing element to the recording element directly by tubes or wires. They opened up new possibilities for in-vivo diagnostics and physiological studies, since tubes and wires restricted the inaccessible regions. Tubes may cause physiological reflexes which disturb the normal body functions under observation. Also,

tubes may cause infection when passed through surgical openings. ERS has none of the above disadvantages. Endoradiosondes are called by different names such as “Radio pill” and “radio telemetering capsule”. Other synonyms include “biological transmitting transducer”, “biotel”, “echo capsule”, “internal biotelemeter”, “subdermal transmitter”, “surgically implanted transmitter”, “telemeter implant”, “tumnik” and “verschluckbaren Intestinalsender” (swallowable intestinal transmitter) [29].

The pioneering work on endoradiosondes was by scientists at the Karolinska Institute, Stockholm and Rockefeller Institute, New York. R. Stuart Mackay and Bertil Jacobson devised a radio method to transmit some variables of interest like temperature and pressure. After the emergence in late 1950’s, it’s popularity declined until 20 years, when a radio pill was used to record the physiological patterns inside the human bowel [30]. Several radio pills have been developed since then. Integrated microcircuit technologies have made it possible to build lightweight, low-power and low-cost medical diagnostic devices.

Small size camera and batteries are being used in implantable pills and following recent significant improvements in the technology. Visual sensor systems require a high frequency link for better resolution and miniaturisation of the implant. Table 2.1 summarises the recent telemetry systems developed for the electronic pill technology.

Reference	Frequency	Data Rate	Modulation	Power
(Mackay, 1957) [31]	100 kHz	–	FM	–
(Valdistri, 2004) [32]	433 MHz	13 kbps	ASK	–
(Johannessen, 2006) [33]	433 MHz	4 kbps	OOK	15.5 mW
(Lei Wang, 2007) [34]	30-40 MHz	5 kbps	–	5-6 mW
(Fouri K, 2008) [35]	UHF	250 kbps	–	–
(Chen, 2009) [36]	433 MHz	267 kbps	FSK	24 mW

Table 2.1: Recent prototype pill specifications.

The pill in [33] uses a simple OOK wireless system to transmit physiological data-pH and temperature. Valdastr *et al.*, developed a similar pill with a multi-channel feature to transmit different physiological parameters of interest [32]. In [36], a wireless endoscope system employs a commercial RF transceiver at 433 MHz to achieve a data rate of 267 kbps. Complex compressing techniques

are used by an ASIC to achieve higher transmission rate of images for low data rate systems. K. Fouri *et al.*, have developed a fluorescence-based electronic pill system that uses UV light by illumination LEDs to get clear images [35]. This device consumes power higher than the other available systems because of the power hungry LEDs. From Table 2.1, it seems that the transmission frequency is limited around UHF (0.3-3 GHz) frequencies and the data rate achieved at these frequencies is small for visual sensors used with an electronic pill. Moreover, it is desirable to achieve high data rates at lower frequencies to minimise the absorption of electromagnetic waves at higher frequencies of operation.

2.3.1 Principle

The two main units of an endoradiosonde are:(1)The transmitter and (2)the receiver.

The wireless link between the two is established by electromagnetic fields. An active telemetry system is one wherein the transmitter emits the fields that is modulated by the variable under study. The energy required is supplied by a power source within the transmitter. Alternatively, the transmitter can also be powered from outside by means of a second electromagnetic field of different frequency. In both the cases radio-frequency energy is generated in an oscillator circuit. A passive endoradiosonde consists of a tuned circuit made up of reactive elements. It doesn't have it's own power source. The energy is supplied from an external source in the form of pulsed electromagnetic field of a frequency close to that of the tuned circuit. The energy is absorbed by the tuned circuit and re-emitted in a modulated form between pulses. These are sometimes called "back-scatter" telemetry systems.

2.3.1.1 Transmitter

The main parts of an active ERS transmitter consist of a transducer, an oscillator to generate the radio waves for communication, a transmitting antenna, a battery source and various mechanical components such as capsule case and a protective membrane. One or more of these components provide dual functions that lead to the overall volume minimisation of the radio pill. For instance, the transistor can

serve both as a transducer (temperature) and an active element in the oscillator circuit. A coil can be an antenna and also a part of the tuned circuit in the radio frequency oscillator.

Small size, long battery life, operational range, satisfactory stability and linearity dictate the design of the transmitter. Stability against variations in temperature and power supply is very difficult to achieve in a limited space and seldom do the published technical descriptions of the radiosonde pills contain data on stability and attainable accuracy.

2.3.2 Modulation

Modulation of the data to be telemetered is determined by the nature of the data being telemetered. Physiological variables vary in the frequency range $100 \frac{\text{cycles}}{\text{second}}$ to $1 \frac{\text{cycle}}{\text{day}}$. Amplitude modulation and frequency modulation are the most common forms of communication schemes employed to transmit information. Amplitude modulation has a disadvantage that any variation in the received signal strength due to the movement of the transmitter or receiver and a decrease in battery voltage would result in erroneous results at the receiver. Pulse modulation schemes can be used to overcome these drawbacks. Instead frequency modulation is often easier to apply and hence has been the preference for ERS transmitter circuits.

2.3.3 Wavelength

The ERS operates from within a human body and hence present a totally different scenario. The choice of operating frequency depends on several factors. A certain percentage of radio waves passing through the tissues is absorbed and this percentage increases with frequency. As a result electromagnetic waves in VHF (Very high frequency) or UHF (Ultra high frequency) range are usually employed to exchange information. At low frequencies the antenna tend to become inconveniently large. Another important factor to be taken into account is that there should be minimum amount of interference from conventional transmitters.

2.3.4 Transmitting Range

The extent to which a transmitter can convey information depends on several factors.

1. The power delivered by the transmitter
2. The relative orientation of the transmitting and receiving antenna
3. Electrical interference
4. The signal to noise ratio of the receiver

The power transmitted by a transmitter falls rapidly with distance. The outpower must be increased considerably for a range of several metres. Pulse modulation can be effective in reducing the average energy consumption of the transmitter.

2.3.5 Active and Passive Systems

The design for a passive system was first proposed by Marchal and Marchal in 1956 [37]. A quartz-tuned circuit was activated by an external pulsed electric field at the same resonant frequency as the tuned circuit. Transmitter was on when there was “ringing” in the quartz crystal and off when there was no ringing; this is the way in which the transmitter sent information.

Haynes and Witchev developed a passive system that re-radiated absorbed energy from a pulsed electromagnetic field whose frequency was close to the frequency of a tuned circuit [38]. The resonance frequency was modulated by the variable under study.

The disadvantage of a passive transmission is that the coupling between the external and internal coils is highly dependent upon their mutual orientation.

2.4 Implanted Transmitters

An implantable biotelemetry unit is a device usually designed to sense physiological event and transmit this information over few centimetres of tissue to an

external receiver [39, 40]. In many cases, primarily in animal studies, a transmitter is surgically placed within the body rather than through a normal body opening. The primary concern is the battery life of the power source and the stability of the transducer in its interaction with the biological system. An experiment wherein the activity of four surgically implanted transmitters in a Rhesus monkey has been reported [31]. The transmitters are each active simultaneously on a different frequency. The number of transmitters utilised depends largely on the demands of the experiment. When several variables can be sensed in one region, it is convenient to employ a single transmitter to send several pieces of information. A similar example is the study of peristalsis in cold-blooded animals by a single transmitter of pressure and temperature, swallowed by the subject. The transmitter was passed out of the subject in the usual way.

Medical applications require the use of microscale telemetry devices. Gastrointestinal diagnostics portray a strong event-related character [41]. Hence wireless sensor systems have been incorporated in a capsule format which is noninvasive and perform endoscopic functions within the Gastrointestinal (GI) tract. Mackay was the first to demonstrate in 1961 [42].

The ingestible capsule moves from mouth to anus due to peristalsis force and it is egested. Temperature, chemical concentrations and images can be captured within the GI tract and the data relayed wirelessly to a body-worn device. Size, cost, circuit complexity, power requirements, sensors, nature of data to be transmitted and performance dictate the design of a biotelemeter. A block diagram of a telemetry system is shown in Fig. 2.1 [1]. Various transducers pass the physiological signals through a stage of amplification and processing circuits for the generation of a subcarrier and modulation for transmission. The receiver consists of a tuner to select transmitting frequency, a demodulator to separate the signal from the carrier wave to obtain the desired information. It is either displayed or recorded. Information to be transmitted is imprinted upon the carrier by a process known as modulation. The information bearing signal is called the modulating signal. Amplitude-modulated (AM) and frequency-modulated (FM) carriers have been used in biotelemetry systems. In an AM system, amplitude of the carrier is caused to vary with the transmitted information and in a FM system, frequency of the carrier is caused to vary with the modulating signal.

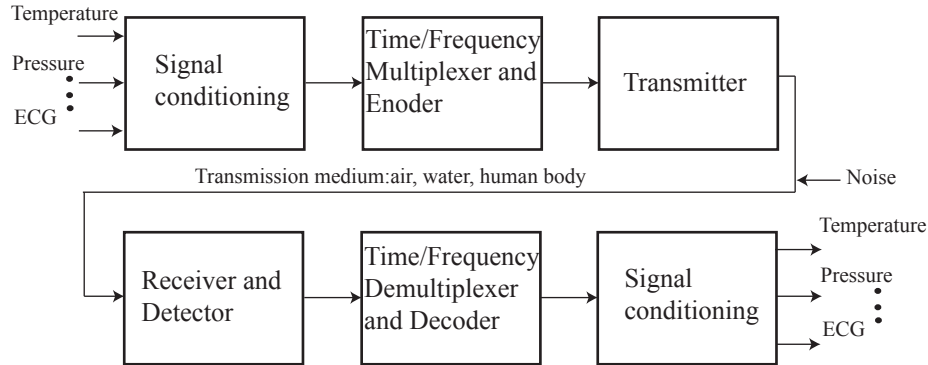


Figure 2.1: Block Diagram of a Biotelemetry System [1].

In biotelemetry systems, physiological signals are sometimes used to modulate a low frequency carrier, called a subcarrier. Radio frequency (RF) carrier of the transmitter is then modulated by the subcarrier. The advantage of this type of transmission is that various physiological signals can be transmitted simultaneously as each signal is impressed upon a subcarrier of a different frequency and all of the subcarriers are combined to simultaneously modulate the RF carrier. This process of transmitting many channels of data on a single RF carrier is called frequency multiplexing. At the receiver, a RF carrier is first demodulated to recover each of the separate subcarriers and then demodulated to retrieve the original physiological signals [43]. Depending on the the modulation scheme employed for the subcarrier and the carrier, the system is designated either as FM/AM or FM/FM. Most of the other approaches use a technique known as pulse modulation, in which the transmission subcarrier is generated in a series of short pulses. If the amplitude of the pulses is used to represent the transmitted information, the method is called pulse amplitude modulation (PAM) . If the width (duration) of the pulse is varied according to the information, then pulse width modulation (PWM) or pulse duration modulation (PDM) results. Pulse position modulation (PPM) refers to the variable timing of a pulse with respect to a reference pulse. Pulse code modulation (PCM) and pulse interval modulation (PIM) are the other denotions wherein information is represented by a sequence of coded pulses in the former and by spacing between constant width pulses in

the latter [44]. All these systems can be defined as PIM/FM, PWM/FM, and so on. However, time multiplexing is used instead of frequency multiplexing. Each of the physiological signal is sampled and used to control either amplitude, width or position of one pulse, depending upon the type of pulse modulation. The FM transmitted signal is received and tuned to the correct frequency. The subcarrier is removed from the RF carrier and then demodulated to reproduce the original data [45].

2.4.1 Wireless Transmission Schemes

In the early 1950s, methods used for the accurate measurement and recording of pressure changes within the human gastrointestinal tract required the passage of tubes through the mouth, nose, or anus, or through an artificial opening [46]. Scientists at the Rockefeller institute devised an instrument that could perform non-invasively under approximately physiological conditions. The capsule called the “echo capsule”, was made of a rigid, plastic cylinder. It measured 3.0 cm in length and 1.0 cm in diameter. The transducer was sensitive to the intraluminal pressures and had a radio transmitter powered by a battery to transmit the recorded information wirelessly. The battery had a life of upto 15 hours. The information was frequency modulated by the transmitter and these signals were accepted by the antenna of a frequency modulation receiver. The signal was demodulated and the pressure variations were displayed on an oscilloscope.

During the same year, another group at the Karolinska Institute, Stockholm, Sweden demonstrated that a capsule could measure and transmit both temperature and pressure simultaneously [47]. Using off-the-shelf components the capsule was 2.8 cm long and 0.9 cm in diameter. The transmitter was simply a Hartley oscillator and the emitter was grounded. The phase difference between the collector and base allowed the use of a single tapped coil. The base was connected to the emitter through a capacitor which not only provides bias to the emitter from a single battery, but also if its capacity is high, gives a blocking or quenching action. The frequency of transmission carried the information regarding pressure and the repetition rate of the radio frequency bursts transmitted temperature. A standard radio receiver was tuned to retrieve the pressure information and the

tone of its output signal indicated temperature.

Iowa transmitters were developed in 1961 by Essler and Folk [48]. It was typically an implantable, long life, short range radio telemetry device. The frequency modulated transmitter operated between 200 kHz and 500 kHz. Each transmitter consists of a two-stage transistor amplifier and a transistor oscillator which utilizes a varicap for frequency modulation. The electrical impulses, about 1 mV, was picked up from the heart beat by two electrodes on the transmitter. The amplifier provided a gain of about 100. After amplification, this voltage is applied across the varicap which causes the frequency of the oscillator to vary, thus providing modulation. The signal from the transmitter was picked up by a loop antenna of several turns of wire encompassing the animal's enclosure. The audio receiver recorded the data onto a magnetic tape or provision was also made for the demodulated data to be recorded onto a standard electrocardiograph (EKG). But these transmitters suffered from the problem of corrosion when implanted inside animals. The moisture from the body of the animals made the transmitters damp. This problem was overcome later by filling the transmitters with an epoxy sealer, silicone rubber, or vaseline to eliminate all trapped air space [49].

All the designs discussed above used a single-stage, frequency modulated transmitters. The emphasis was placed on small size and long battery life. At the receiver, a beat-frequency oscillator was used to count the number of pulses sent out by the transmitter. To improve the range of transmission a small steady oscillator was placed near the receiver and tuned so that the signal combines with the transmitter signal to give an audible tone, then the presence of the transmitter signal is noticeable whenever it is on. The problem with such receivers is instability due to either the radio frequency oscillator or beat-frequency oscillator drift. FM systems were used for the study of the transient temperature and readings were only taken at half hour intervals [50, 51]. This sometimes resulted in missing data at the extreme point which is undesirable. To overcome this problem, a complex transmitter, though shorter in life, evolved. The frequency modulated subcarrier/amplitude modulated carrier FM/AM telemetry system had a complicated transmitter, but less complicated receiver [2]. A block diagram of the system is shown in Fig. 2.2. The system used a separate transmitting unit placed at different locations inside a single animal or in a number of different animals.

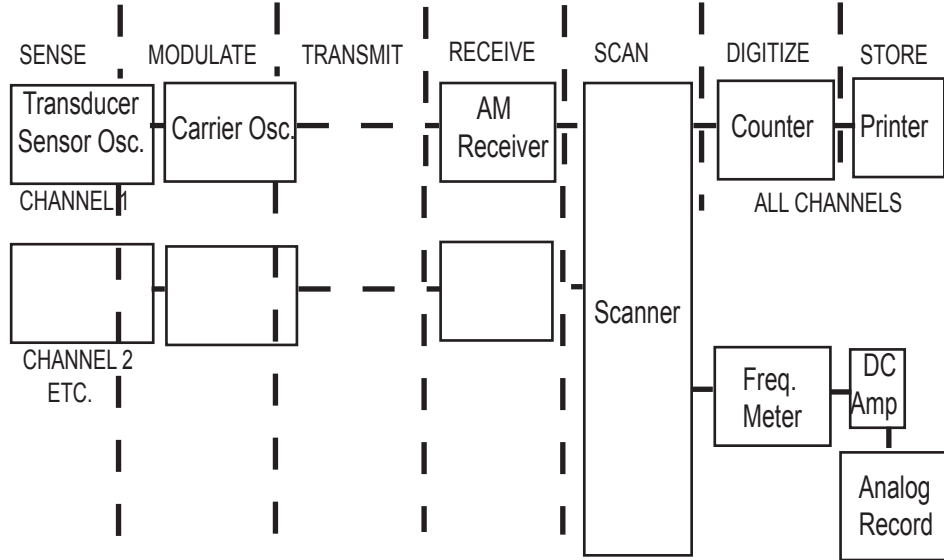


Figure 2.2: FM/AM Telemetry System [2].

The receiver used was a simple AM receiver capable of receiving radio signals in the 180-420 kHz band. A scanner acted as a switch between different inputs. Each input was sequentially sampled, digitized by the counter and printed in its numerical value. To maintain an analogue record of the selected channels, a frequency meter was used to convert the audio signal to a suitable voltage and then amplified by a dc amplifier to gain sufficient power to drive a galvanometer-type recorder. The sensing unit and transmitter consists of a phase-shift oscillator and Colpitt's oscillator respectively as shown in Fig. 2.3. Thermistors were a part of the feedback network of a phase-shift oscillator and the angular frequency of oscillation is given by

$$\omega^2 \approx 1/(6R^2 + 4R_L R)C^2 \quad (2.1)$$

where R is the value of the thermistor and C is the capacitor of the feedback network. For $R_L \approx R$ the resonant frequency is

$$f \approx 1/2\pi\sqrt{10}RC \quad (2.2)$$

High-gain germanium transistors were used at a voltage of 3 V and the col-

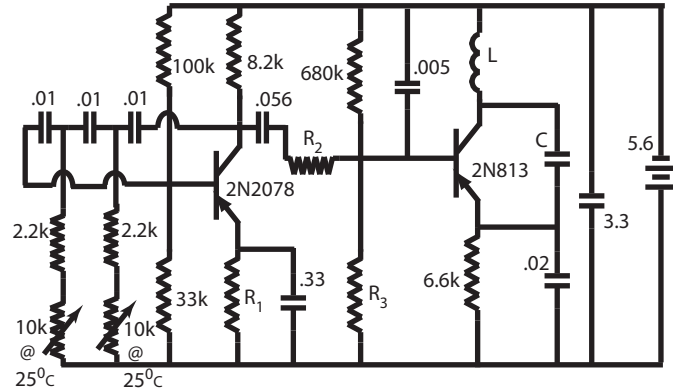


Figure 2.3: Transmitter and the Sensing Unit [2].

lector current was estimated to be $100 \mu\text{A}$. The design method was effective in minimising the receiving equipment, was geometrically small enough to be implanted and also had sufficient signal reception at a radial distance of 1.5 m. But the operation life of the telemetry system was just over 60 days when compared to other frequency modulated transmitters which had an operation life in excess of 150 days.

EEGs and EKGs are low-frequency bioelectric signals. To make use of the maximum available bandwidth of the magnetic tape recorders, a simple time-division multiplexing system was suggested [52]. The system was simple, portable and could be easily realised by commercially available instrumentation. A novel implantable transmitter that could be switched on and off to conserve the battery life was suggested in 1966 [53]. The telemetry system used frequency modulation with a carrier frequency of 100 MHz. The oscillator used was of Hartley type with a variable capacitive reactance. A pulsating oscillator was used to start or stop the implanted transmitter. The oscillator used a grid-circuit time constant of 1.10 s and yielded a pulse rate of approximately one per second. Pulses were 180 s in duration with rise and fall times of less than $1 \mu\text{s}$. The self-blocking oscillations was a result of unusually long time constant in the biasing circuit. Turn-on and turn-off range was reliable upto 25 cm.

Data multiplexing was regarded as the valuable concept that would enable the transmission of biological information of various kinds from a few channels

simultaneously. Fischler et.al [54] claimed that a CW FM/FM multiplex radiotelemetry system was advantageous compared to time multiplexing systems. A six channel FM/FM telemetry system capable of measuring two surface temperatures, an internal temperature, the respiration rate, and position and muscle spasm of a paralysed patient was constructed as a transmission package measuring $0.6 \times 2.5 \times 2.5$ in [55]. The use of single tunnel diodes as voltage controlled relaxation oscillators was unique to such systems. This reduced the overall size and also power consumption. In the same year scientists at the University of California reported the development of an FM/AM radiotelemetry system for multichannel recording of biological data [56]. The difference of this system to the one reported earlier was in the generation of subcarrier signals and the final signal for transmission. The subcarriers were generated using twin-T oscillators modulated in turn by the amplified data signals. The FM carriers were then linearly summed upon a crystal controlled AM transmitter.

In the year 1968, Carl F. Andren *et al.* [3] published a paper that discussed a scheme of high efficiency power and electronic data transfer through the skin to power chronically implanted artificial organs. The electromagnetic energy was transmitted through the skin by a device called the “skin tunnel transformer”. This device was based on the principle that the windings of a transformer need not be in contact with the transformer core but need only link the magnetic flux in the core by the virtue of encompassing it. Fig. 2.4 shows the skin tunnel transformer with the secondary coil completely buried under the skin. Using plastic surgical techniques, a tunnel was created through the center of the buried coil so that the core and the primary coil can be constructed around the secondary coil. The primary coil is connected to a remote ac power source. The alternate configuration provided improved transformer geometry but was less desirable surgically.

Fig. 2.5 shows the power and telemetry system. The incoming power signal is frequency modulated by a subcarrier and for outgoing signals, a frequency which is different from the power carrier is used. The advantages of such a system are low impedance and low losses to maximise the signal-to-noise ratio. The disadvantage was that it required a surgical change to change the normal body geometry of the patient. Also, provision to send the data signal would make the telemetry system bulky as separate coils were to be used for the transmission of

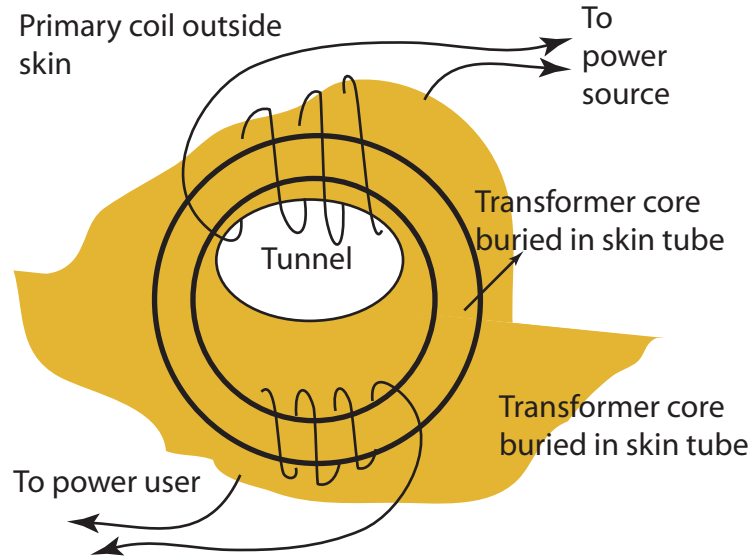


Figure 2.4: Skin Tunnel Transformer.

signal and energy.

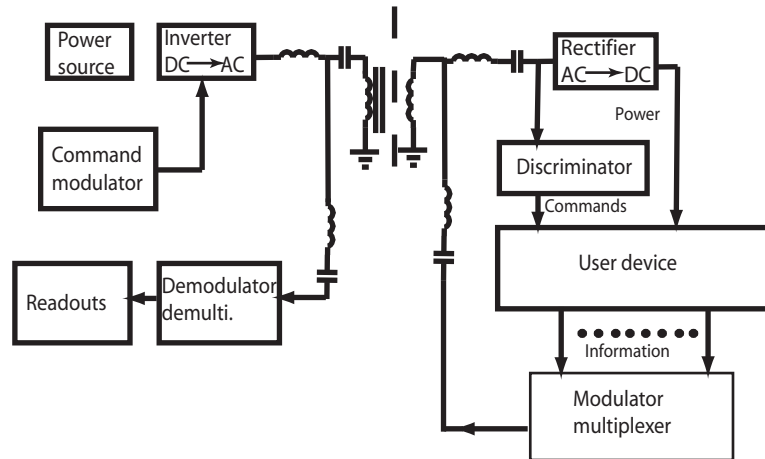


Figure 2.5: Power and Telemetry System of a Skin Tunnel Transformer [3].

Overall size and weight of the implantable telemetry systems was of prime concern and this dictated the design strategies involved in such complicated systems. Use of single RF frequency for energy transfer and signal transmission was suggested to reduce the volume of the implant unit and to simplify the total

equipment [4]. The principle was based on time sharing multiplexing as shown in Fig. 2.6. The system was used to send ECG signals from a Rhesus monkey strapped in a chair. The RF coupling coil was an eight inch diameter loop, which encircled the chair and the monkey. The axes of the implant tank coil and the coupling coil was maintained almost parallel at all times. The control pulse generator modulated the burst of RF pulses generated by the RF oscillator. The pulse train was amplified to the desired level and delivered to the coupling coil to power the implant tank coil. The induced voltage and power is rectified and stored in a capacitor to supply the dc power to the implant electronics. The implant sends the physiological information during the OFF state of the RF oscillator. The information is transmitted by very narrow RF pulses, which are pulse modulated. The time delay between the trailing edge of the RF powering pulse and the transmitted signal pulse carries the necessary information regarding the amplitude of the ECG signals. The signal is received by the same RF powering coil and is fed to the RF amplifier through an isolation network. The signal is then demodulated and provided for a display unit. The most important section of the implant unit was the oscillator which not only provided RF power detection but also oscillation and transmission of the signal. The oscillator circuit used was a Colpitt's oscillator.

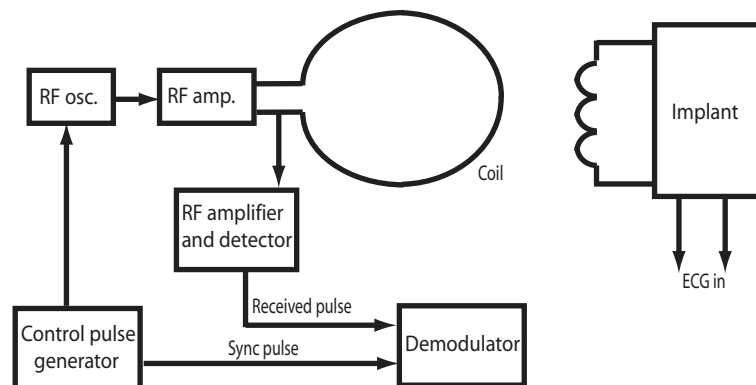


Figure 2.6: Block Diagram showing the use of a single RF frequency for energy transfer and signal transmission [4].

Bruce C. Towe [5] proposed a novel method to telemeter ECG waveforms which had the advantages of greater range and low power consumption compared to the telemetry system discussed earlier. The technique involved the transmission of bioelectric waveforms by encoding the information at a rate by which a passive L-C circuit is shifted between two different resonant frequencies. When such a pseudo frequency shift keying circuit is brought near a properly tuned base unit, power from the base unit is alternately absorbed and not absorbed resulting in a small periodic voltage amplitude change in the base unit antenna loop. The concept can be best understood by considering the system as a loosely coupled resonant transformer where changes in the secondary loading are reflected as a change in the current flow in the primary. When the secondary coil is resonant with the primary, increased power transfer occurs from the primary to the secondary through the effect of reflected impedance [57].

The reflected load resistance from the secondary to the primary of two loosely coupled coils is given by

$$R_e = \frac{Rk^2Q_1Q_2}{R + Q^2R_2}R_1 \quad (2.3)$$

where R_e is the reflected equivalent resistance, R_1 and R_2 are load resistances of the primary and the secondary windings, Q_1 and Q_2 are the quality factors of the primary and secondary L-C resonant windings, R is the a.c. equivalent coil load resistance. The condition of loose coupling is satisfied for very small values of k . k remains small for two coils separated by distances comparable to the diameter of the larger coil. For a fixed value of Q_1 and R associated with a base unit, changing the value of Q_2 in the remote unit by a change in the resonant frequency will cause a change in R_e at the base unit. This subsequently changes the voltage at the primary. These changes are detected by a suitable circuitry.

Fig. 2.7 shows the remote unit to cause a periodic frequency keying of the resonant circuit. In the present unit, Q_2 is periodically reduced from approximately 30 to 0 by shifting the L-C circuit to another resonant frequency by providing an alternate path to an additional capacitance across the circuit. This shifting is accomplished by turning on an FET transistor. The frequency was set nominally to 1 KHz. The timer used allowed the frequency modulation of its nominal rate by

the external amplified bioelectric signals. The remote unit was resonated to 450 kHz by a small trimmer capacitor. The coil consisted of 30 turns and measured 4 cm in diameter. The base unit was simply a sinusoidal generator which could be tuned to 450 kHz. The transmit loop antenna measured 70 cm in diameter and had 12 turns. The system used to detect the reflected impedance signal was a simple direct conversion receiver coupled to a one turn link winding over the base unit loop antenna.

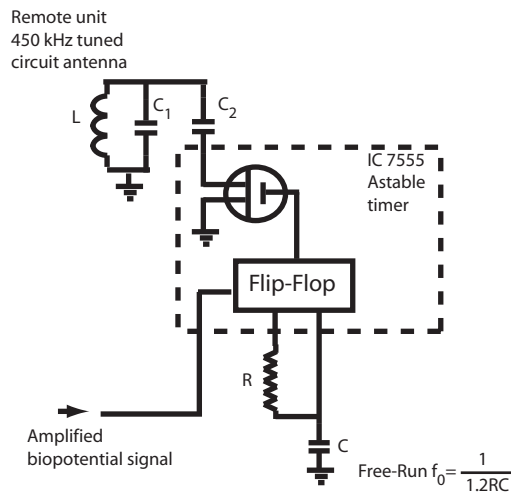


Figure 2.7: Circuit used to cause a periodic frequency keying of the remote unit L-C circuit [5].

The drawback of this system was that it was fairly difficult to tune for sufficient range. It also required the use of several items of test equipment to adequately align and adjust the system. Also the transmit frequencies and subcarrier frequencies must be adjusted to exactly match each other. The system was able to receive and demodulate the bioelectric signal waveforms received inside a volume defined by the size of the base unit loop antenna in the horizontal direction with a vertical separation distance of up to 1 m. The signal fell rapidly outside the cylinder. For maximum range, the base unit and the remote unit had to be maintained parallel and hence this system could pose some problems in certain direction independent applications. Use of orthonormal antennas might have solved this problem [31].

Implantable biomedical devices underwent a great development due to ad-

vances in micromachining technologies and Complementary Metal-Oxide Semiconductor (CMOS) microelectronic systems [18]. Miniature size, low power consumption, high reliability, low cost and superior functionality are the significant features of such implantable systems. Mixed signal design techniques were explored and the transceiver system now could incorporate digital modulation schemes of communication to exchange data.

A multichannel neuromuscular microstimulator was used for functional neuromuscular stimulation [6]. It could receive power and data through wireless RF telemetry. The BiCMOS IC also incorporated voltage regulators, clock recovery, data detection, output drivers and an active on-chip transmitter. It measured $1.4 \text{ mm} \times 13.5 \text{ mm}$ and dissipated only 40 mW of power. Fig. 2.8 shows the overall system block diagram and on-chip transmitter circuit diagram. The most important feature of this device was the on-chip transmitter that could be automatically turned on and off.

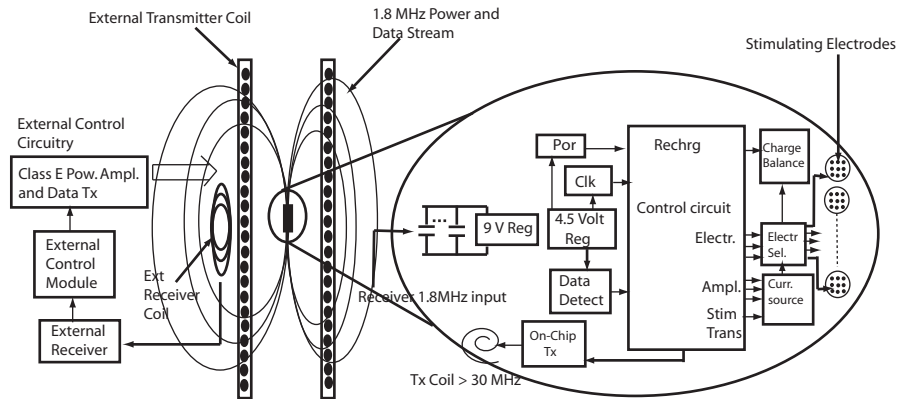


Figure 2.8: Overall system block diagram for the multichannel microstimulator [6].

The transmitter, as shown in Fig. 2.9, consisted of a coil of inductance L_t for RF telemetry, a capacitor C_t for tuning the LC resonance of the transmitter coil, tuning capacitor C_{set} for frequency setting of the self oscillating NAND-inverter-inverter loop, an NMOS drive transistor for driving the inductor and a transmit signal to the NAND gate that turns the oscillator on and off. An electroplated nickel coil with low losses for data transmission was fabricated. The coil was $20 \mu\text{m}$ thick and had 10 turns with average dimensions of $1.24 \text{ mm} \times 7.42 \text{ mm}$.

The system was first of its kind to provide all the necessary functions needed for future wireless instrumentation systems.

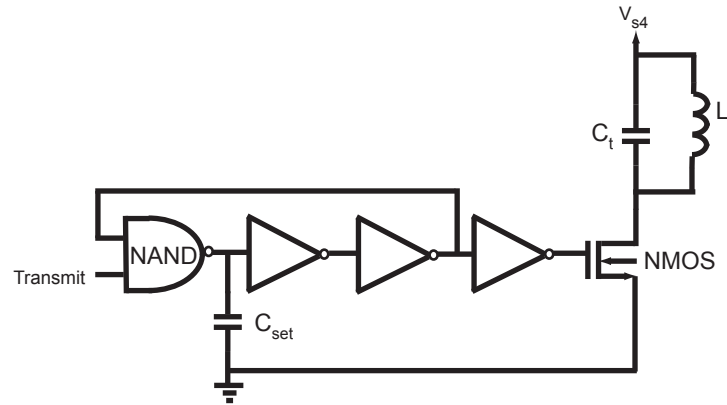


Figure 2.9: On-chip transmitter circuit design [6].

A microcontroller based implantable system was developed to study the nerve activity in small animals [27]. The microcontroller controlled a series of operations of the implantable telemeter. It adjusted the gain of the ECG and neural signal amplifiers. The amplified signals were then applied to the analogue-digital converter (ADC). The 8 bit digitised serial data was then telemetered by a series RLC circuit. The entire implantable system had minimal number of components and the use of microcontroller offered flexibility. A computer was central to the entire system which sent a power command and gain control codes of the ECG and NS amplifiers in the implantable telemeter, to the backpack by an infrared beam. The backpack had a power controller, an oscillator, a tuned amplifier and a FM transmitter. The power was delivered to the implant externally by the oscillator which generated $9 V_{p-p}$ sinusoidal wave at 200 kHz to drive a transmitting primary spiral coil. The communication scheme used was on-off keying. The FM transmitter then relayed the implant information back to the computer. The system used off the shelf components. The implant could communicate over a distance of 8 cm.

Miniature size passive implantable systems had a major drawback that the antenna was inefficient in receiving the radiated power due to its limited physical size. Hence the data acquisition and transmission system had to be optimised for

low power consumption. Based on the principle of load-shift keying [58], Qiuting Huang *et al.* at the Swiss Federal Institute of Technology published a paper that discussed the design of a passive telemetry IC that could telemeter information using PPM-AM signals and function at very low power without the use of an internal battery [59]. The changes in the sensor resistance results in the amplitude and phase change of the receiver current which can be detected by suitable demodulator circuits. While doing so the transponder absorbs very little power thus making the transmission possible that would otherwise be impossible with the available power of few milliwatts. Clements *et al.* suggests a similar telemetry system using inductive power and data link for retinal prosthesis [60]. The power was transferred using magnetic coupling and since only a small fraction of the magnetic field in the primary coil coupled to the secondary coil, a class E amplifier topology was made the choice to fit the design requirements of such a weakly coupled system. The amplitude of the ac carrier is varied according to the PWM waveform and the data signal is thus coupled to the implant coil. The amplitude shift keying (ASK) demodulator recovers the digital waveform from the envelope of the inductively coupled ASK waveform. The demodulator detects amplitude shifts by comparing it to an averaged version. A bi-directional and multi-channel wireless telemetry capsule that could transmit images from inside the human body and receive a control signal from an external unit was proposed in 2002 [61]. It measured 11 mm in diameter and used two 10 mm diameter loop antennas, one to transmit the signals from inside the human body at 315 MHz and the other to receive the external control signals at 433 MHz. The data from the CMOS image sensor is AM modulated and mixed with a local oscillator running at 315 MHz. It is then amplified and fed to the loop antenna. Since 315 MHz is a commercial cable channel frequency, a television (TV) receiver can be tuned and the images can be seen on a TV. The loop antenna receives the control signal at 415 MHz and a commercialized ASK/OOK (on-off keying) superheterodyne receiver demodulates the data. The decoder then interprets the serial information to control the ON/OFF of the CMOS image sensor. The system was efficient because it saved the power by switching the camera off during the dead-time. The drawback was that the data rate was only 100 bps. No information regarding the range of transmission was presented in the paper.

A microcontroller-based multichannel telemetry system was proposed that had the advantages of programmability and versatility in order to fulfill different application requirements [32]. The device could transmit information from three sensors, selecting one channel at a time with a carrier frequency of 433.92 MHz. The data was ASK modulated before being transmitted and each channel had a data rate of 13 kb/s. Unlike other telemetry systems a helical antenna was used instead of a loop antenna. It had a length of 17 mm and diameter of 5 mm. A quarter wave-length whip antenna along with a commercial ASK signal receiver was used for signal reception. The transmitter and its transmission capabilities through biological tissues was tested in vitro. It was found that the range of transmission was more than 5 m. A wireless sensor network could be easily built by using different carrier frequencies for transmission of radio signals. This paper demonstrated that microcontrollers provide flexibility and reprogrammability for implantable systems. The IDEAS (Integrated Diagnostics for Environmental and Analytical Systems) project developed a multisensor microsystem in the format of a pill using system-on-a-chip and lab-on-a-chip technologies [15, 62]. The pill had a range of sensors for measuring temperature, conductivity and pH along with a chemical sensor to measure the dissolved oxygen content in the intestine. An inductive link provided the communication between the transmitter and receiver. FSK (Frequency Shift Keying) was used to modulate the digital data and the maximum data rate was 5 kbps. Recently an implantable system developed on a ZigBee platform was proposed [63]. The system had the advantage of long battery lifetime and also provided an opportunity to build a wireless network of wearable sensors and implantable systems because of the ZigBee standard hardware and software architectures. They claimed that reliable communication could be achieved for a signal frequency of 2.4 GHz and also exposure levels to electromagnetic fields were within the reference level for general public exposure to time-varying electric and magnetic fields, fixed at 10 W/m^2 [64]. Exposure to electric and magnetic fields results in energy absorption and also temperature rise in the body. This phenomenon is significant at frequencies above 100 kHz and for high powers, and hence the distribution of heating within the body has to be assessed by dosimetric measurement and calculation in order to ensure safety. International Commission on Non-Ionizing Radiation Protection (ICNIRP) has

provided the basic restrictions and the reference levels of exposure to time varying electric, magnetic and electromagnetic fields [65]. Public exposure limits are specified for anyone who is exposed to radiation outside the work site (a site where a person is employed) or visitors to the work site who are not at work. Occupational exposure limits are specified to those who are exposed to electromagnetic field radiation during the course of their employment. People who are exposed to such radiation are trained to be aware of the potential risk and take necessary precautions. By contrast, the general public comprises individuals of all ages and of varying health status, and may include particularly susceptible groups or individuals. In many cases, the general public is not even aware of their exposure to electromagnetic field radiation and therefore stringent exposure restrictions are generally considered for the public exposure limits. The restrictions can be relaxed for particular individuals who are going to be diagnosed for critical ailments with an implantable pill by considering the benefits over the health risks (due to radiation exposure) that the person might have to bear. Moreover the exposure of the tissue or living cells to electric and magnetic fields from the implant will be only for a couple of days and the diagnostic results from the test might be very crucial for the patients long term well-being.

2.5 Impulse radio

The modern era in impulse radio communication began with the work of time-domain electromagnetics in the early 1960's [66] and was led by Harmuth, Ross and Robins at Sperry Rand Corporation [67, 68, 69]. It was first referred to as baseband radio as the information was transmitted by a series of pulses. The important distinguishing feature is that the instantaneous bandwidth of such systems is many times greater than the minimum required to deliver a particular message. At the heart of the system is a pulse generator for generating subnanosecond pulses. Silicon planar transistors in avalanche mode of operation were used to generate pulses, with widths ranging between 0.3 ns and 120 ns [70]. Step recovery diodes were also used in pulse shaping [71]. These circuits suffered from limitations for use in integrated configurations. Kim *et al.* [72] published a paper on the integrated implementation of a Scholtz monocycle generator. It has

several advantages including low cost and low power integration with other components. A CMOS programmable pulse generator has been proposed by Marsden *et al.* [73]. The pulse is generated by controlling the timing and sequence of transistor switching. The pulses generated have to be modified in accordance with the message to be transmitted. Hence timing between successive pulses is varied to convey digital information. The simplest is the amplitude modulation or on/off keying (OOK). The more advantageous modulation techniques include pulse position modulation (PPM), biphasic pulse polarity modulation (antipodal PAM) and pulse width modulation (PWM).

A UWB system is similar to a spread spectrum system in transmitting the information over a wide bandwidth. A spread spectrum accomplishes this task by the means of a spreading signal, often called a code signal, which is independent of the data. A UWB system refers to impulse based waveforms that follow different modulation schemes such as PAM, PPM, etc., The transmitted signal consists of a train of impulses carrying information in their position or amplitude. The narrow pulses, in the order of a nanosecond, result in an electromagnetic radiation of wider spectrum of several GHz and thus it is termed as an UWB transmission.

In a spread spectrum system, the input binary data is directly multiplied with the pseudo-random sequence, which is independent of the binary data to produce the baseband signal. This signal is modulated by a high frequency carrier wave [74]. Fig. 2.10 shows a binary phase shift keying spread spectrum transmitter. The spreading code is purely a pseudo random noise (PN) code that is easy to generate, has randomness and long periods. Randomness properties include balance, run and correlation as described for binary signals [43].

Good balance requires that in each period of the sequence, the number of binary ones differs from the number of binary zeros by at most one digit. A run is defined as a sequence of a single type of binary digit. The appearance of the alternate digit in a sequence starts a new run. The length of the run is the number of digits in the run. A spread spectrum system needs the same spreading code that was used at the transmitter to correctly decode the sequence received at the receiver. The spread spectrum system has good interference suppressing capability and fine time resolution for determining the time-delay or range measurement. A UWB system attains all the desirable features of a spread spectrum

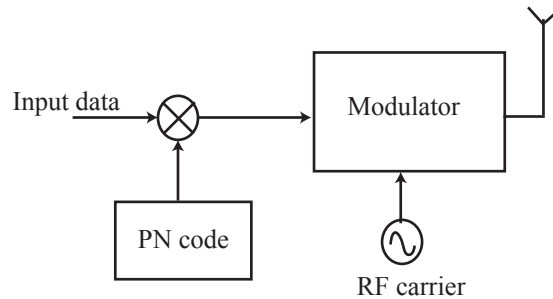


Figure 2.10: Spread spectrum transmitter.

system not by using a pseudo noise code to spread the information bandwidth but employing very short pulses to represent the baseband data. Impulse UWB is also carrier free transmission as the subnanosecond pulses are directly transmitted by a wideband antenna. This greatly simplifies the transmitter architecture of a UWB communication system and the pulse generator becomes the crucial block for generating pulses suitable for transmission by a ultra wideband antenna.

Ultra wideband technology shows great promise for realising low-power and high data rate link transceiver systems [75]. This has led to the development of prototypes for use in implanted systems. The notable one is an impulse radio system for cochlea implants [76]. A theoretical work on UWB for implanted systems has been published recently [77]. But much of UWB signalling capabilities has yet to be exploited. Some of the challenges that has to be overcome include [78]: synchronisation, antenna size and absorption by tissues at high frequencies.

Pulse shaping plays a major role in producing spectrally efficient [79, 80, 81, 82] and frequency tolerant communication systems. Hence the need for pulse shaping circuits. This would unnecessarily increase the complexity and pose an hindrance for use in implantable systems.

The UWB spectral mask is illustrated in Fig. 2.11. UWB antenna design has been greatly helped by the allocation of 3.1-10.6 GHz spectrum for unlicensed use by FCC. This has presented innumerable exciting opportunities and challenges to market commercial UWB communication products. As it is evident a wide bandwidth causes the systems to operate at low power and hence coexist with

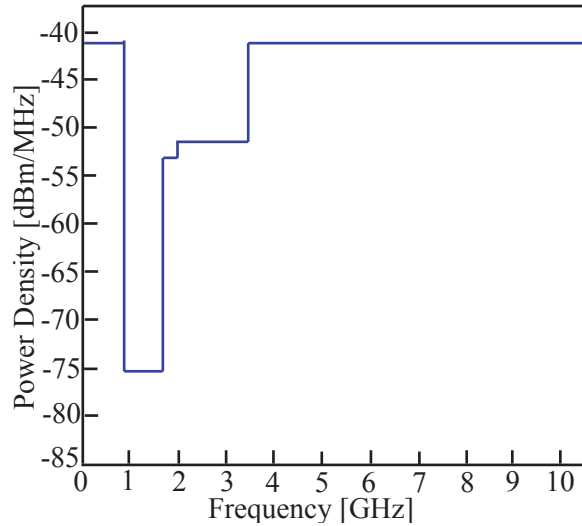


Figure 2.11: FCC spectral mask for indoor unlicensed UWB transmission.

traditional narrow band systems. The remarkable feature in designing UWB antennas is maintaining a high radiation efficiency over a bandwidth of nearly 7.5 GHz. Besides achieving a wide impedance bandwidth, the communication engineers have to stop thinking of an antenna performance in terms of frequency domain characteristics and consider temporal characteristics in designing UWB antennas. A Voltage Standing Wave Ratio (VSWR) of at most 2:1 is required across the entire frequency band for an ideal UWB antenna to be efficient. As the data may be contained in the shape or precise timing of a very short pulse, a clean impulse response is considered a primary requirement. Hence, a linear phase shift with constant magnitude over frequency guarantees proper pulse reception without any distortion. Since the transmit power is low, a high radiation efficiency is required.

2.6 Antennas

The propagated signal is received at the receiving antenna and the distance transmitted is called the range of the system. The range of the system depends on power and frequency of the transmitter, relative locations of transmitting and receiving antennas and sensitivity of the receiver. At ranges of a few metres, the

transmission can be thought of taking place rather in the fashion of the transfer of energy from the primary windings of a transformer into the secondary winding. For longer range transmissions, up to many kilometers, the more usual concepts of radio transmission apply.

Short range physiological observations can become useless because of a weak signal. The transmitter strength needs to be maximal and prevent the signal from being lost in any background noise. Changes in orientation can also cause signal loss which might otherwise be strong. Thus a signal from an ingested transmitter can vanish as the capsule moves away along the turns of the gastrointestinal tract. Omnidirectional systems hence become a necessity to make sure that signal is present in atleast one of the directions. Usually more than one antenna is employed in an omnidirectional system. This type of antenna suitable for placement under a cage [31]. Cyclic scanning of the output from the three coils or suitable combination into a single signal will prevent the signal from being lost for any orientation of the transmitter. Telemetry users should be aware of some useful tips whilst using antennas. Some of these factors are as follows:

1. Keep clear of the antenna when taking a bearing.
2. Do not stand within $1/2$ wavelength of the antenna elements.
3. Protect the antenna elements to prevent them from getting bent out of shape.
4. Keep all metal objects from interfering with the antenna.

This will help to avoid confusion and success rate in tracking will be increased [83].

2.6.1 Antenna Design

The design of antenna has come of age and a large number of texts are available to discuss this engineering discipline [84, 85]. But one thing in common in all these texts is that the antenna is placed in a non-conducting medium with a relative permittivity of 1, or close to 1. In other words, the antenna is placed in air or vacuum. An antenna inside a human body presents a completely different situation.

The antenna is surrounded by a lossy medium of high permittivity. The electrical properties such as conductivity and permittivity are dependant on frequency [86]. Also, the antennas used are electrically small making them inefficient radiators. Hence the use of finite difference time domain (FDTD) . This technique becomes an efficient alternative to determine the radiation characteristics and would ultimately help in designing more efficient telemetry systems. The application of FDTD analysis to implanted radiators in 418 MHz biotelemetry systems has been dealt with [87]. The paper suggests that the radiation losses increase with an increase in the operating frequency. This is due to the fact that human body is 60-70% water which absorbs electromagnetic waves strongly and the absorption increases as the frequency increases. Hence the RF frequency should be low, in the high frequency (HF) rather than very high frequency (VHF) or ultra high frequency (UHF) to minimise the radiation losses. Also the energy efficiency and battery life of the transmitter improves. But the design of an efficient radiator at HF is difficult as the necessary size of an antenna is inversely proportional to the frequency. The choice of frequency of operation has a direct relevance to the compactness and efficiency of the biotelemetry system being developed.

Wang *et al.* [34] have discussed the performance of two wireless transmission schemes *in situ*, one in the 868 MHz ISM band and the other in a VHF transmission band. The radiation characteristics of a loop antenna, operated in the frequency range 300 kHz-30 MHz, was compared with a helical and patch antenna, both operating in the 868 MHz ISM band. The loop antenna occupied only 1//700th volume of the helical antenna and 1/1000th volume of the patch antenna. FSK was preferred for communication over a single channel. The novelty of the system was in exchanging information in the near-field region surrounding the loop antenna. The low-frequency transmission scheme also consumed less power than its high-frequency counterparts. But it suffered from drawbacks such as low data rate (5 kbps compared to 10 kbps for high-frequency antenna configurations) and operating distance (<0.5 m). Nevertheless the paper claims that near-field transmission schemes are best suited for wireless implants because of high signal-to-noise ratio (SNR) and less interference to other narrow band communication systems.

2.7 Summary

In this chapter, a review of wireless technologies developed for integrated sensor communication is presented. The features and shortcomings are carefully assessed as a precursor to developing a novel near-field wireless communication system. Literature on antennas for ingestible devices was revisited. Ultra wideband, a promising wireless communication standard was reviewed to become known with its notable characteristics. It delivers great promise as an emerging standard for far-field wireless sensor communication systems. The next chapter will present a novel near-field pulse radio communication system and its design strategies.

CHAPTER 3

SYSTEM DESIGN

Contents

3.1	Introduction	41
3.2	Implantable Microsystem	41
3.3	Communication Transceivers	42
3.3.1	Near-field electromagnetic wireless communication	43
3.3.2	Far-field electromagnetic wireless communication	43
3.4	Baseband wireless communication	43
3.5	Pulse Shaping Mechanism	45
3.5.1	Filter Response	48
3.5.2	Input Impedance	50
3.5.3	Radiation Power Density	53
3.6	Wave Propagation	54
3.6.1	Tissue Properties	55
3.7	Antenna	58
3.7.1	Dipole or Linear-wire Antenna	58
3.7.2	Loop Antenna	61
3.8	Lumped Element Equivalent Circuit-Dipole Antenna	62

3.8.1 The Three-Element Equivalent Circuit	62
3.8.2 The Four-Element Equivalent Circuit	64
3.9 Results and Discussion	66
3.10 Summary	68

3.1 Introduction

The previous chapter reviewed the literature relevant to communication systems developed so far, for use in implants. This chapter presents a novel idea in designing transmitters for wireless sensor systems. The underlying principle governing the information exchange is mutual induction between two loosely coupled coils. Transmitting coil resonance determines the operating conditions in conventional short-range telemetry links. But the approach taken to convey information in this particular system is unique in the sense that transmitting coil acts as a data modulator. It does so by shaping the pulses.

3.2 Implantable Microsystem

A conceptual diagram of a generic biomedical device is shown in Fig. 3.1.

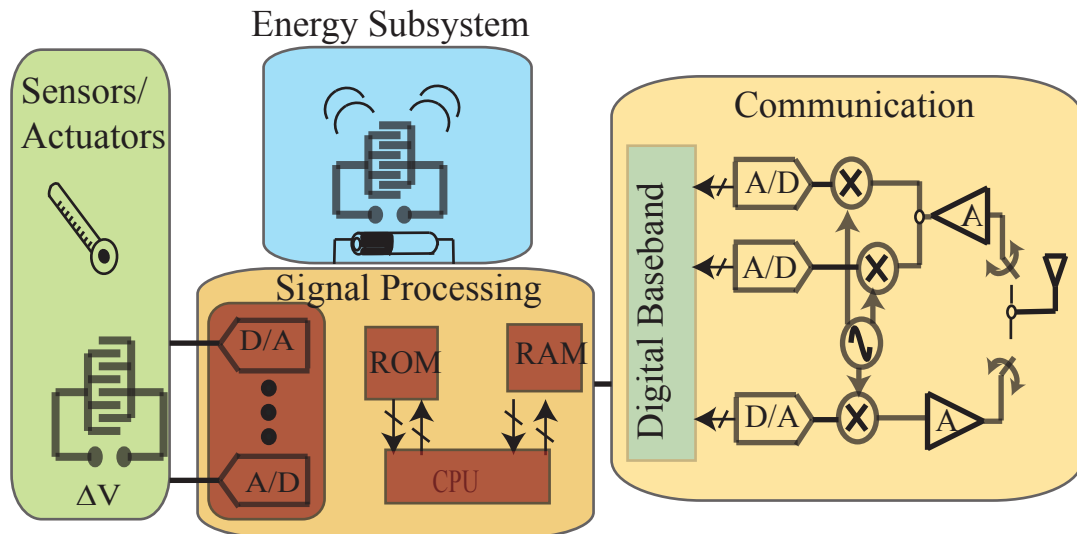


Figure 3.1: Generic Biomedical Device- A Conceptual Diagram [7].

Sensors interface the biomedical environment with signal processing circuits. The data conversion of biomedical signals becomes necessary to take advantage of the sophisticated digital signal processing circuitry. This is achieved by an analog-to-digital converter (ADC) with a certain amount of pre-processing to improve

the system performance. ADC power consumption is considered to optimise system bandwidth and dynamic range. The energy per conversion, an important metric for ADCs, increases as the dynamic range and sampling rate requirements increase. An empirical figure of merit (FOM) for ADCs normalizes their power consumption to the Nyquist sampling rate (F_s) and the dynamic range, expressed as 2^{ENOB} (where ENOB is the effective number of bits at the output) [88]:

$$FOM = \frac{P}{2^{ENOB} F_s} \quad (3.1)$$

An FOM as low as 4.4 fJ per conversion step has been reported [89]. Successive approximation register and oversampling ADCs are considered to be the best suitable candidates for most biomedical applications as they can achieve optimal FOM [7].

3.3 Communication Transceivers

The communication subsystem makes sending and receiving of information to and from biomedical devices possible. The information can be commands, such as configuration instructions or data samples from a sensor. For pill like devices, wireless communication is preferred as it is needed to traverse through the gut region and send information from inaccessible regions inside the human body to the outside world.

Communication between implants inside the human body and the outside world is achieved by electromagnetic waves through air. Depending upon the frequency of operation and the dimensions of the radiating element it is classified as either near-field wireless transmission or far-field wireless transmission. Recently a paper suggested using the human body as a transmission medium [90]. However the system uses electrodes attached to user's skin to transmit information through electrostatic coupling. This is of particular discomfort to patients and the movements are severely restricted. Moreover information from inaccessible places, like the gastrointestinal tract, cannot be obtained.

3.3.1 Near-field electromagnetic wireless communication

The primary method of wireless communication is via electromagnetic waves in air. At low frequency, near-field inductive coupling is predominant and is usually bidirectional. For implanted systems, constrained in volume and energy, the forward link consists of a high-powered transmitter that transmits both power and data whereas a reverse link transmits only data. As discussed in Chapter 2, a load configuration modulator can be used to convey information on the reverse link. It is typically limited in range to a few centimetres.

The main drawback of such an inductively coupled communication system (apart from low range) is low data rates. To support high data rates using near-field communications, low quality factor antenna coils have been used [91]. Nevertheless high frequency, far-field wireless communication is preferred for unidirectional data links.

3.3.2 Far-field electromagnetic wireless communication

For communication to be possible in a far-field, the frequencies of operation should be at least hundreds of megahertz and above. The link only provides data between an implant and a receiver outside the body. In other words the communication is half-duplex. The range of operation is over few centimetres. New standards have emerged to ensure coexistence and interoperability between devices. Some of the key ones are MICS, WMTS, Bluetooth and Zigbee.

3.4 Baseband wireless communication

This chapter introduces and explains in-depth a novel idea of communication suitable for miniature wireless devices such as diagnostic pills. The implant is extremely restrained in size and volume that demands an efficient and simple transmitter design. This poses innumerable challenges in antenna design as traditionally radiators ought to be a certain fraction of operational wavelength. Therefore we confine the functionality of our system to near-field. In order to make communication plausible, an efficient way of radiating fields has to be found.

The wireless communication is possible only in the near-field as the desired frequency of operation is low. Electromagnetic fields are strongly absorbed inside a human body and the absorption increases as the frequency increases [92]. Hence the range of frequencies usable is in HF rather than VHF or UHF region. Magnetic fields are offered a low reluctance path by biological tissues and therefore the transmission losses can be kept to be a minimum [93]. The human body is considered to be a non-magnetic material and there will be negligible magnetic field losses [94]. This argument supports the use of magnetic antennas in implants rather than electric antennas. Magnetic antennas are simply those antennas whereby magnetic fields are predominantly caused by a circular loop of current. The best example is a loop antenna. On the other hand electric antennas are explained as radiators that have an electric field emanated by time varying electric charges. Both types of antennas radiate electromagnetic waves that are associated with electric and magnetic fields but it largely depends on the sensitivity of any antenna to a particular field.

In traditional narrow-band communication system design techniques, the information signal to be transmitted is modulated by changing its amplitude, frequency or phase. The modulating signal is normally a high frequency carrier wave and the resulting signal after modulation is called a modulated signal. It is then mixed with other high frequency carrier waves (depending upon the application) before being amplified to a suitable power level by a power amplifier. The end frequency nearly matches the antenna's resonant frequency.

The approach taken in this research work is to minimise the number of blocks, especially modulators, mixers and power amplifiers in the design. We propose the idea of sending baseband or information bearing signal without modulation, thereby reducing the number of blocks in the overall system. Digital communication has been the trend as it offers many advantages over its analogue counterpart. The instantaneous bandwidth of the digital signal suggests that it might propagate without a carrier. A block diagram of the proposed near-field wireless communication system is shown in Fig. 3.2.

The implementation is much simpler than a conventional wireless communication system due to the omission of oscillator circuits and mixers, used for up-conversion. The source generates the message in binary. The pulse shaping

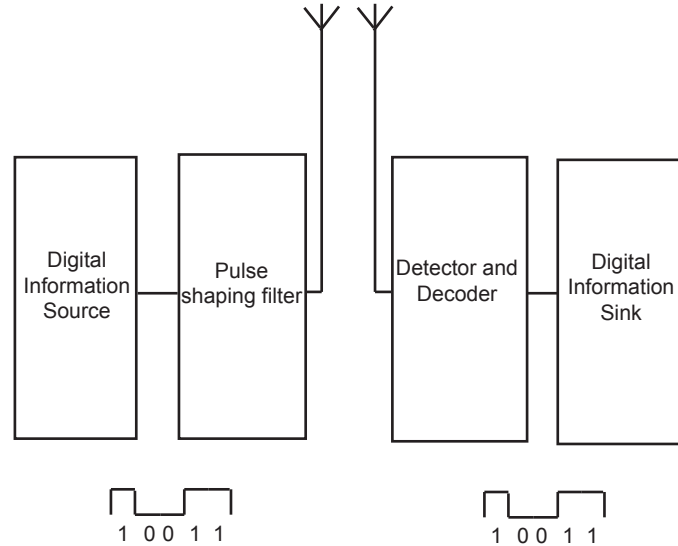


Figure 3.2: A Block Diagram of the Near-Field Communication System.

filter along with an antenna is instrumental and utmost importance is given in designing it. In this design, an antenna acts as a radiator as well as a pulse shaping filter. At the receiver a detector and decoder receives pulses without distorting them. Finally, the data is stored on a computer.

3.5 Pulse Shaping Mechanism

Antenna can be regarded as filters that can be tuned to a particular resonant frequency. In essence an antenna can be represented by a lumped-equivalent circuit consisting of a capacitance in series with a small frequency dependent resistance [95]. This has two distinct disadvantages: 1)the equivalent circuit becomes grossly inaccurate at or near the resonant frequency of the antenna; and 2)the value of the resistance has to be varied for different frequencies. Subsequent models developed then accounted for this by inserting an inductance into the circuit. The radiation resistance is still dependent on the frequency of operation even with the inductance placed in series [96, Chapter 2].

A filter's frequency response will help determine the magnitude and phase changes that occur with frequency. This information will suffice in determining

the distortion suffered by a pulse. It is vital for communication to make sense as the proposed transmission is a waveform transmission. A failure in controlled distortion will result in making the entire transmission scheme worthless. The feasibility of using antennas as pulse shaping filters is investigated in the following sections. This ultimately will result in direct emanation of pulses from antennas without modulation and make low-frequency near-field transmission a possibility for implants.

In digital communication systems, there are various filters throughout the system (reactive circuit elements such as inductors and capacitors)- in the transmitter, receiver and the channel. At the transmitter, the information symbols, characterised as impulses or voltage levels, modulate pulses which are then filtered to comply with some band-width constraint [43]. In baseband systems the pulses are distorted by distributed reactances associated with the cables and in bandpass systems the channels are characterised by fading that results in signal distortion. A receiving filter called the equalizing filter can be configured to compensate for the distortion caused by both the transmitter and channel. The system transfer function can be represented as

$$H(f) = H_t(f) H_c(f) H_r(f) \quad (3.2)$$

where $H_t(f)$ is the response of the transmitting filter, $H_c(f)$ the filtering within the channel and $H_r(f)$ the receiving/equalizing filter. Due to the effects of filtering the received pulses can overlap one another such that the tail of one pulse can smear into adjacent symbol intervals thereby interfering with the detection process. Such an interference is termed intersymbol interference (ISI). To minimise the effects of filtering and channel-induced distortion, $H_c(f)$ is specified and the problem remains to determine $H_t(f)$ and $H_r(f)$ such that the ISI is minimised at the output of $H_r(f)$. Nyquist showed that if the system transfer function $H(f)$ is made rectangular its impulse response will be of the form $h(t) = \text{sinc}(t/T)$ and then the pulses can be detected without ISI. In practical systems, the channel's frequency transfer function $H_c(f)$ and its impulse response $h_c(t)$ are not known with sufficient precision to allow a receiver to yield zero ISI for all time. Therefore the transmit and receive filters are chosen

to be matched so that

$$H_f = H_t(f)H_r(f) \quad (3.3)$$

The receiver equalizer transfer function needed to compensate for channel distortion is simply the inverse of the channel transfer function. This equalisation procedure is similar to specifying the antenna's response to transmit the digital data pulses directly from a suitable antenna without any modulation. The transfer function that is often used to describe the system transfer function of a digital communication system is a raised-cosine filter. Without the filtering effects of the channel, the transmitting and the receiving filter will each have a transfer function that is the square root of the raised cosine. Whenever a separate equalising filter is introduced to mitigate the effects of channel-induced ISI, the receiving and equalising filters are configured to compensate for the distortion caused by both the transmitter and the channel so as to yield an overall system transfer function characterised by zero ISI. The equalizer transfer function needed to compensate for channel distortion will be simply the inverse of the channel transfer function. A training sequence that is often noise-like is chosen to estimate the channel frequency response and in its simplest sense a single pulse is transmitted over a system designated to have a raised-cosine transfer function and the channel induced ISI will result in a distorted received pulse. The distortion is viewed as positive or negative echoes occurring both before and after the main lobe and therefore an equaliser will generate a set of canceling echoes at predetermined sampling times.

By using a matched filter at the receiver the reconstruction of the original data pulse is not required for its optimal detection. A matched filter is designed to provide maximum signal-to-noise power ratio at its output for a given symbol transmitted waveform. A known signal $s(t)$ plus additive white gaussian noise $n(t)$ can be considered to be the input to a linear, time-invariant receiving filter and is sampled at regular intervals. At time $t = T$, the sampler output $z(t)$ consists of a signal component a_i and a noise component n_o . The instantaneous signal power to average noise power, $(S/N)_T$, at time $t = T$, is

$$\left(\frac{S}{N}\right)_T = \frac{a_i^2}{\sigma_o^2} \quad (3.4)$$

The transfer function $H_o(f)$ that maximises (3.4) has the impulse response which is the mirror image of the message signal $s(t)$ delayed by the symbol duration T . The maximum signal-to-noise ratio is given by

$$\max \left(\frac{S}{N}\right)_T = \frac{2E}{N_o} \quad (3.5)$$

where the energy E of the input signal $s(t)$ is

$$E = \int_{-\infty}^{\infty} |S(f)|^2 df \quad (3.6)$$

$S(f)$ is the fourier transform of the input signal $s(t)$. The maximum output thus depends on the input signal energy and the power spectral density of the noise and not on the particular shape of the waveform that is used.

3.5.1 Filter Response

This section attempts to investigate the two most basic forms of antennas namely: 1) Loop Antenna; and 2) Dipole Antenna. Input impedance is one of the most important antenna parameters that ought to be considered for designing near-field transmission antennas. It has already been mentioned that magnetic fields are offered low reluctance path when antennas are used in ingestible devices. The total power density surrounding an antenna is made up of reactive and radiated power densities. This space is usually subdivided into three regions: a) reactive near-field, b) radiating near-field (Fresnel) and c) far-field (Fraunhofer) regions as shown in Fig. 3.3 [8].

The reactive near-field is defined as “*that portion of the near-field region immediately surrounding the antenna wherein the reactive field predominates*”. For most antennas, the outer boundary region of this region is commonly taken to exist at a distance $R < 0.62\sqrt{D^3/\lambda}$ from the antenna surface where λ is the wavelength and D is the largest dimension of the antenna. The radiating near-field (Fresnel) region is defined as “*that region of the antenna field between the reac-*

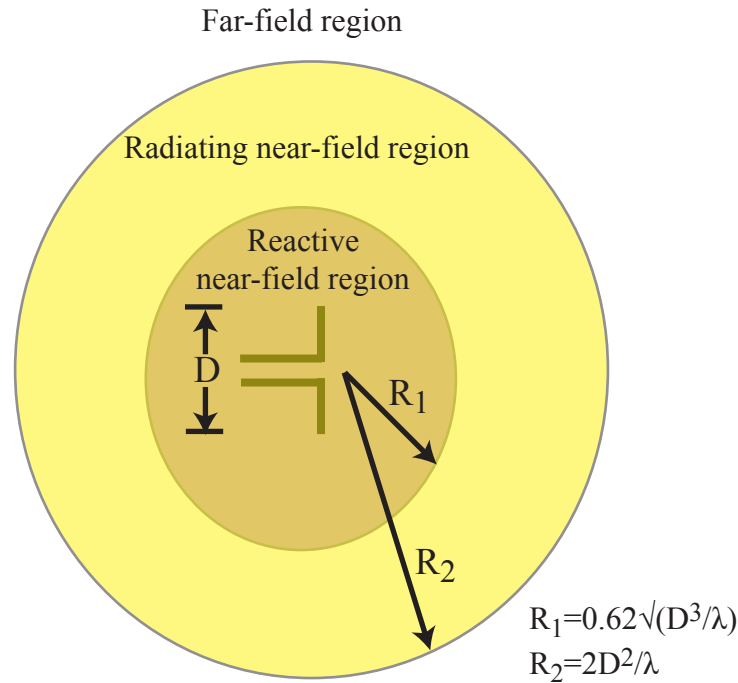


Figure 3.3: Antenna Field Regions [8].

tive near-field region and the far-field region wherein radiation fields predominate and wherein the angular field distribution is dependent upon the distance from the antenna". This region does not exist if the maximum dimension of the antenna is not large compared to the wavelength. The inner boundary is taken to be the distance $R \geq 0.62\sqrt{D^3/\lambda}$ and the outer boundary distance $R < 2D^2/\lambda$. Far-field region is defined as "that region of the field of an antenna where the angular field distribution is essentially independent of the distance from the antenna". The far-field region is commonly taken to exist at distances greater than $2D^2/\lambda$ for antenna with a maximum overall dimension D .

To design a near-field transmission scheme, a particular parameter of interest is the input impedance of an antenna. This is considered to be important because it is through the mechanism of radiation resistance (real part of the input impedance) that power is transferred from guided wave to the free-space wave. The other interesting aspect of this parameter is that the imaginary part is re-

lated to reactive energy stored in antenna's near-field. This gives us an insight into the type of energy (electric or magnetic) that encompasses an antenna.

3.5.2 Input Impedance

The input impedance is defined as the impedance presented by an antenna at its terminals or the ratio of the voltage to current at a pair of terminals or the ratio of the appropriate components of the electric to magnetic fields at a point. An antenna in transmitting mode can be represented as shown in Fig. 3.4.

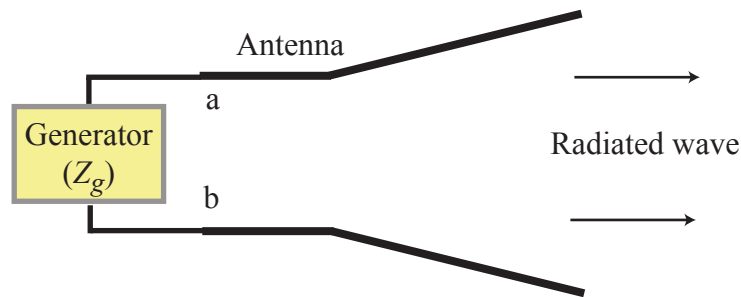


Figure 3.4: Antenna in transmitting mode.

The antenna input terminals $a-b$ can be considered to be the output nodes of a Thevenin equivalent circuit. An impedance Z_A representing antenna's impedance can be connected between terminals $a-b$. This can be defined by:

$$Z_A = R_A + jX_A \quad (3.7)$$

where

Z_A = antenna impedance at terminals $a-b$

R_A = antenna resistance at terminals $a-b$

X_A = antenna reactance at terminals $a-b$

A Thevenin equivalent circuit of an antenna is shown in Fig. 3.5.

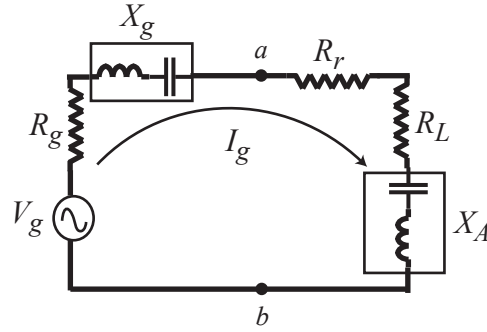


Figure 3.5: Thevenin equivalent circuit of an antenna.

It is assumed that a generator provides power to the antenna. Its internal impedance is given by:

$$Z_g = R_g + jX_g \quad (3.8)$$

where

R_g = resistance of generator impedance

X_g = reactance of generator impedance

In general the resistive part of Z_A consists of two components; that is

$$R_A = R_r + R_L \quad (3.9)$$

where

R_r = radiation resistance of the antenna

R_L = loss resistance of the antenna

The current I_g developed within the loop is given by:

$$I_g = \frac{V_g}{(R_r + R_L + R_g) + j(X_A + X_g)} \quad (3.10)$$

Its magnitude is given by

$$|I_g| = \frac{|V_g|}{\sqrt{(R_r + R_L + R_g)^2 + (X_A + X_g)^2}} \quad (3.11)$$

where V_g is the peak generator voltage. The power P_r delivered to the antenna for radiation in the far-field is given by

$$P_r = \frac{1}{2}|I_g|^2 R_r = \frac{|V_g|^2}{2} \frac{R_r}{\sqrt{(R_r + R_L + R_g)^2 + (X_A + X_g)^2}} \quad (3.12)$$

The power P_L is dissipated as heat in R_L and is given by

$$P_L = \frac{1}{2}|I_g|^2 R_L = \frac{|V_g|^2}{2} \frac{R_L}{\sqrt{(R_r + R_L + R_g)^2 + (X_A + X_g)^2}} \quad (3.13)$$

The remaining power is dissipated as heat on the internal resistance R_g of the generator, and is given by

$$P_g = \frac{1}{2}|I_g|^2 R_g = \frac{|V_g|^2}{2} \frac{R_g}{\sqrt{(R_r + R_L + R_g)^2 + (X_A + X_g)^2}} \quad (3.14)$$

It has been customary to match antenna's impedance with the generator impedance. This is called conjugate matching; and it occurs when

$$R_r + R_L = R_g \quad (3.15)$$

$$X_A = -X_g \quad (3.16)$$

Conjugate matching maximises the power delivered to an antenna. As a result radiation resistance increases and it is mainly advantageous for far-field communication systems wherein energy is radiated as plane waves. However our system operates in the near-field and we want the energy to be stored in fields (preferably magnetic) immediately surrounding an antenna. The other condition as shown in (3.16) can be achieved by resonance. At resonance, there is a continuous interchange of energy between electric and magnetic fields. This condition might seem feasible for designing near-field communication systems but resonance occurs at a particular frequency called the “resonant frequency” and any attempt to radiate pulses by a resonant antenna will result in severe distortion. This is what needs to be avoided as we intend to contain information in the shape of a transmitted pulse. This is one of the salient features of the system proposed in this thesis.

3.5.3 Radiation Power Density

Electromagnetic waves carry information from one point to another through various media such as air, water, a wave guide, etc., Waves are thus associated with energy and power. A quantity called the instantaneous Poynting vector describes the power associated with an electromagnetic wave and is defined as

$$\mathcal{W} = \mathcal{E} \times \mathcal{H} \quad (3.17)$$

where

\mathcal{W} = instantaneous Poynting vector

\mathcal{E} = instantaneous electric-field intensity

\mathcal{H} = instantaneous magnetic-field intensity

The total power crossing a surface can be obtained by integrating the normal component of the Poynting vector over the entire surface. In equation form

$$\mathcal{P} = \oiint_S \mathcal{W} \cdot ds = \oiint_S \mathcal{W} \cdot \hat{n} da \quad (3.18)$$

where

\mathcal{P} = instantaneous total power

\hat{n} = unit vector normal to the surface

da = infinitesimal area of the closed surface

In order to calculate the instantaneous \mathcal{E} and \mathcal{H} when the fields vary harmonically in time, the following relations can be used:

$$\mathcal{E}(x, y, z; t) = \text{Re}[E(x, y, z)e^{j\omega t}] \quad (3.19)$$

$$\mathcal{H}(x, y, z; t) = \text{Re}[H(x, y, z)e^{j\omega t}] \quad (3.20)$$

Using the definitions of (3.19) and (3.20) and the identity $\text{Re}[Ee^{j\omega t}] = \frac{1}{2}[Ee^{j\omega t} + E^*e^{-j\omega t}]$, (3.17) can be written as

$$\mathcal{W} = \mathcal{E} \times \mathcal{H} = \frac{1}{2}\text{Re}[E \times H^*] + \frac{1}{2}\text{Re}[E \times He^{2j\omega t}] \quad (3.21)$$

The first term of (3.21) is not a function of time while the time variations of

the second are twice the given frequency. The average Poynting vector or average power density can be written as

$$W_{av}(x, y, z) = [\mathcal{W}(x, y, z; t)]_{av} = \frac{1}{2} \text{Re}[E \times H^*] \quad (3.22)$$

The average (real) power density represents the power density associated with far-field electromagnetic fields. The imaginary part represents the reactive (stored) power density associated with the near-field electromagnetic fields. It can be either positive or negative depending upon the antenna being electric or magnetic in nature. This is the same quantity represented as X_A in Thevenin's equivalent circuit, as shown in Fig. 3.5.

The above discussion helps in concluding that radiation power density provides a judgment as to whether an antenna stores electric or magnetic fields in its near-field. Thevenin's equivalent circuit converts the physical fundamental parameters into their electrical equivalents. By combining these a design procedure is suggested that facilitates the designing of a near-field low frequency communication system for ingestible devices.

3.6 Wave Propagation

The previous sections discussed the electric and magnetic forms of energy density associated with fields surrounding an antenna. The electric and magnetic fields undergo different levels of attenuation as they traverse through different media. Therefore it becomes necessary to discuss the effects of the medium surrounding an antenna.

The medium surrounding the antenna influences its performance. An implantable antenna is encompassed by a human body. In a sense, the human body can be regarded as a very large, lossy, non-magnetic substance which extends from the absolute near-field to, at least in some directions, the far-field. Any material can be characterised by its permittivity (ϵ), permeability (μ) and conductivity (σ), which in general are complex and frequency dependent [9]. The permittivity ϵ and the conductivity σ can be expressed by their real and imaginary parts as:

$$\epsilon = \epsilon' - j\epsilon'' \quad (3.23)$$

$$\sigma = \sigma' - j\sigma'' \quad (3.24)$$

The complex permittivity ϵ_c of a medium is then defined as

$$\epsilon_c = \epsilon_e - j\frac{\sigma_e}{\omega} \quad (3.25)$$

Here the effective permittivity ϵ_e and effective conductivity σ_e are defined as

$$\epsilon_e = \epsilon' - \frac{\sigma''}{\omega} \quad (3.26)$$

$$\sigma_e = \sigma' + \omega\epsilon'' \quad (3.27)$$

The loss due to conductivity in the matter is expressed as a dissipation factor or a loss tangent $\tan \delta$. They are defined as:

$$\tan \delta = -\frac{\text{Im} [\epsilon_c]}{\text{Re} [\epsilon_c]} = \frac{\sigma_e}{\omega\epsilon_e} \quad (3.28)$$

where $\text{Re}[\]$ and $\text{Im}[\]$ denote real and imaginary parts, respectively.

3.6.1 Tissue Properties

The relative permittivity ϵ_r and conductivity σ_e of different human tissues at three different frequencies are given in Tabs. 3.1, 3.2 and 3.3 [97].

Tissue	ϵ_r	σ_e (S/m)
Muscle	170.73	0.61683
Fat	13.767	0.029152
Skin (dry)	361.66	0.19732
Skin (wet)	221.81	0.366

Table 3.1: Tissue Parameters at 10 MHz.

The tables suggest that the conductivity increases as the frequency increases. This increases the loss tangent and hence as frequency increases the absorption

Tissue	ϵ_r	σ_e (S/m)
Muscle	65.972	0.70759
Fat	6.0741	0.036295
Skin (dry)	72.929	0.49122
Skin (wet)	65.969	0.5232

Table 3.2: Tissue Parameters at 100 MHz.

Tissue	ϵ_r	σ_e (S/m)
Muscle	57.129	0.79631
Fat	5.5798	0.041119
Skin (dry)	46.787	0.68806
Skin (wet)	49.896	0.66894

Table 3.3: Tissue Parameters at 400 MHz.

Tissue	ϵ_r	σ_e (S/m)
Muscle	57.1	0.797
Fat	5.6	0.041
Skin (dry)	46.7	0.69
Skin (wet)	49.8	0.67

Table 3.4: Tissue Parameters at 403.5 MHz.

increases. Johansson carried out an one-dimensional FDTD simulation to study the effect of a human body on an impinging plane wave [9]. The human body is modelled as a block of muscle tissue with certain thickness and extending to infinity in the other two dimensions. The other tissues are added as layers of finite thickness to the existing layer of the muscle tissue. The simulation was carried out for the MICS band frequency of 403.5 MHz and Tab. 3.4 gives the corresponding tissue parameters. Fig. 3.6 shows the magnitude of the electric and the magnetic fields varying with distance. The muscle tissue is assumed to be at $z = 1.0$ m and the thickness of the slab was 144 mm [98]. It can be seen that the magnetic field is strengthened at the surface between the body block and the air which suggests that a magnetic antenna might be beneficial for implant communication. Johansson *et al.* developed more complex models to study the effect of the fat layer in between the skin and the muscle layer. Figs. 3.7 and 3.8 show the E and H plots for fat layers of thicknesses 0, 5, 10, 25 and 50 mm.

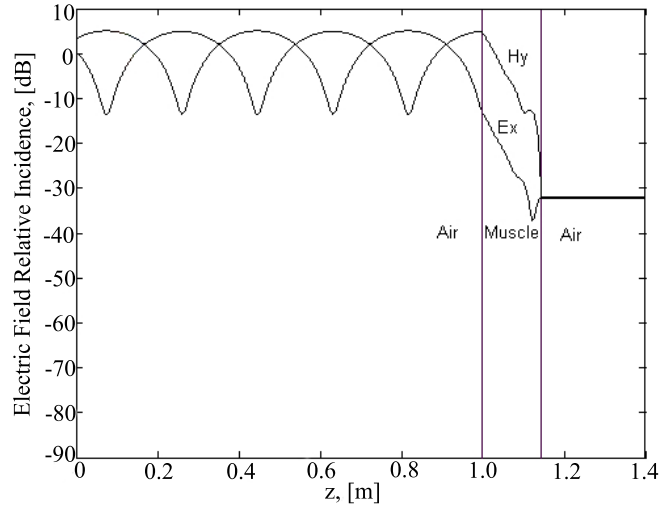


Figure 3.6: The variations in RMS electric and magnetic fields when a plane wave travelling in the positive z direction impinges upon a simple 1D phantom [9].

There was a dependence on the fat layer but the variations were not larger.

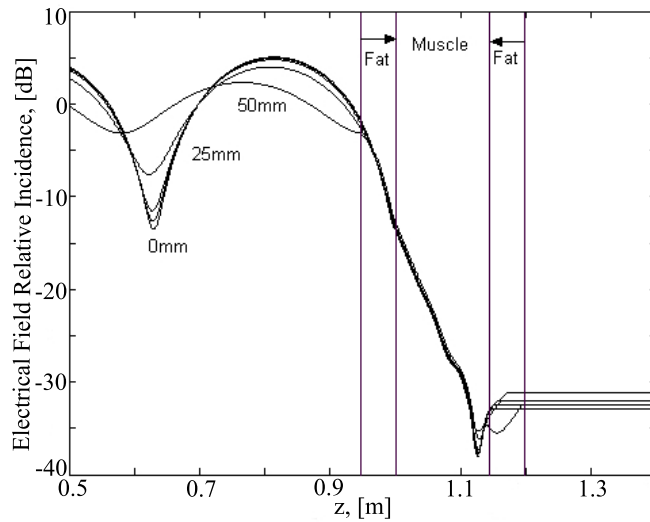


Figure 3.7: Electrical field strength dependence on fat layer thickness [9].

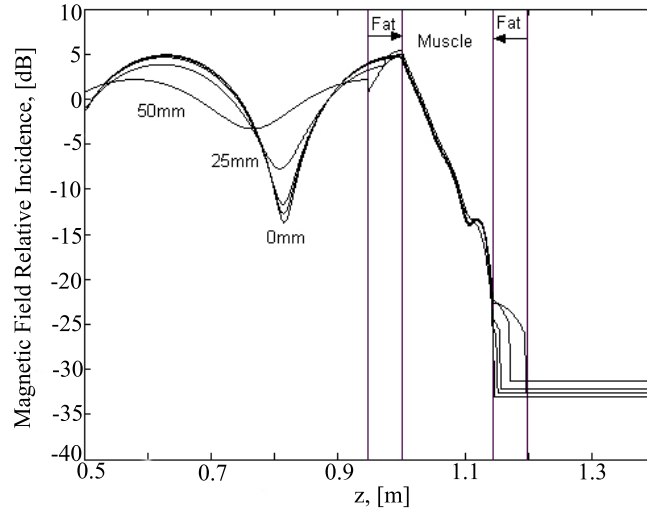


Figure 3.8: Electrical field strength dependence on fat layer thickness [9].

3.7 Antenna

The most common forms of antennas are dipoles and loop antennas; they are the most versatile types for many applications. Desirable features for an implant antenna include compact size and acceptable radiation efficiency, for the fields pass through biological tissue. They have to be omnidirectional too. To investigate the suitability of these antennas for use in near-field implant communication, the radiated fields are analysed to determine whether power density is predominantly inductive or capacitive. It is also established if any of these antennas can modulate the data pulses.

3.7.1 Dipole or Linear-wire Antenna

A dipole is simply a linear wire that is used to radiate fields into free space. In order to use a dipole in implants, its length has to be in the order of a few centimeters, for the pill that houses all the circuitry including antenna normally measures $11 \text{ mm} \times 25 \text{ mm}$. The frequency should be low for absorption of radiated fields by tissues [99]. Therefore a dipole's length l is usually much smaller than the wavelength λ . It can be considered as an infinitesimal dipole for which the fields E and H are given by

$$E_r = \eta \frac{I_0 l \cos \theta}{2\pi r^2} \left[1 + \frac{1}{jkr} \right] e^{-jkr} \quad (3.29)$$

$$E_\theta = j\eta \frac{kI_0 l \sin \theta}{4\pi r} \left[1 + \frac{1}{jkr} - \frac{1}{(kr)^2} \right] e^{-jkr} \quad (3.30)$$

$$E_\phi = 0 \quad (3.31)$$

$$H_r = H_\theta = 0 \quad (3.32)$$

$$H_\phi = j \frac{kI_0 l \sin \theta}{4\pi r} \left[1 + \frac{1}{jkr} \right] e^{-jkr} \quad (3.33)$$

The power density of an antenna, as discussed in Section 3.5.3, can be computed if E and H fields are known. Using (3.29)-(6.5), the complex Poynting vector for a dipole antenna can be written as

$$W = \frac{1}{2} (E \times H^*) = \frac{1}{2} (\hat{\mathbf{a}}_r E_r + \hat{\mathbf{a}}_\theta E_\theta) \times (\hat{\mathbf{a}}_\phi H_\phi^*) = \frac{1}{2} (\hat{\mathbf{a}}_r E_\theta H_\phi^* - \hat{\mathbf{a}}_\theta E_r H_\phi^*) \quad (3.34)$$

The subscripts \mathbf{r} , θ and ϕ represent resolved vector components of a spherical coordinate system. The power density of a dipole antenna has radial W_r and transverse W_θ components. They are given by

$$W_r = \frac{\eta}{8} \left| \frac{I_0 l}{\lambda^2} \right| \frac{\sin^2 \theta}{r^2} \left[1 - j \frac{1}{(kr)^3} \right] \quad (3.35)$$

$$W_\theta = j\eta \frac{k |I_0 l|^2 \cos \theta \sin \theta}{16\pi^2 r^3} \left[1 + \frac{1}{(kr)^2} \right] \quad (3.36)$$

The complex power moving outward radially can be computed by integrating (6.8)-(3.36) over a closed sphere of radius r . It can be written as

$$P = \oiint_S \mathbf{W} \cdot d\mathbf{s} = \int_0^{2\pi} \int_0^\pi (\hat{\mathbf{a}}_r W_r + \hat{\mathbf{a}}_\theta W_\theta) \cdot \hat{\mathbf{a}}_r r^2 \sin \theta d\theta d\phi \quad (3.37)$$

which reduces to

$$P = \int_0^{2\pi} \int_0^\pi W_r r^2 \sin \theta d\theta d\phi = \eta \frac{\pi}{3} \left| \frac{I_0 l}{\lambda} \right|^2 \left[1 - j \frac{1}{(kr)^3} \right] \quad (3.38)$$

The transverse component W_θ of the power density does not contribute to the integral. This is because of the way in which the power pattern is defined. It is a measure, as a function of direction, of the average power density radiated by an antenna in a direction normal to the infinitesimal area dA on the sphere of radius r . However as W_θ moves in the transverse direction, it (3.38) does not represent the total complex power radiated by the antenna. The second term of (3.38) along with (3.36) should be used to determine the total reactive power of the dipole antenna.

(3.38) can also be written as

$$P = P_{rad} + j2\omega (\tilde{W}_m - \tilde{W}_e) = \eta \frac{\pi}{3} \left| \frac{I_0 l}{\lambda} \right|^2 \left[1 - j \frac{1}{(kr)^3} \right] \quad (3.39)$$

where

P =power in radial direction

P_{rad} =time-average power radiated

\tilde{W}_m =time-average magnetic energy density in radial direction

\tilde{W}_e =time-average electric energy density in radial direction

$2\omega (\tilde{W}_m - \tilde{W}_e)$ =time-average imaginary (reactive) power in radial direction

From (3.39)

$$P_{rad} = \eta \frac{\pi}{3} \left| \frac{I_0 l}{\lambda} \right|^2 \quad (3.40)$$

$$2\omega (\tilde{W}_m - \tilde{W}_e) = -\eta \frac{\pi}{3} \left| \frac{I_0 l}{\lambda} \right|^2 \frac{1}{(kr)^3} \quad (3.41)$$

(3.41) is of particular interest as it clearly shows that magnetic radial energy is less than electric radial energy. Additionally for large values of kr ($kr \gg 1$), the reactive power abates and vanishes when $kr \rightarrow \infty$. For use in implants, antennas are preferred to be magnetic rather than electric. It was previously reported in Section. 3.3 that the human body can be used as a medium for electrostatic coupling. This prompts for a need to verify if these antennas can shape the pulses

and make communication possible.

3.7.2 Loop Antenna

A loop antenna is equivalent to an infinitesimal **magnetic dipole** whose axis is perpendicular to the plane of the loop. The magnetic dipole is assumed to have a length l and constant magnetic spatial current I_m given by

$$E_r = E_\theta = H_\phi = 0 \quad (3.42)$$

$$E_\phi = -j \frac{k I_m l \sin \theta}{4\pi r} \left[1 + \frac{1}{jkr}\right] e^{-jkr} \quad (3.43)$$

$$H_r = \frac{I_m l \cos \theta}{2\pi \eta r^2} \left[1 + \frac{1}{jkr}\right] e^{-jkr} \quad (3.44)$$

$$H_\theta = j \frac{k I_m l \sin \theta}{4\pi \eta r} \left[1 + \frac{1}{jkr} - \frac{1}{(kr)^2}\right] e^{-jkr} \quad (3.45)$$

The term $I_m l$ is called the magnetic moment of the magnetic dipole. It is equivalent to a small electric loop of radius a and constant electric current I_o provided that

$$I_m l = j S \omega \mu I_o \quad (3.46)$$

where

$S = \pi a^2 = \text{area of the loop.}$

As discussed in Section (3.7.1), for a dipole antenna the power in the near-field region ($kr \ll 1$) is predominantly reactive and in the far-field real. The complex power for a loop antenna is given by

$$W = \frac{1}{2} (E \times H^*) = \frac{1}{2} [(\hat{\mathbf{a}}_\phi E_\phi) \times (\hat{\mathbf{a}}_r H_r^* + \hat{\mathbf{a}}_\theta H_\theta^*)] = \frac{1}{2} (-\hat{\mathbf{a}}_r E_\phi H_\theta^* + \hat{\mathbf{a}}_\theta E_\phi H_r^*) \quad (3.47)$$

The radial W_r and transverse W_θ components of complex power density are given by

$$W_r = \eta \frac{(ka)^4}{32} |I_0|^2 \frac{\sin^2 \theta}{r^2} \left[1 + j \frac{1}{(kr)^3} \right] \quad (3.48)$$

$$W_\theta = \eta \frac{(ka)^2}{16} |I_0 a|^2 \frac{\sin \theta \cos \theta}{r^3} \left[\frac{1}{r} \left(1 - \frac{k}{r} \right) - j \left(k + \frac{1}{kr^3} \right) \right] \quad (3.49)$$

By integrating (3.47) over a closed sphere of radius r , the power moving outward radially is given by

$$P = \eta \left(\frac{\pi}{12} \right) (ka)^4 |I_0|^2 \left[1 + j \frac{1}{(kr)^3} \right] \quad (3.50)$$

From (3.50)

$$2\omega \left(\tilde{W}_m - \tilde{W}_e \right) = \eta \left(\frac{\pi}{12} \right) (ka)^4 |I_0|^2 \frac{1}{(kr)^3} \quad (3.51)$$

A comparison between (3.51) and (3.41) indicates that the reactive energy for a dipole is negative whereas it is positive for a loop antenna. In other words for a dipole the radial power density in the near-field is capacitive but inductive for a loop antenna.

3.8 Lumped Element Equivalent Circuit-Dipole Antenna

Chu [100] and Storable *et al.*, [101] proposed two simple equivalent circuits to represent short dipole antennas. These were, respectively

1. a three-element equivalent circuit from [100]
2. a four-element equivalent circuit from [101]

3.8.1 The Three-Element Equivalent Circuit

Chu's equivalent circuit can be represented by three lumped elements as shown in Fig. 3.9. The values of lumped elements depend on the physical dimensions

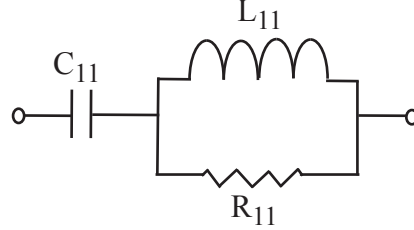


Figure 3.9: Three-element equivalent circuit of a dipole.

of a dipole and not on the frequency of operation. This aspect of frequency-independent lumped elements is crucial for carrying out time-domain analysis, in order to determine the pulse shape at the terminals of an antenna. The antenna feed point impedance $Z_a = R_a + jX_a$ may be obtained by finding the equivalent impedance of the network shown in Fig. 3.9. The value of C_{11} is determined from the reactance of the antenna at a frequency (f) much lower than the resonant frequency. While doing so L_{11} and R_{11} can be ignored and C_{11} is given by

$$C_{11} = \frac{|X_a|}{2\pi f} \quad (3.52)$$

But the value of C_{11} is related to the dipole half-length (h) and radius (a) by [102]

$$C_{11} = \frac{27.82 \times 10^{-12}}{\ln(2h/a) - 1.693} \quad (3.53)$$

The inductance L_{11} and R_{11} can be evaluated at the resonant frequency (ω_o) at which the reactance of the antenna vanishes. The radiation resistance R_{ao} is related to all the lumped elements by the following relations:

$$L_{11} = \frac{1}{\omega_o^2 C_{11}} + C_{11} R_{ao}^2 \quad (3.54)$$

$$R_{11} = \frac{L_{11}}{C_{11} R_{ao}} \quad (3.55)$$

This circuit suffered from problems of predicting high radiation resistance below resonance. Nevertheless the values of reactance were most accurate.

3.8.2 The Four-Element Equivalent Circuit

Similar to the three-equivalent circuit the dipole is approximated by lumped elements independent of frequency. The difference is an addition of a resistance in series with the capacitance [101]. This is shown in Fig. 3.10.

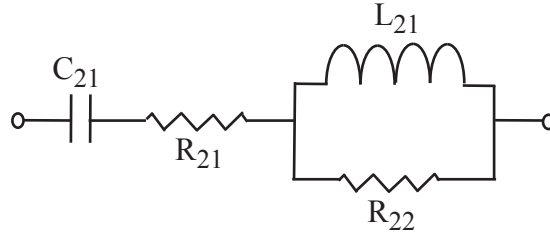


Figure 3.10: Four-element equivalent circuit of a dipole.

The values of R_{21} , R_{22} , C_{21} and L_{21} are given by:

$$R_{21} = 0.663 \Omega \quad (3.56)$$

$$R_{22} = 2200.6 \Omega \quad (3.57)$$

$$C_{21} = \frac{0.002721}{\pi c} \text{ F} \quad (3.58)$$

$$L_{21} = \frac{434.55l}{\pi c} \text{ H} \quad (3.59)$$

where

$$c = 3 \times 10^8 \text{ (m/s)}$$

$$l = 2h = \text{total length of the dipole (m)}$$

This equivalent circuit also has some disadvantages. It predicted input impedances with large-errors especially when frequencies were below the resonant frequency and the radiation resistance is less than approximately 2Ω . This is an impediment when designing near-field pulse based communication systems because the

radiation resistance is expected to be low, as much of the energy is stored in its reactive fields.

Thus it was decided to use a modified version of the four-element lumped equivalent circuit representing a dipole for carrying out a necessary time-domain analysis. It also consisted of four elements and was of similar configuration to the three-element equivalent circuit of Chu [95]. The values of the elements of Fig. 3.11 are given by:

$$C_{31} = \frac{12.0647h}{\log(2h/a) - 0.7245} \text{ pF} \quad (3.60)$$

$$C_{32} = 2h \left\{ \frac{0.89075}{[\log(2h/a)]^{0.8006} - 0.861} - 0.02541 \right\} \text{ pF} \quad (3.61)$$

$$L_{31} = 0.2h \{ [1.4813 \log(2h/a)]^{1.012} - 0.6188 \} \text{ } \mu\text{H} \quad (3.62)$$

$$R_{31} = 0.41288 [\log(2h/a)]^2 + 7.40754 (2h/a)^{-0.02389} - 7.27408 \text{ k}\Omega \quad (3.63)$$

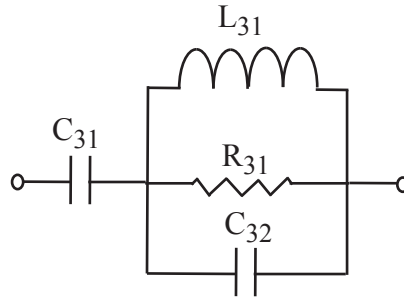


Figure 3.11: New four-element equivalent circuit of a dipole.

These empirical equations consider the physical dimensions of the dipole, viz., half-length (h) and radius (a) which are expressed in meters. It is worth pointing out the fact that unlike Chu's equivalent circuit, the resonance frequency ω_o does not appear in the expressions. This suggests that a complete frequency response

can be obtained by evaluating equations (3.60)-(3.63).

3.9 Results and Discussion

Owing to the requirement of compact size antennas in implantable devices, the new four-element equivalent circuit of a dipole was investigated for half-lengths $h = [0.5 \ 1 \ 1.5]$ cm to know the nature of waveforms at the antenna terminals. Dipoles of such lengths can be easily integrated in a pill-shaped ingestible device. The values of C_{31} , C_{32} , L_{31} and R_{31} can be evaluated by solving (3.60)-(3.63). The antenna impedance between the open terminals can be calculated by (3.64) and (3.65):

$$\frac{1}{Z_{eq}} = \frac{1}{R_{31}} + \frac{1}{j\omega L_{31}} + j\omega C_{32} \quad (3.64)$$

$$Z_{total} = Z_{eq} - \frac{j}{\omega C_{31}} \quad (3.65)$$

h [cm]	C_{31} [fF]	C_{32} [fF]	L_{31} [nH]	R_{31} [k Ω]	Input Impedance [Ω]
0.5	83.192	18.104	1.548	0.433	$0.87e^{-6} - j0.95e^6$
1.0	117.58	24.769	4.009	0.718	$3.53e^{-6} - j0.68e^6$
1.5	150.54	31.447	6.815	0.921	$7.96e^{-6} - j0.53e^6$

Table 3.5: Lumped Element Values.

The entries in the table were generated for a frequency $f = 2$ MHz and radius $a = 0.3455$ mm. The input impedance suggests that the radiation resistance is practically non-existent. However an interesting observation is that the reactance of a dipole is negative for such small dimensions. In other words the energy stored is mainly capacitive. Advanced Design System software (ADS) was used to simulate the behaviour of a dipole antenna when excited by a pulse. A square pulse of peak amplitude 1 V is applied across the terminals of the dipole through a series resistance of 5 Ω . The values of all the lumped components that form the new four-element equivalent circuit were taken from the entries in the first row of Table 3.5. It was observed that dipole antenna behaved like a capacitor and the entire voltage appeared across its terminals as shown in Fig. 3.12 (a). The voltage

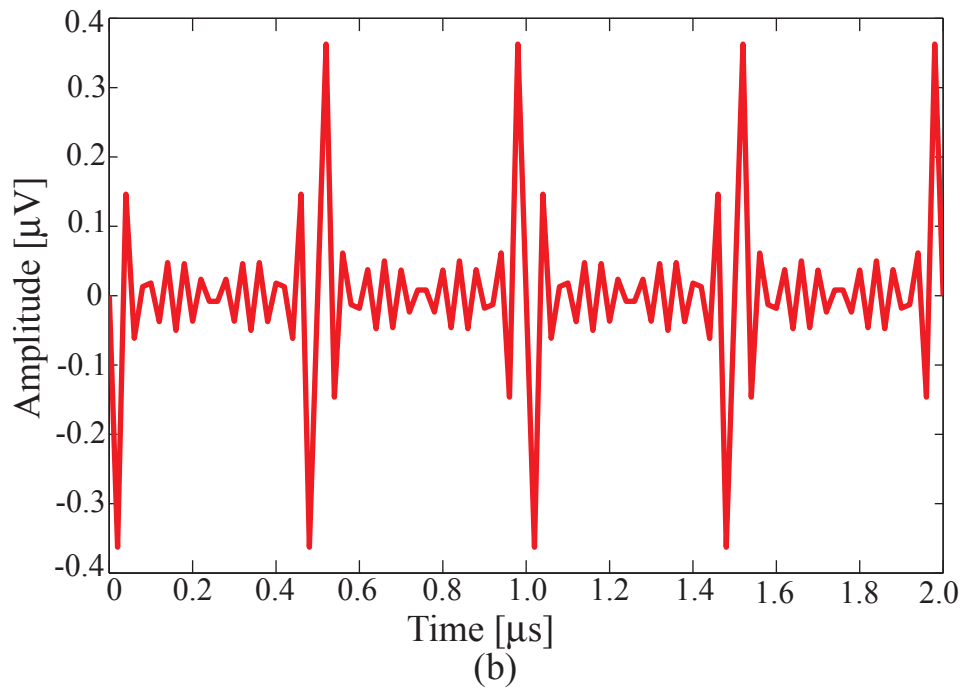
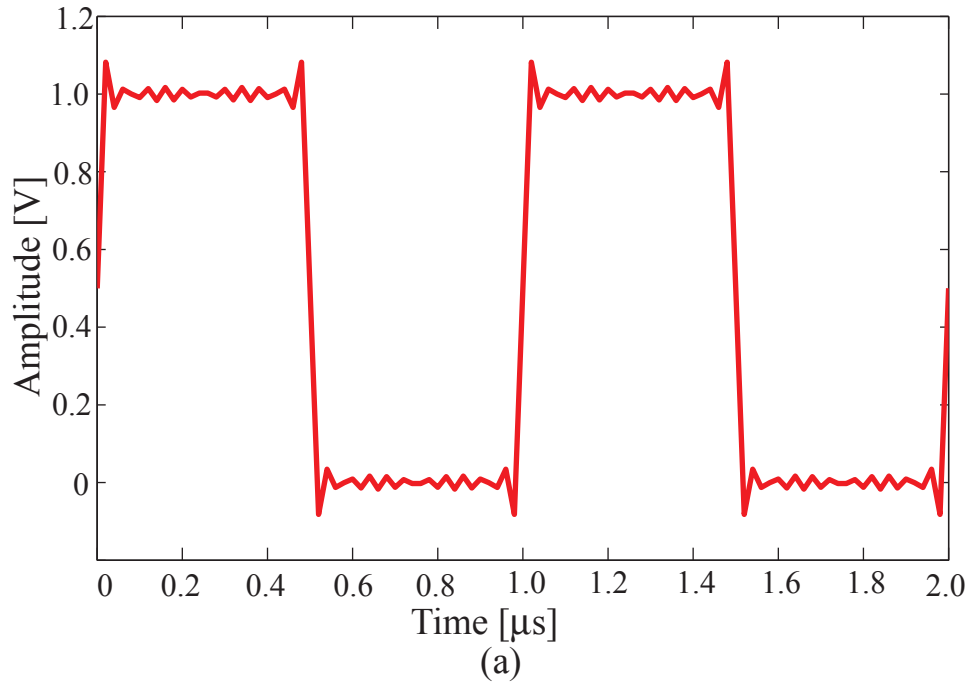


Figure 3.12: Simulated voltage waveforms:(a)Electric energy waveform; and (b)Magnetic energy waveform

that appears as magnetic energy in a dipole is shown in Fig. 3.12 (b). As expected the amplitude levels are too low and hence the signal will be lost in background noise. For increasing dipole half-length there is also a corresponding increase in its inductance. This did not increase the amplitude levels significantly and the waveform shape also remained the same. To couple the electric energy from one dipole to another, one should opt for electrostatic coupling. This necessitates for the dipole (once implanted) to be in contact with bodily fluids which is not desirable. Thus use of dipoles in near-field communication implantable systems was considered not to be a feasible option. In general it can be concluded that the electric antennas are unsuitable for use in low frequency pulse radio near-field implantable systems.

3.10 Summary

In this chapter, a novel design scheme for radiating pulses is presented. The scheme called the near-field baseband communication, is attractive for implantable systems owing to its low power requirements and reduced complexity. This chapter carefully considers the antenna choices (electric or magnetic) to be made. It is central for the communication system as antenna not only acts as a radiator, but also, an encoder. The suitability of a dipole was studied and was found that it is not an ideal candidate for near-field wireless systems. The next chapter discusses the loop antennas and investigates different circuit topologies to make near-field communication system viable.

CHAPTER 4

LOOP ANTENNA DESIGN FOR PULSE RADIO

Contents

4.1	Introduction	70
4.2	Coil Properties	70
4.2.1	External Inductance	71
4.2.2	Internal Impedance	71
4.2.2.1	Skin Effect	72
4.2.2.2	Proximity Effect	73
4.3	Simulation Results and Verification	76
4.3.1	External and Internal Inductance	76
4.4	Pulse Shaping Filter	79
4.4.1	Filter Design	80
4.4.1.1	Filter Analysis	82
4.4.1.2	Pulse Characterisation	89
4.5	Antenna Bandwidth	90
4.6	Summary	92

4.1 Introduction

The previous chapter included a description of electric and magnetic antennas and also explained the shortcomings of electric antennas for use in near-field low frequency implantable systems. This chapter concentrates on establishing the use of loop antennas as magnetic antennas to radiate low frequency pulses effectively. A comprehensive theory has been developed for designing low frequency pulse radio systems. The loop antenna is treated as a lumped equivalent circuit to determine the distortion suffered by a pulse at the antenna terminals. This is very important for an efficient detection of the pulse at the receiver. An expression for the fractional bandwidth of such low frequency pulse antennas has been developed.

4.2 Coil Properties

A coil can be represented by lumped components as shown in Fig. 4.1.

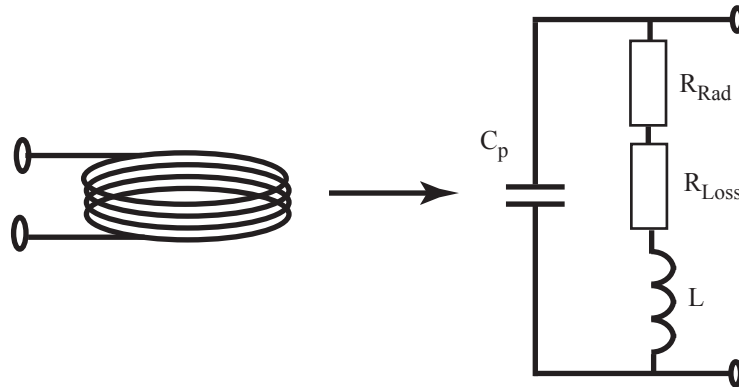


Figure 4.1: Equivalent Circuit of a Loop Antenna.

R_{Rad} the radiation resistance, R_{Loss} the loss resistance, L the inductance and C_P the parasitic capacitance constitute the lumped equivalent circuit components [103].

4.2.1 External Inductance

The external inductance of an inductor depends upon its geometry and can be readily calculated by various expressions. The most common geometries are long solenoid, a toroid and a spiral shaped coil. The external inductance for coils, whose height is large in comparison to the radius, is given by [104]:

$$L_e = \frac{\mu N^2 A}{l} \quad (4.1)$$

where

μ =permeability of the medium, Hm^{-1}

N =number of turns on solenoid

A =cross-sectional area of solenoid, m^2

l =length of solenoid, m

The external inductance of any coil whose height is small in comparison to its radius is given by [105]:

$$L_e = N^2 a \mu \left[\ln \left(\frac{8a}{d} - 2 \right) \right] \quad (4.2)$$

where

N =number of turns

μ =permeability of the medium, , Hm^{-1}

a =loop radius

d =wire radius

It is assumed that the loop radius a is much greater than the wire radius d .

4.2.2 Internal Impedance

An alternating current (AC) in a wire generates a magnetic field inside and around it. The internal magnetic field penetrates the wire to a certain depth. Thus the field decreases to $1/e$ of its initial value, while the field penetrates to a distance δ . This is called the $1/e$ *depth of penetration* and the phenomenon is often called *skin effect*. The depth of penetration is given by:

$$\delta = \frac{1}{\sqrt{f\pi\mu\sigma}} \quad (4.3)$$

where

δ =1/e depth of penetration, m

f =frequency, Hz

σ =electrical conductivity of the medium, Um^{-1}

The above equation (4.3) indicates that the internal impedance is dependent upon the frequency. For an electrically small single-turn loop antenna, the internal impedance is generally taken to be that of a straight conductor in length to the circumference of the loop [106]. But in case of multiturn loops the current distribution is somewhat cumbersome to be predicted as the current re-distribution can also be a result of the magnetic field generated currents in nearby turns. This occurrence is called the proximity effect. These effects are important to be considered for electrically small coils as the loss resistance tends to be much larger than the radiation resistance [13]. Fig. 4.2 represents the internal impedance in a single conductor and a system of two adjacent conductors.

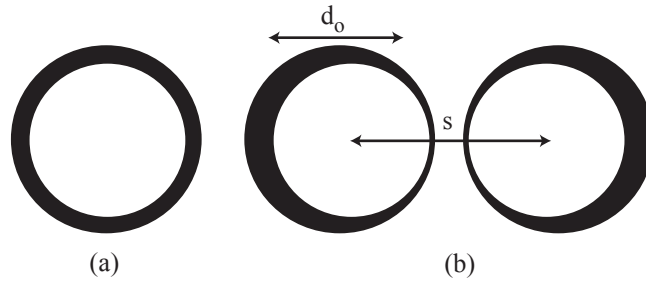


Figure 4.2: (a)Skin Effect in a Single Conductor; and (b)Proximity Effect and Skin Effect in Adjacent Conductors.

4.2.2.1 Skin Effect

An increase in the internal impedance per unit length due to the skin effect is given by [105]:

$$Z_i = R + j\omega L_i = \frac{jR_s}{\sqrt{2}\pi d} \left[\frac{Ber(q) + jBei(q)}{Ber'(q) + jBei'(q)} \right] \quad (4.4)$$

where

$$R_s = \frac{1}{\sigma \delta} = \sqrt{\frac{\pi f \mu}{\sigma}} \quad (4.5)$$

$$q = \frac{\sqrt{2}d}{\sigma} \quad (4.6)$$

d =wire radius

The Ber and Bei functions and their derivatives Ber' and Bei' respectively are defined as follows:

$$Ber(v) + jBei(v) = J_0(j^{-1/2}v) \quad (4.7)$$

$$Ber'(v) + jBei'(v) = \frac{d}{dv} (Ber(v) + jBei(v)) = j^{-1/2} J_0'(j^{-1/2}v) \quad (4.8)$$

where

J_0 =Bessel function of the first kind of order zero

Low and High frequency approximations are suggested for (4.4) that can be useful in knowing the nature of internal impedances for variations in either frequency f or loop radius a . It is given by:

$$Z_i \approx \frac{1}{\pi d^2} \left[1 + \frac{1}{48} \left(\frac{d}{\delta} \right)^2 \right] + j \frac{\omega \mu}{8\pi} \quad \Omega/\text{m} \quad (4.9)$$

The high frequency expression is given by:

$$Z_i \approx \frac{(1+j)}{2\pi d} R_s \quad \Omega/\text{m} \quad (4.10)$$

4.2.2.2 Proximity Effect

Proximity effect is important in loop antennas as it can affect the radiation efficiency. The radiation and loss resistances determine the radiation efficiency. In practice, multiturn loops are used to increase the radiation efficiency. However, the current distribution in a multiturn loop is quite complex as a result of which

great confidence has not yet been established in determining the radiation efficiency of a small multiturn loop antenna analytically. Experimental techniques such as the Wheeler method and Q method are used to measure radiation efficiency [107].

G. S. Smith made a theoretical analysis to evaluate the proximity effect [108]. The total ohmic resistance for an N -turn circular-loop antenna with loop radius a , wire radius b , and loop separation $2c$ is given by:

$$R_{\text{ohmic}} = \frac{Na}{b} R_s \left(\frac{R_p}{R_o} + 1 \right) \quad (4.11)$$

where

$R_s = \sqrt{\frac{\omega \mu_o}{2\sigma}}$ = surface impedance of conductor

R_p = ohmic resistance per unit length due to proximity effect

$R_o = \frac{NR_s}{2\pi b}$ = ohmic skin effect resistance per unit length

The normalised values of additional ohmic resistance per unit length due to proximity effect $\frac{R_p}{R_o}$ are reproduced for reference in Table 4.1 [13]. It is evident that for close spacing the additional resistance due to the proximity effect is twice as large as that in the absence of the proximity effect. Smith claims that these results are valid for almost all practical wire sizes used to make loop antennas as long as the frequency of operation is above 1 MHz.

Most of the formulae presented so far require the loop antennas to be electrically small. A coil is generally considered to be electrically small if the total length of the conductor is less than a tenth of the wavelength [84]. The system proposed in this thesis is operable in the near-field. The maximum theoretical frequency for near-field transmission depends on the required range r given by [109]:

$$r = \frac{\lambda}{2\pi} \quad (4.12)$$

where

λ = wavelength

Since the desired operational range is to be within a metre (in the near-field) or so, the maximum frequency permitted would be less than or equal to 48 MHz. Therefore the minimum wavelength will be equal to 6.25 m. As the

c/b	Numbers of conductors						
	2	3	4	5	6	7	8
1	0.333						
1.05	0.316	0.743	1.231				
1.10	0.299	0.643	0.996	1.347	1.689	2.020	2.340
1.15	0.284	0.580	0.868	1.142	1.400	1.643	1.872
1.20	0.268	0.531	0.777	1.002	1.210	1.401	1.577
1.25	0.254	0.491	0.704	0.896	1.068	1.224	1.365
1.30	0.240	0.455	0.644	0.809	0.956	1.086	1.203
1.40	0.214	0.395	0.546	0.674	0.784	0.880	0.965
1.50	0.191	0.346	0.470	0.572	0.658	0.732	0.796
1.60	0.173	0.305	0.408	0.492	0.561	0.620	0.670
1.70	0.155	0.270	0.358	0.428	0.485	0.532	0.573
1.80	0.141	0.241	0.316	0.375	0.423	0.462	0.495
1.90	0.128	0.216	0.281	0.332	0.372	0.405	0.433
2.00	0.116	0.195	0.252	0.295	0.330	0.358	0.382
2.20	0.098	0.161	0.205	0.239	0.265	0.286	0.304
2.40	0.082	0.135	0.170	0.197	0.217	0.234	0.247
2.50	0.077	0.124	0.156	0.180	0.198	0.213	0.225
2.60	0.071	0.114	0.144	0.165	0.182	0.195	0.206
2.80	0.061	0.098	0.123	0.141	0.154	0.165	0.174
3.00	0.054	0.085	0.106	0.121	0.133	0.142	0.150
3.50	0.040	0.062	0.077	0.087	0.095	0.101	0.106
4.00	0.031	0.048	0.058	0.066	0.072	0.076	0.080

Table 4.1: Normalised additional ohmic resistance per unit length due to the proximity effect R_p/R_o [13].

antenna should fit in a small pill, its dimensions will always satisfy the criteria of electrically small antennas. The conclusion is that all the equations presented so far can be used for near-field transmission system design. Another condition that ought to be tested is that skin depth should be less than the wire radius for the operational frequencies concerned. The field should not be able to penetrate to the centre of the conductor and therefore the wire radius should be greater than 4.6 skin depths. Table 4.2 is created which suggests minimum wire radius for various frequencies concerned. While doing the computations, it was assumed

Frequency	40 MHz	20 MHz	10 MHz	1 MHz
Wire Radius	0.048 mm	0.068 mm	0.096 mm	0.306 mm

Table 4.2: Minimum wire radius for Smith's proximity effect analysis to be valid for various near-field frequencies.

that wire was made of copper, which has a conductivity of $\sigma = 5.7 \times 10^7$ S/m at $25^\circ C$ [8].

4.3 Simulation Results and Verification

All the effects discussed so far are simulated for near-field frequencies and the variations observed over the specified range of near-field frequencies. This will help in determining the value of the series resistance in the lumped equivalent circuit. A frequency and time response will then be carried out in order to determine the pulse response of the loop antenna.

4.3.1 External and Internal Inductance

The proximity effect does not give the internal inductance of multiturn loop coils. It mainly affects the resistance of coils given by:

$$\frac{\text{ac resistance}}{\text{dc resistance}} = H_B + u \left(\frac{d_o}{s} \right)^2 G \quad (4.13)$$

where

H_B =resistance of isolated wire taking into account the skin effect

G =a proximity effect factor

u =a constant

d_o =wire diameter in cm

s =spacing between centres of adjacent turns

The internal inductance of a single coil is however given by the skin effect. Fig. 4.3 shows that internal inductance is negligible in comparison to the external inductance. Also, internal inductance decreases for increasing frequency.

Proximity effect quantifies an increase in the additional ohmic resistance and

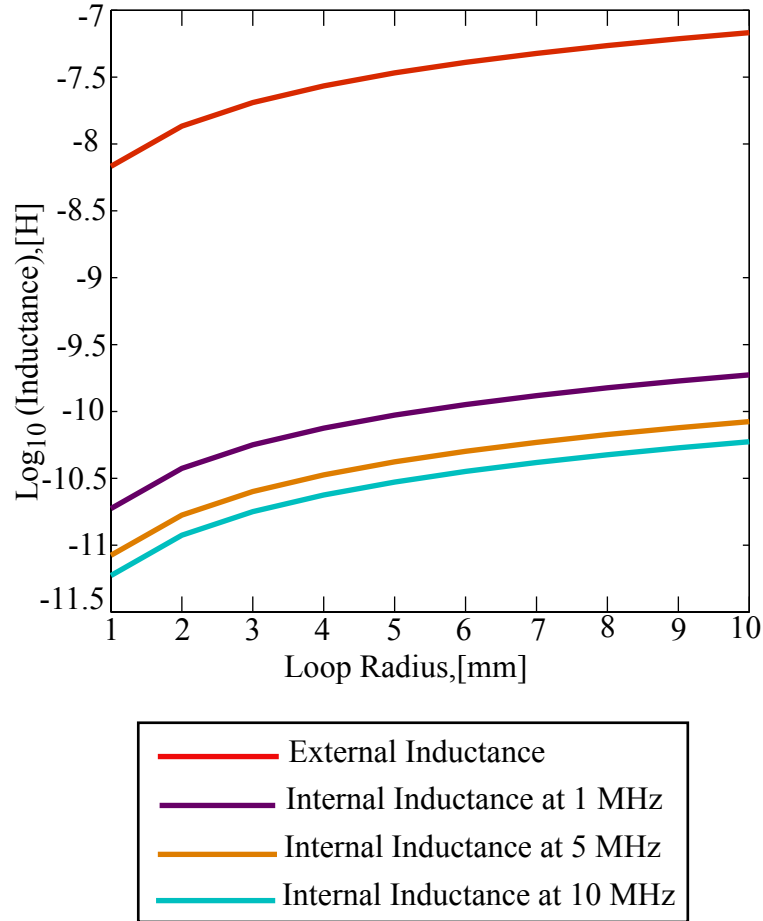


Figure 4.3: Variations of external and internal inductances of a single coil.

it is important to consider this. The resistance alters the shape of the pulse to be transmitted. Hence the variation of ohmic resistance with frequency needs to be determined. Smith’s effect on a loop antenna at near-field frequencies can be beneficial for determining the effect of a loop’s resistance on the shape of a pulse. The parameters that influence the total ohmic resistance are the ratio between conductor spacing and wire radius, frequency, conductivity and number of turns. Figs. 4.4, 4.5, 4.6 and 4.7 show the variation of total ohmic resistance with frequency for various combinations of wire radius and loop radius. In all the four cases, the resistance decreased with an increase in the spacing to wire radius ratio. Hence Smith’s proximity effect is less pronounced in widely-spaced coils.

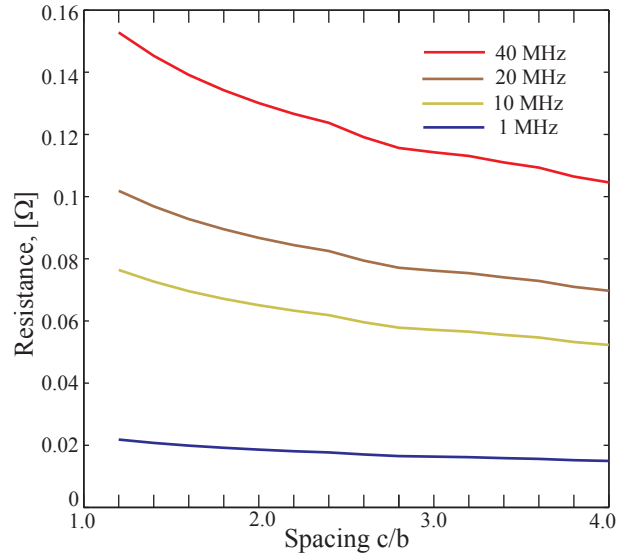


Figure 4.4: Smith’s proximity effect theory for a four turn coil of radius 5 mm with a wire radius of 0.355 mm.

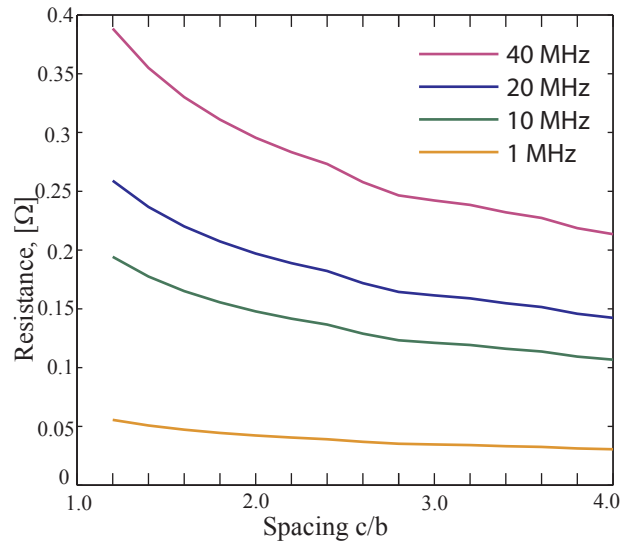


Figure 4.5: Smith’s proximity effect theory for an eight turn coil of radius 5 mm with a wire radius of 0.355 mm.

As the wire radius increases, the resistance decreases, but the difference is small. It can be seen clearly in Figs. 4.4 and 4.6. An increase in the number of turns results in an increase in the total ohmic resistance. It was decided to use Smith’s proximity effect results to predict the distortion suffered by a pulse.

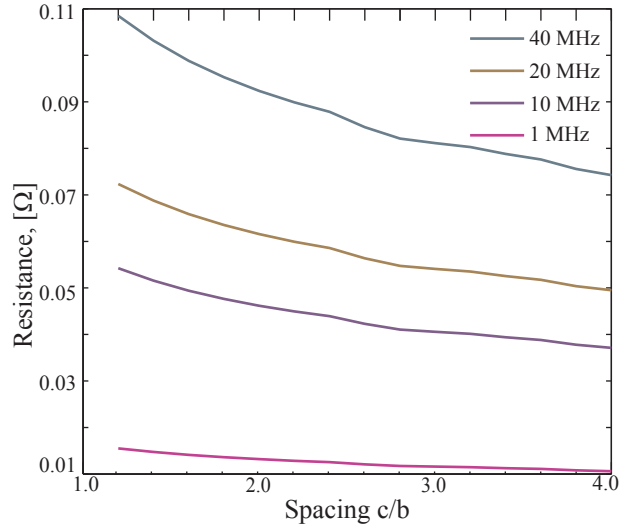


Figure 4.6: Smith's proximity effect theory for a four turn coil of radius 10 mm with a wire radius of 1 mm.

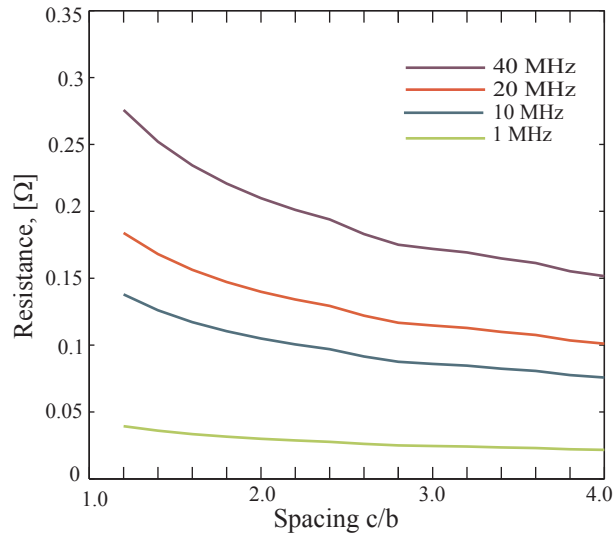


Figure 4.7: Smith's proximity effect theory for an eight turn coil of radius 10 mm with a wire radius of 1 mm.

4.4 Pulse Shaping Filter

The pulse shaping filter plays a crucial role in the overall system design. The design can be realised by considering the antenna as a filter whose parameters can be defined by the help of all the equations presented in the above discus-

sions. The pulse is distorted by an antenna, but in a controlled manner, and the information is conveyed through mutual coupling. This principle is analogous to ultra wideband radio or impulse radio. UWB systems are becoming attractive at microwave frequencies [110, 111]. These systems comprise some type of fast rise-time step or pulse generator [112, 113]. The shape of the pulse in an ideal impulse radio is a Gaussian monocycle of nanosecond duration. Hence dedicated pulse shapers are used to shape the incoming pulse. Data is then transmitted using techniques such as PPM. The pulse shaping adds complexity to the system that in the present case we would like to avoid. In contrast, the system presented in this work, uses the antenna itself as a pulse shaper. It is made up of purely passive elements thereby minimising power consumption. Another major difference is that the near-field baseband pulse radio system operates in the near-field, coupling energy through the reactive fields, unlike an UWB system that operates in the far-field by harnessing energy in the radiated fields. Owing to its simplicity, the baseband pulse radio system becomes attractive and applies itself readily to low frequency near-field communication systems.

4.4.1 Filter Design

ADS software was used to facilitate the design of the near-field baseband communication system. It was the first priority to determine whether a loop antenna can effectively radiate pulses in a manner that can make the information intelligible. With the antenna being predominantly magnetic, it has to also build inductive reactive energy in the form of magnetic fields. These fields of energy can then be coupled to an another receiving antenna, the design of which will be discussed in a later chapter.

Loop antennas come in different shapes and sizes. There are several analytical expressions to calculate their inductance. To understand the principle of designing a loop antenna for the near-field communication systems, it was decided to consider a solenoidal shaped antenna. Importantly, the solenoidal shaped antenna when integrated inside the case of a pill, utilises the available volume efficiently. This is necessary as the field produced by a magnetic dipole is proportional to the area of the loop as shown by (3.46). However the principle can be easily extended

to a loop antenna of any shape and size. The inductance of a solenoid is given by:

$$L = \frac{\mu_o \mu_r N^2 A}{l} \quad (4.14)$$

where μ_o is the permeability of free space, μ_r is the relative permeability, N is the number of turns, l is the length of the solenoidal coil and A is the area of cross-section of the solenoid.

$$|IV| = \left| LI \frac{\Delta I}{\Delta t} \right| \quad (4.15)$$

The capacitance is very small and does not influence the antenna design. However this statement is invalid for the design of a receiving antenna. Hence its discussion is deferred until Chapter 7. The resistances in the equivalent circuit of the loop antenna are small with values normally between 0.1 and 0.5 Ω . The equivalent circuit shown in Fig. 4.1 is modified to have just an inductance and a resistance. The solenoidal loop antenna was assumed to have 10 turns, a loop radius of 5 mm and a total length of 25 mm. Using (4.14), the inductance was found to be 0.394 μH .

The inductor was excited by a square pulse of amplitude 0.5 V. Figs. 4.8 and 4.9 show the input and output waveforms at the terminals of the equivalent circuit representing the loop antenna respectively. This helps us to observe the effect in the time domain and it can be seen that during the rising edge of the pulse, the voltage across the inductor (or antenna terminals) is at its maximum. At this instant the inductor appears as an open circuit. For a constant amplitude, the voltage across the inductor should decay and reach zero amplitude. This decay time depends upon the values of resistance and inductance, given by the time constant τ as in $\tau = \frac{L}{R}$. It approximately takes 5 time constants for a pulse of amplitude A to reach nearly zero. Since the resistance is very small, the decay time is large and the voltage across the antenna never reaches zero. This severely restricts the rate at which energy is taken away from the inductor, in other words, the rate at which magnetic energy is building up in an inductor.

Analytically this can be explained with the help of (4.15). The magnetic field is proportional to the current. If the decay time (Δt) is small, then all the energy

in the magnetic field has to dissipate in a short time. The current thus flows through the antenna for a very short time and a large magnetic field develops around the antenna. This aids in the conversion of almost all the electric energy available to magnetic energy. However the resistance has to be at an acceptable value to minimise losses in heating. A few changes have to be incorporated to achieve the desired result. This includes the addition of a resistance and capacitance.

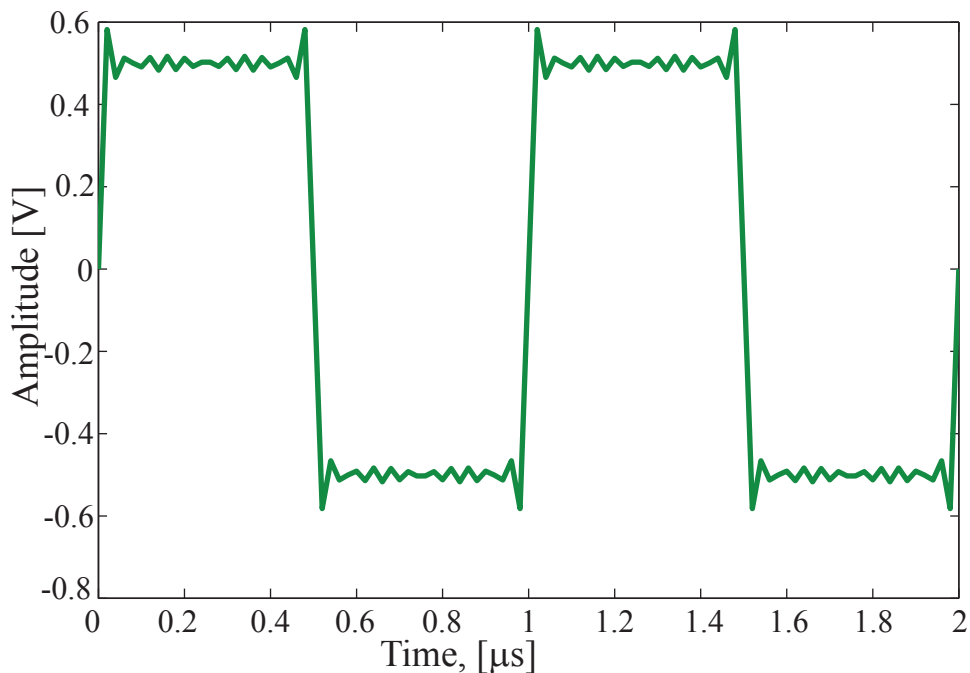


Figure 4.8: Input Square Pulse of Amplitude 0.5 V.

4.4.1.1 Filter Analysis

A novel procedure is suggested to design an antenna for near-field baseband pulse transmission systems. It has been explained that a stand alone loop antenna cannot operate efficiently. A design methodology is proposed here to enhance the features of a loop antenna. The design can feature either as a series RLC circuit or a parallel RLC circuit. The inductor “ L ” in both designs serves as a loop antenna. Loop antennas are perfectly suitable for implantable applications because of their omnidirectionality [114]. An analysis should be carried out in a

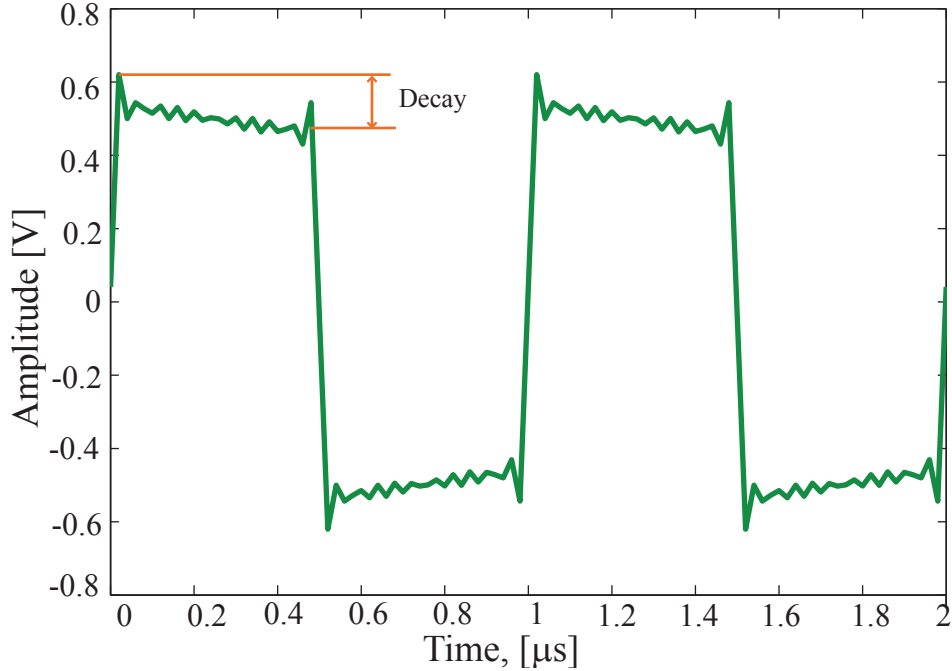


Figure 4.9: Output at the Antenna Terminals.

manner that helps determine the behaviour of a loop antenna circuit over a range of frequencies and how this translates to variations in voltage over time axis. In essence, an antenna can be regarded as a black box, which requires inductance, capacitance and resistance as inputs to produce the temporal characteristics of the loop antenna. The digital pulse is becoming shorter to increase the speed at which a system can operate and therefore a loop antenna has to respond quickly by building and decaying the magnetic energy during the rising and falling edges of the digital pulse. This can be achieved by including an external resistance and capacitance with the loop antenna and in order to determine the values of these elements one has to determine the magnitude and phase characteristics of the loop antenna together with the resistance and capacitance. The resistance and capacitance can either be connected in series or in parallel with a loop antenna.

The series RLC and parallel RLC circuits are shown in Figs. 4.10 (a) and 4.10 (b). As shown previously, the winding resistance is usually small and hence neglected. The transfer functions $H(\omega)$ of a series and parallel circuit are given by 4.16 and 4.17 respectively.

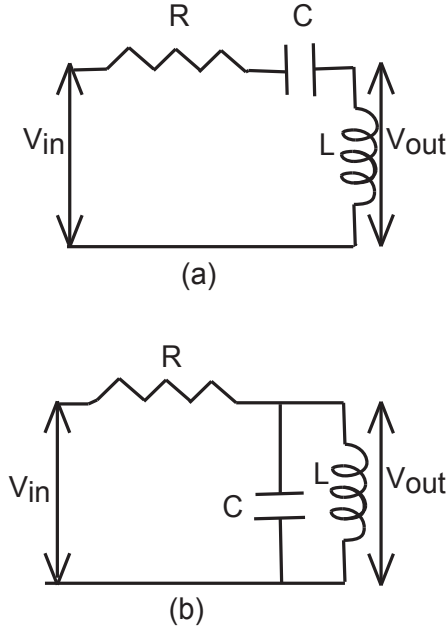


Figure 4.10: (a)Series RLC Circuit; and (b)Parallel RLC Circuit.

$$H_S(\omega) = \frac{j\omega^2 LC}{\omega RC + j(\omega^2 LC - 1)} \quad (4.16)$$

$$H_P(\omega) = \frac{j\omega L}{(R - \omega^2 RLC) + j\omega L} \quad (4.17)$$

$$\theta_S = 90^\circ - \tan^{-1} \left(\frac{\omega^2 LC - 1}{\omega RC} \right) \quad (4.18)$$

$$\theta_P = 90^\circ - \tan^{-1} \left(\frac{\omega L}{R - \omega^2 RLC} \right) \quad (4.19)$$

$$\omega_o = \frac{1}{\sqrt{LC}} \quad (4.20)$$

where

ω_o is the resonance frequency.

A tank circuit can appear to be predominantly inductive, capacitive or resistive depending upon the frequency ω of the input signal V_{in} . In the present case,

the input to the antenna is a rectangular pulse. A pulse is made up of several harmonics. These harmonic frequencies suffer varying levels of attenuation in magnitude and phase, depending on the position of individual frequency components above or below the resonant frequency (ω_o). While designing the antenna, this factor has to be taken into account and the antenna, which is a black box, has to appear inductive to the harmonics. Hence the need to analyse the *RLC* circuits with the help of phasor diagrams. These diagrams help to visualise the resultant voltage V_r (or current I_r) as a vectorial sum of voltages (or currents) across (flowing through) the resistance V_R , inductance V_L and capacitance V_C . Figs. 4.11 (a) and 4.11 (b) show the phasor diagrams for a series and parallel *RLC* circuit respectively.

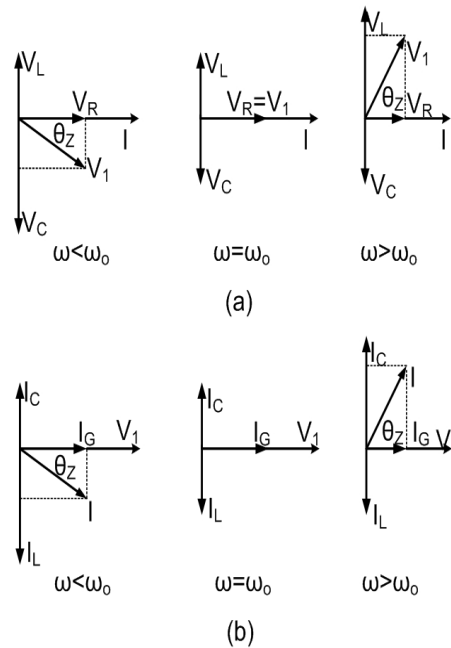


Figure 4.11: Phasor Diagrams:(a)Series *RLC* Circuit; and (b)Parallel *RLC* Circuit.

For a series circuit, when $\omega < \omega_o$, $V_C > V_L$, resultant phase θ_r is negative and the resultant voltage V_r lags the current. When $\omega = \omega_o$, θ_r is zero and the voltage V_r is in phase with the current. If $\omega > \omega_o$, $V_L > V_C$, θ_r is positive and the voltage V_r leads the current. Similar statements can be made for the parallel

circuit with the voltage variable replaced by the current variable.

To design the filter, parameters like Q -factor, damping coefficient α and damping ratio ζ can be used. All the parameters are dependent upon each other. It was decided to use ζ , as it can be expressed in terms of R , L and C , which are the plug-ins for the black box. ζ is given by (4.21) and (4.22) for a series and parallel RLC circuit respectively. The value of ζ can be less than, equal to or greater than 1. Fig. 4.12 shows the amplitude and phase characteristics of the series and parallel RLC circuits for various values of ζ and it can be seen that the magnitude response becomes wider for increasing values of ζ in the case of a series RLC circuit and narrower for a parallel RLC circuit. The effect of ζ on a pulse has to be analysed in the time domain to determine the distortion suffered by a pulse.

$$\zeta_s = \frac{R}{2} \sqrt{\frac{C}{L}} \quad (4.21)$$

$$\zeta_p = \frac{1}{2R} \sqrt{\frac{L}{C}} \quad (4.22)$$

The time domain response of a parallel RLC circuit was analysed for various values of ζ as shown in Fig. 4.13. The input was a square pulse of amplitude 0.5 V.

The pulse was severely distorted in all the cases except Fig. 4.13 (d). In Figs. 4.13 (a) and 4.13 (b), the value of ζ is 0.05 but the time domain response of both of them is different. These anomalies have to be addressed as the shape of the pulse is crucial to make the communication scheme viable. An expression containing the frequency and time domain information of the pulse and the tank circuit will help in designing the loop antenna for use in pulse radio communication systems. A discussion on the tank circuit's bandwidth becomes ever more important and a critical analysis has been carried out, the description of which is in Sec. 4.5. As expected the time domain response of the loop antenna, with an external resistance and capacitance, was found to be oscillatory as shown in Figs. 4.13 (a) and 4.13 (b). A small damping ratio makes the magnitude response sharply peaked. It can be seen that the pulse spreads in the time domain due to "ringing". The amplitude of the pulse in the time domain is very small as the antenna is

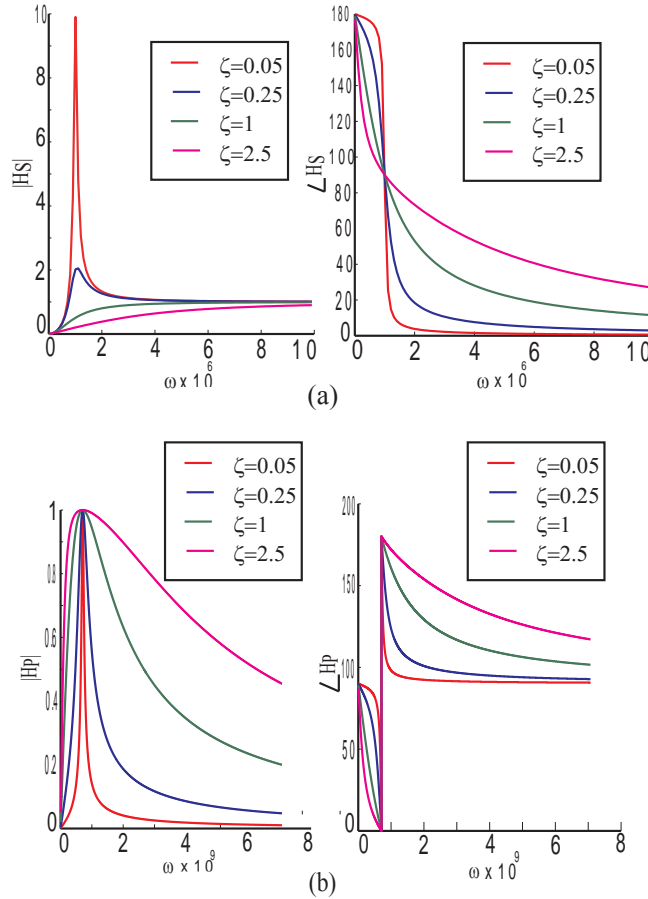


Figure 4.12: Amplitude and phase characteristics of (a)Series RLC and (b)Parallel RLC circuits for varying values of ζ . $|H|$ is the magnitude and $\angle H$ is the phase of the transfer function, with subscripts s and p denoting either a series or parallel RLC circuit respectively.

highly selective. This is undesirable as the detection at the receiver would be a difficult task. In Fig. 4.13 (c), it can be seen that the temporal response is still oscillatory and the pulse has undergone less distortion when compared to cases (a) and (b). The amplitude of the pulse is also larger. This can be attributed to the fact that the frequency response of the loop antenna is not as sharply peaked as those before and the antenna becomes less selective in the pass band. On the other hand, a flat magnitude response curve implies that there will be no ringing and pulses can be shaped perfectly. This is the case when ζ is above 1 as shown in Fig. 4.13 (d). Therefore, the decision was made to design a tank circuit

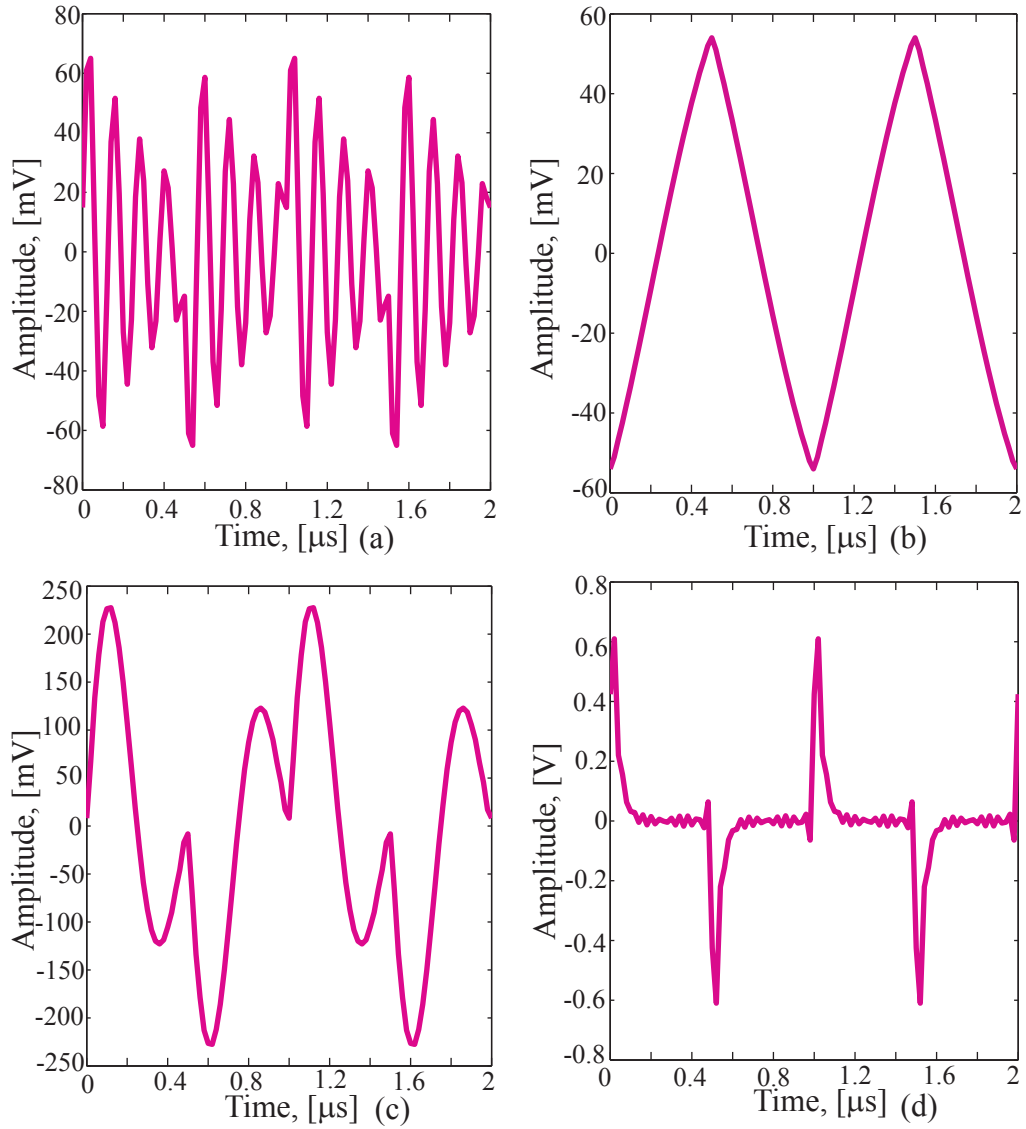


Figure 4.13: Time Domain Response of a Parallel RLC Circuit:(a) $\zeta=0.05$; (b) $\zeta=0.05$; (c) $\zeta=0.2$ and (d) $\zeta=18.5$. In all the cases except (b), $L=0.3 \mu\text{H}$, $R=10 \Omega$ and in (b), $L=20 \text{ nH}$. C was different in all cases.

(that included the loop antenna) with a smooth magnitude response and a phase response which was almost linear.

4.4.1.2 Pulse Characterisation

The transmitted pulse is characterised by its amplitude and width in the time domain. An analytical treatment helps in determining these characteristics. A knowledge of these parameters will help in designing an antenna that will meet the specifications of a pulse transmitter. It can be seen from the previous section that a transmitted pulse will be made shorter in width by the antenna. Characteristic equations for series and parallel RLC circuits can be solved for a step response. (4.23) gives the general form of the characteristic equation of a bandpass filter.

$$s^2 + 2\zeta\omega_o s + \omega_o^2 = 0 \quad (4.23)$$

$$V_{ls}(t) = \frac{V_S}{2\omega_o\sqrt{\zeta^2 - 1}}(s_1 e^{s_1 t} - s_2 e^{s_2 t}) \quad (4.24)$$

$$V_{lp}(t) = \frac{V_S \zeta}{\sqrt{\zeta^2 - 1}}(e^{s_1 t} - e^{s_2 t}) \quad (4.25)$$

where

$$s_1 = -\zeta\omega_o + \omega_o\sqrt{\zeta^2 - 1} \text{ and } s_2 = -\zeta\omega_o - \omega_o\sqrt{\zeta^2 - 1}.$$

The step responses of series and parallel RLC circuits are given by (4.24) and (4.25). s_1 and s_2 are the poles of the characteristic equation. They also form the roots of the characteristic equation. A careful observation reveals that poles determine the time it takes for a pulse to decay to approximately zero amplitude. The filter is said to be in an “overdamped” state. Under this condition, the poles are real. s_1 will be less than s_2 and the pulse amplitude V_s will decay to zero amplitude in time, approximately equal to $5\left(\frac{1}{s_1}\right)$.

The design procedure can be summarised as below:

- R should be as small as possible.
- The circuit should be overdamped.
- The resonance frequency of the coil should be greater than the resonance frequency of the circuit.

4.5 Antenna Bandwidth

In this section, the theories of the filter design and antenna design are merged to arrive at a relationship between pulse widths and antenna bandwidths in terms of the frequency spectra. From Sec. 4.4, it can be deduced that the bandwidth of the filter must be extremely wide and the loading factor ζ should be greater than 1 to transmit the pulses efficiently. How wide should the bandwidth be, can be answered by the help of the knowledge of a rectangular pulse in frequency domain. A rectangular pulse has a width t_p . It is assumed to be repetitive after every T instants in time. The Fourier series representation of the rectangular pulse is given by (4.26).

$$v(t) = \frac{At_p}{T} + \sum_{n=1}^{\infty} \left(2A \frac{t_p}{T} \right) \left(\frac{\sin n\pi t_p/T}{n\pi t_p/T} \right) \cos 2\pi (nf_o) t \quad (4.26)$$

In the limit as the period T increases to infinity without bound, the amplitude spectra become indistinguishable from one another and the continuous curve can be described by (4.27) which is nothing but the Fourier transform of $v(t)$ to the frequency domain as $V(f)$. Fig. 4.14 shows the normalised energy spectral density of the pulse in blue, bipolar pulse in red and the magnitude response of the tank circuit in green.

The bipolar pulse had positive and negative amplitudes of A and width equal to $t_p/2$. In order to arrive at the expression for the bandwidth of the composite system (loop antenna with an external resistance and capacitance) two terms of the filter's passband, namely f_l and f_h have to be determined. The antenna is inductive at frequencies below the resonance frequency f_o and capacitive above f_o . For frequencies above f_o the antenna appears as a constant gain antenna and therefore f_h can be equated to f_o .

$$V(f) = At_p \frac{\sin \pi t_p f}{\pi t_p f} \quad (4.27)$$

To begin with, the frequency f is normalised with the pulse width t_p as ft_p . This will change f_l and f_h to $f_l t_p$ and $f_h t_p$ respectively. As the antenna has to radiate almost all the frequencies, $f_l t_p$ has to be as small as possible. It cannot be zero as a voltage of zero frequency as the antenna acts as a short circuit. So

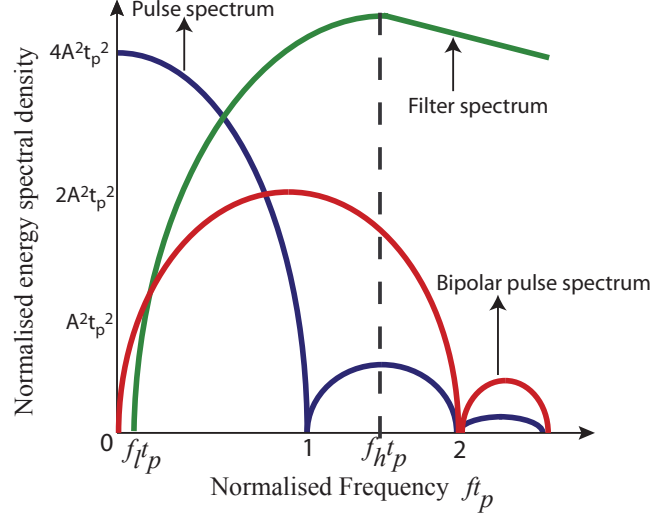


Figure 4.14: Normalised Magnitude Spectrum of the Pulse and Pulse-Shaping Filter.

it was decided to set $f_l t_p = 0.1$. Any variation in f_h affects f_o ($f_h = f_o$) which in turn changes ζ . In Sec. 4.4.1.2, it was reasoned that the antenna has to act as an overdamped filter. Hence, changes in ζ have to be tracked. Before varying f_h , the damping ratio has to be set to a fixed value. This can be achieved by maintaining a constant ratio of L/C . For a fixed value of ζ and $f_l t_p$, the effects of varying $f_h t_p$ on antenna's fractional bandwidth B_f , given by (4.28), is observed.

$$B_f = 2 \frac{f_h - f_l}{f_h + f_l} \quad (4.28)$$

The energy of the pulse spectrum is concentrated at lower frequencies and when such a pulse below the resonant frequency f_o of the antenna undergo attenuation due to capacitive mismatch and above f_o generally act as constant gain antennas. The region around the point of resonance is also of concern as this might induce the “ringing” effect. In essence the resonance frequency splits the spectrum into two parts. It was experimentally observed that for ζ equal to 2, 10 and 20, perfectly shaped pulses were possible only when $f_h t_p$ was greater than or equal to 5, 20 and 40 respectively. When these values were substituted in (4.28),

B_f was nearly equal to 2. Hence, (4.29) gives the fractional bandwidth of the proposed near-field pulse radio system. This analysis helps to design the loop antenna for any pulse width. All that is required is to determine the values of L and C of the loop antenna. Then it has to be made sure that $f_h t_p$ is greater than or equal to 2ζ .

$$B_f \approx 2 \quad (4.29)$$

The bipolar pulse spectrum has no dc component and thus the average losses in the antenna are reduced. Moreover one of the difficulties posed in radiating low frequency is the antenna size. This is because the antenna must be at least a substantial fraction in size of the wavelength of the frequency of electromagnetic waves. Because of the huge size requirement of the antenna, radiation of dc or near dc frequencies is not feasible for communication purposes. The bipolar signals have a better signal-to-noise ratio and require low energy per bit to achieve a good bit error probability rate than the unipolar signals.

4.6 Summary

In this chapter, the design of loop antennas for low frequency near-field pulse radio system is presented. The approach is new in the sense that the loop antenna was not made to resonate at one particular frequency, but instead excited by a pulse which is made up of several harmonics. A detailed analysis was carried out to determine the lumped parameters of the loop antenna's electrical equivalent circuit. The skin effect and the proximity effect was considered in determining the total ohmic resistance of a loop antenna. It was found that these effects contributed insignificantly to a loop's ohmic resistance. Certain changes were required to make the loop antenna more effective in radiating pulses. This included an addition of a series resistance and a parallel capacitance. The main content of this chapter is the estimation of the bandwidth required by loop antennas that are ought to be used in low frequency pulse radio systems. The next chapter discusses different encoding schemes that can be employed in this particular communication scheme. A microcontroller produces the required pulses and a

digital signal processor decodes the data at the receiver.

CHAPTER 5

HFSS AND ANTENNA MODELLING

Contents

5.1	Introduction	95
5.2	Antenna	95
5.2.1	Printed Loop Antenna	97
5.2.2	Solenoidal Loop Antenna	99
5.2.3	Result Interpretation	102
5.3	Experimental Results	104
5.4	Summary	108

5.1 Introduction

The previous chapter dealt with the loop antenna design for the near-field base-band communication system. The approach taken to the design was to regard the loop antenna as a filter that can be represented by a lumped equivalent circuit. This was crucial as it aids in designing the system to meet the desired characteristics in the time and frequency domain. A perfectly shaped pulse in the time domain makes the communication system practically viable. This chapter discusses the electromagnetic design of the magnetic antennas that is central to the near-field wireless communication scheme. Planar loop and solenoidal loop antennas are investigated and an optimal shape among the two is suggested. Ansoft HFSS, a finite element based modelling tool is used to simulate and analyse the electromagnetic fields around these antennas.

5.2 Antenna

In Chapter 4, it was explained that the loop antenna can be treated as a lumped equivalent circuit to determine the time and frequency domain responses. This investigation is necessary to know the effects of the antenna on the pulse and engineer the design of the loop antenna to enable the pulse transmission by encoding information in its shape. A complementary information to this understanding will be the radiation pattern of a loop antenna in the near-field. A radiation pattern is defined as “*a mathematical function or a graphical representation as a function of space coordinates. In most cases, the radiation pattern is determined in the far-field region and is represented as a function of the directional coordinates*” [8]. It was intended to choose the most suitable radiating structure from various shapes and sizes of loop antennas possible. The structures that are to be analysed are: (a) Printed loop antennas and (b) Solenoidal loop antennas. The reasoning credited for choosing to analyse these shapes is the practicality associated with these antenna shapes. The printed loop antennas can be easily integrated with a system-on-chip (SOC) technology. A solenoidal loop antenna can be easily wound in the form of a coil and encased within the pill shaped object. HFSS aids in providing a solution to the complex electromagnetic fields

surrounding the antenna. This will help in developing an understanding of how the fields decay with distance.

The design of loop antennas for the near-field baseband pulse transmission is not dissimilar to radio frequency identification (RFID) links. RFID is an identification method based on the remote retrieval of information via radio waves from miniature electronic circuits called RFID tags [115]. An RFID system has two components: (a) A reader and (b) A tag. RFID tags fall into two main categories depending upon their source of power [116]. RFID tags can be powered by their own power source usually in the form of an on board battery. These are known as active RFID tags. Active tags can operate over a larger read range (20-100 m) as they can emit a strong signal. They operate at higher frequencies - 433 MHz, 2.45 GHz or 5.8 GHz depending upon the data rates and memory requirements [117]. Passive tags are often employed when the data rate is not critical and a smaller range of operation is required. The magnetic field emanated by a reader is linked to the tag antenna and thus communication is made possible. These tags offer the advantages of low power, compactness and low cost. Impedance reflection modulation is popular with such passive tag architectures. The near-field RFID can be represented as a magnetic link between two weakly coupled resonant coils. Resonance is very crucial for such devices and the power transfer is enhanced by matching the resonant frequency of the reader coil with the tag coil. The coils thus have a high Q-factor. High-Q coils are very selective and have a sharp frequency response. This is unattractive for pulse based near-field communication systems as explained in Sec. 4.4.1. Nevertheless the value of inductance is very important for the proposed design principle as it controls the decay rate of the transmitted pulse.

The aim of this analysis is to determine the inductance value of the printed planar square loop antenna and the solenoidal antenna. This is followed by the observation of the near-field radiation pattern and the decay of the electromagnetic fields with distance. The results are then compared with the experimental observation and an appropriate structure among the two is suggested for use in the near-field baseband wireless communication system.

5.2.1 Printed Loop Antenna

The printed loop antenna is square in shape. A printed square loop antenna is characterised by the number of turns in the loop and substrate properties such as dielectric constant and thickness. The planar inductor can be directly printed on the printed circuit board (PCB). The copper track can be considered as the windings of the planar inductor.

Simple accurate expressions for the inductance of square, hexagonal, octagonal and circular spiral inductors have been presented with reasonable accuracy [118]. These analytical expressions are used to compare the inductance value obtained by simulations. Fig. 5.1 shows the layout of a simple square planar inductor.

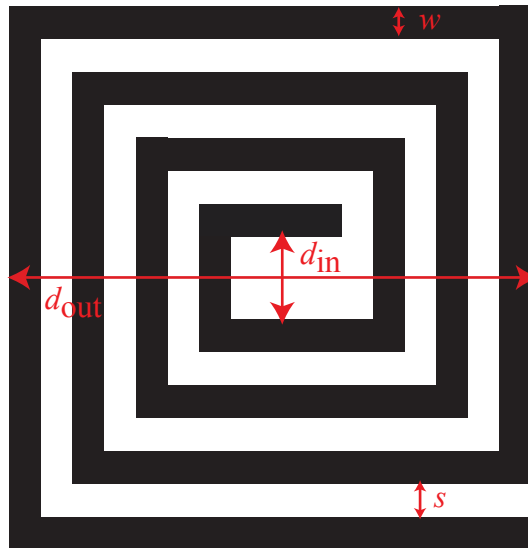


Figure 5.1: Square Planar Inductor.

It can be seen that the square inductor is completely specified by the number of turns n , the turn width w , the turn spacing s . Arithmetic geometrical averages like the average diameter d_{avg} and the fill ratio defined as ρ have to be computed. These are given by (5.1) and (5.2) respectively.

$$d_{avg} = 0.5(d_{out} + d_{in}) \quad (5.1)$$

where d_{in} =the inner diameter and d_{out} =the outer diameter.

$$\rho = \frac{(d_{out} - d_{in})}{(d_{out} + d_{in})} \quad (5.2)$$

In the current scenario, it was decided to use the expression based on approximating the sides of the spirals by symmetrical current sheets of equivalent current densities [118]. There are many expressions to choose from, like Wheeler's expression [119] and optimal expressions using geometric programming [120]. This particular expression was selected owing to its simplicity and accuracy. The resulting expression is given by:

$$L_{gmd} = \frac{\mu n^2 d_{avg} c_1}{2} (\ln(c_2/\rho) + c_3\rho + c_4\rho^2) \quad (5.3)$$

where the coefficients c_i are dependent upon the layout in question. In this case it is a square for which the coefficients are given in Table 5.1. It has a maximum error tolerance of 8% for $s \leq 3w$.

Layout	c_1	c_2	c_3	c_4
Square	1.27	2.07	0.18	0.13

Table 5.1: Coefficients for Current Sheet Expansion.

As shown in Fig. 5.2, a square planar inductor model was setup in HFSS. The model had the following dimensions: $d_{out} = 9$ mm, $d_{in} = 0.45$ mm, $n = 6$, $w = 0.5$ mm and $s = 0.25$ mm. The substrate was made of duroid material, the relative permittivity of which is 2.2, relative permeability is 1 and the dielectric loss tangent is 0.0009. It had a thickness of 1 mm. Although FR4 substrate would be sufficient the reason to choose the duroid substrate was its ready availability. Generally FR4 substrates are used at frequencies less than 2 GHz while duroid substrates are used for providing superior electrical characteristics at higher frequencies. Lumped ports were defined to act as the sources of excitation. They were defined as rectangles from the edge of the trace to the ground. The resistance was set to 50 Ω . An air box of dimensions (9.55 \times 9.05 \times 5) mm was defined as a radiation boundary. The electromagnetic fields were solved at 1 MHz.

Fig. 5.3 shows a plot of the inductance of the planar square loop antenna vs frequency as simulated by HFSS. The variation of the inductance is very small and lies between 0.1 μ H and 0.11 μ H. The value of the inductance was found to

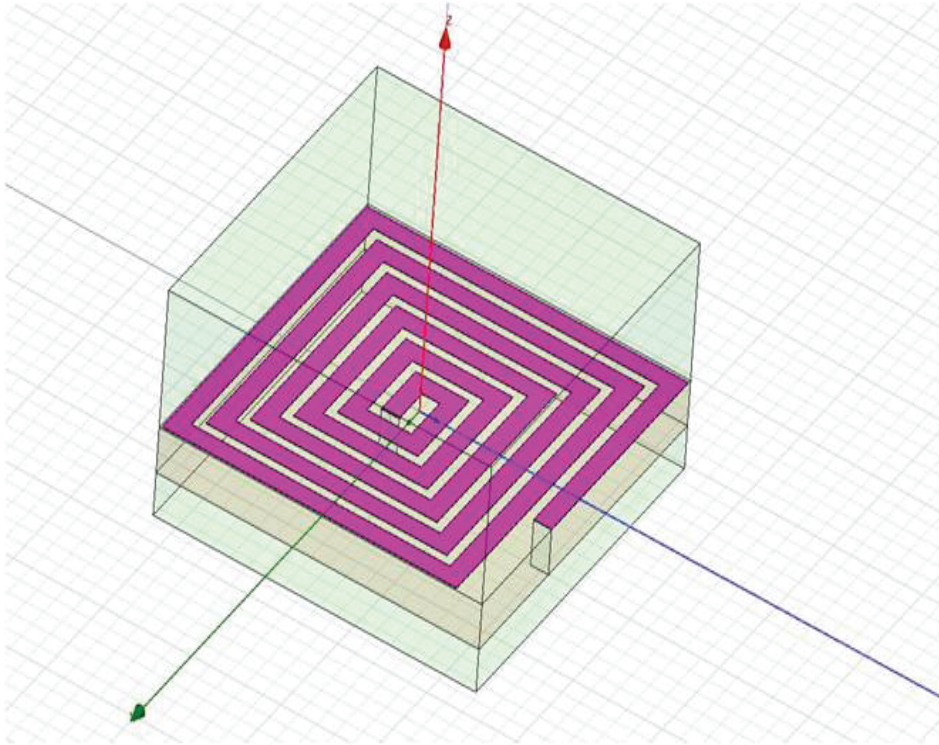


Figure 5.2: Printed Loop Antenna.

be $0.142 \mu\text{H}$ by using (5.3). There is a close agreement between the analytical and the simulated values.

The antenna gain was simulated on a sphere of radius 20 cm defined around the region of the antenna. Figs. 5.4(a) and 5.4(b) show a plot of the antenna gain in the elevation and the azimuthal planes respectively. It can be seen that the gain is constant around the antenna and confirms the omnidirectional pattern associated with such loop antennas.

5.2.2 Solenoidal Loop Antenna

The solenoidal loop antenna is characterised by its number of turns N , pitch p and the loop radius A . Its inductance is given by (5.4). Fig. 5.5 shows the simulation model setup in HFSS. The solenoid had 9 turns, a pitch of 1 mm and a radius of 5 mm. The wire was made of copper that had a radius of 0.355 mm. A radiation box measuring $(75 \times 75 \times 75)$ mm is drawn around the solenoidal loop antenna.

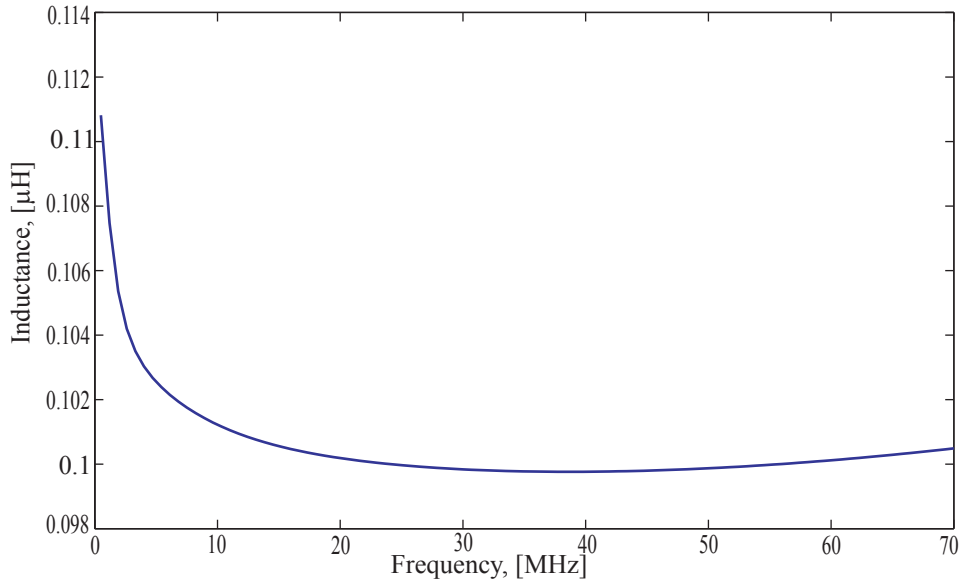


Figure 5.3: Inductance vs Frequency.

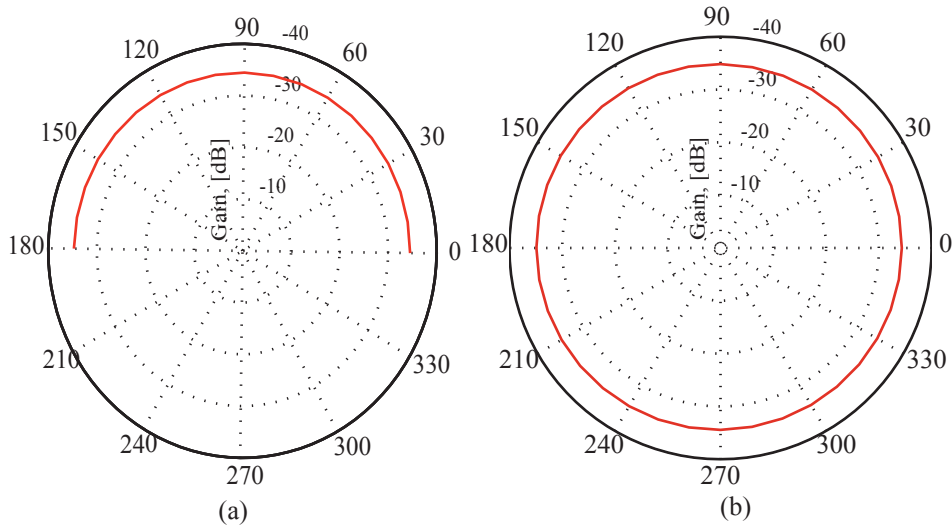


Figure 5.4: Simulated Gain Patterns of the Planar Square Loop Antenna:(a)Elevation Plane ($\phi = 90^\circ$) and (b)Azimuthal Plane ($\theta = 90^\circ$).

Both the ends of the solenoid were extended uniformly to define a single lumped port. The resistance was set to 50Ω as similar to the lumped port resistance of the planar square loop antenna. The electromagnetic field solution was obtained at a solution frequency of 1 MHz.

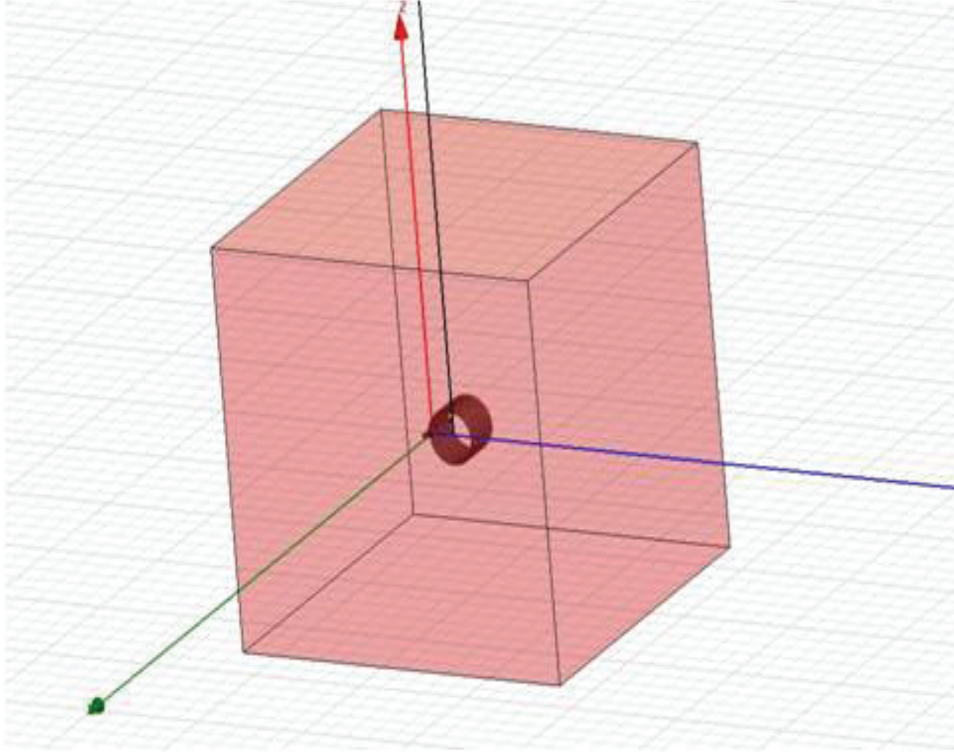


Figure 5.5: Solenoidal Loop Antenna.

$$L_{solenoid} = \frac{\mu_0 \mu_r N^2 A}{l} \quad (5.4)$$

Fig. 5.6 shows the variation of the inductance vs frequency for the solenoidal loop antenna. The value ranges between $0.525 \mu\text{H}$ and $0.54 \mu\text{H}$. Using (3.36), the value of the inductance was found to be $0.605 \mu\text{H}$.

A radiation sphere of radius 20cm was inscribed around the solenoidal loop antenna and the gain plots of the solenoidal antenna were plotted in the elevation and the azimuthal planes as shown in Figs. 5.7(a) and 5.7(b) respectively. The gain patterns are omnidirectional but the magnitude is not constant in every direction. A maximum change of 3-7 dB can be found in the gain patterns of both the elevation and azimuthal plane patterns. The magnitude of the gain is also larger than that of the printed planar square loop antenna.

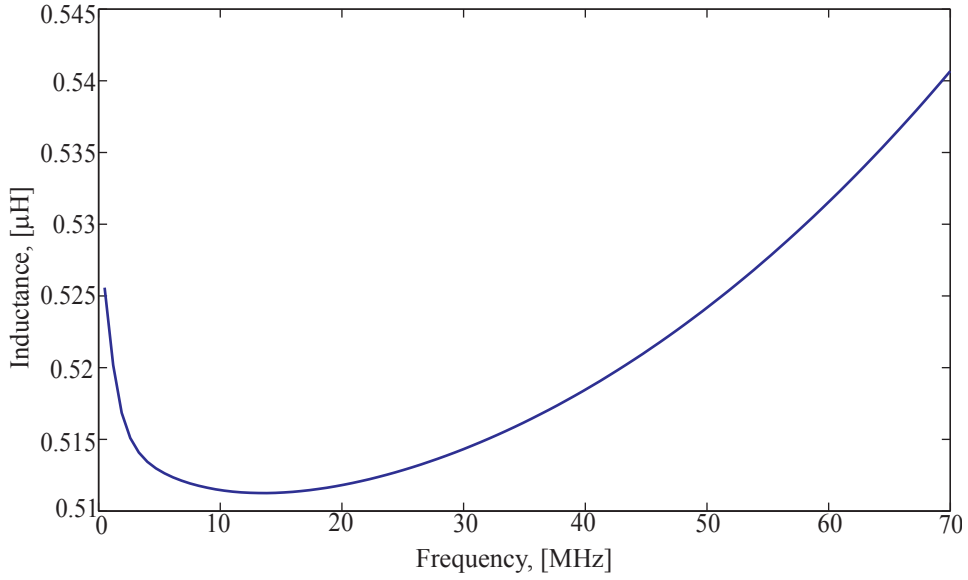


Figure 5.6: Inductance vs Frequency.

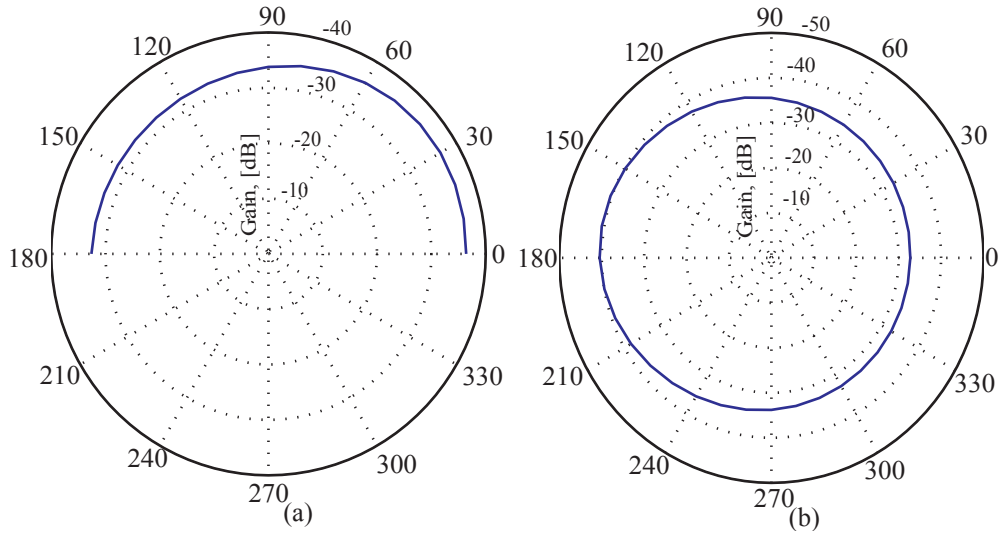


Figure 5.7: Simulated Gain Patterns of the Solenoidal Loop Antenna:(a)Elevation Plane ($\phi = 90^\circ$) and (b)Azimuthal Plane ($\theta = 90^\circ$).

5.2.3 Result Interpretation

The square loop antenna and the solenoidal loop antenna are both omnidirectional suggesting that they can be integrated with pill shaped implants. The location of

the pill will be unknown inside a human body and therefore the omnidirectionality of the implant antennas is one of the salient features that has to be fulfilled. The near-field baseband pulse radio communication system works on the principle of coupling of magnetic fields between the transmitting and receiving antennas. The reactive fields decay rapidly with distance as suggested by (3.41). Hence it becomes necessary that the radiating structure occupies a maximum volume within a confined space. It is clearly evident that the solenoidal loop antenna occupies much larger volume than a printed square loop antenna. Therefore a solenoidal loop antenna is magnetically larger than a planar square loop antenna. This claim can be supported by observing the gain of these antennas over a linear distance of 20 cm. Figs. 5.8(a) and 5.8(b) show the variation of gain with distance along the y axis for planar square and solenoidal loop antennas respectively. HFSS computes the field at a point and hence the distance has to be normalised by the number of points. For this particular case, the distance was normalised to 1000 points.

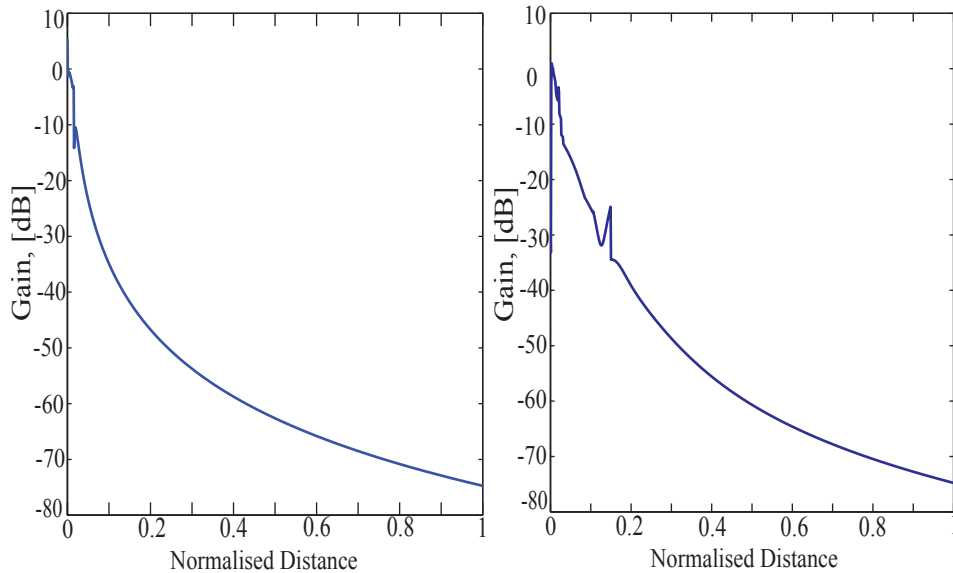


Figure 5.8: Gain vs Distance for Antennas:(a)Planar Square Loop and (b)Solenoidal Loop.

It can be seen that in either case the gain decreases with distance. But a careful observation reveals that the decay of a solenoidal loop antenna, as shown

in 5.8(b), is somewhat slower than the decay of a planar square loop antenna, as shown in 5.8(a). Hence the conclusion that a solenoidal loop antenna is a better choice for use in near-field baseband communication systems. The field is measured from the centre of the solenoidal loop antenna up to a distance of 20 cm. The glitch in Fig. 5.8 (b) occurs as this is the boundary where the coil is positioned.

5.3 Experimental Results

Experimental data is presented to validate the claims made in the previous discussions. A copper wire of cross-sectional area $0.397 (\mu\text{m})^2$ was wound in the form of a solenoid. The radiation efficiency of a single turn loop antenna is small and with the solenoidal shape, it has the advantage that the radiation resistance is increased by a factor of N^2 . The radiation resistance of a coil of N turns is equal to that of a single turn multiplied by N^2 . Table 5.2 lists the properties of the loop antenna. A similar coil acts as a receiving antenna. A dual display LCR meter, Megger B371, was used to measure the inductance of the coils. Air cored coils were chosen over ferromagnetic cored coils, as the magnetic flux tends to concentrate in a ferromagnetic object as shown in Fig. 5.9 [10].

No. of Turns	15
Wire radius	0.355 mm
Coil diameter	10 mm
Length	25 mm
Inductance	0.9uH

Table 5.2: Physical and Electrical characteristics of the loop antenna

The amplitude of the pulse was set to 3 V(p-p) and the width to 1 μs . The peak value and average value of the current entering the composite load consisting of an inductor and capacitor is experimentally determined to be 190 mA and 1.1 mA respectively. The energy per bit transmitted was calculated to be 6.6 nJ, which is smaller than the values of 1 μJ , 2.1 μJ and 2.2 μJ recorded for wireless transmission schemes using carrier frequencies of 32 MHz, 868 MHz and 868 MHz respectively [34]. The frequency domain analysis is carried out on

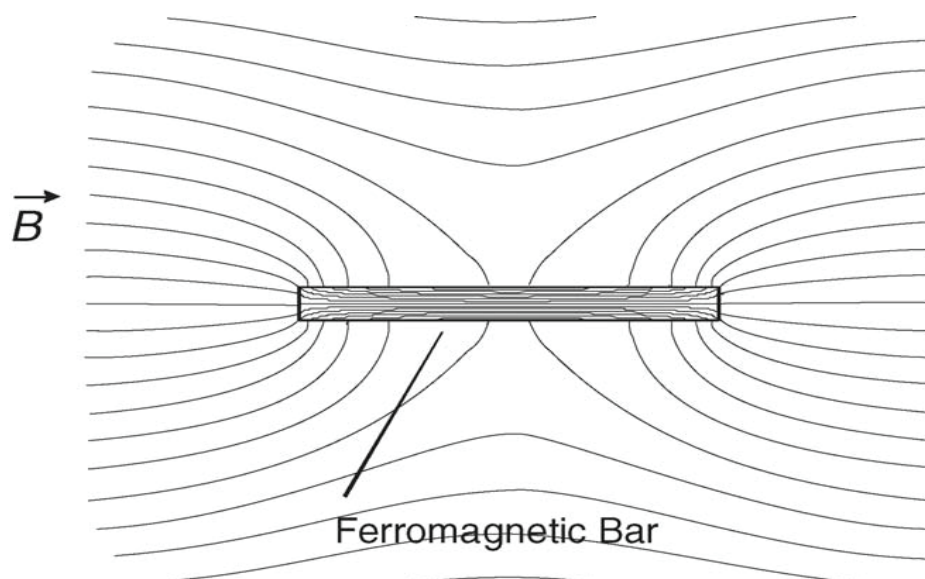


Figure 5.9: Magneto-concentration effect in a ferromagnetic bar. When a high permeability bar is placed in a homogeneous magnetic field parallel with the plate, the magnetic flux tends to concentrate in the bar [10].

the input signal of the bandpass filter and the transmitted signal. Figs. 5.10 and 5.11 show the magnitude spectrum of the input signal and the transmitted signal. The bandpass filter alters the magnitude and phase of the input signal. Changes mainly affect the lower end of the frequency spectrum of the input signal. Therefore the asymptotically decaying nature of the transmitted pulse. It can also be seen that the higher frequency components are not significantly attenuated as the lower frequency components by the solenoidal shaped antenna.

The energy transfer takes place through mutual coupling of fields between the transmitting coil and the receiving coil. Figs. 5.12(a) and 5.12(b) show the measured variation of the signal power ratio at the receiver with distance for a solenoidal coil of 15 turns and a square planar inductor of 6 turns respectively. The receiving coil was the same in both cases. It shows that larger the area of radiating element greater the range of the transmitter. The plots follow the same trend as the results of the simulation presented in Sec. 5.2.3.

To verify the all-round hemispherical coverage of the transmitting antenna, measurements were taken in the elevation and the azimuthal plane, from 0° to

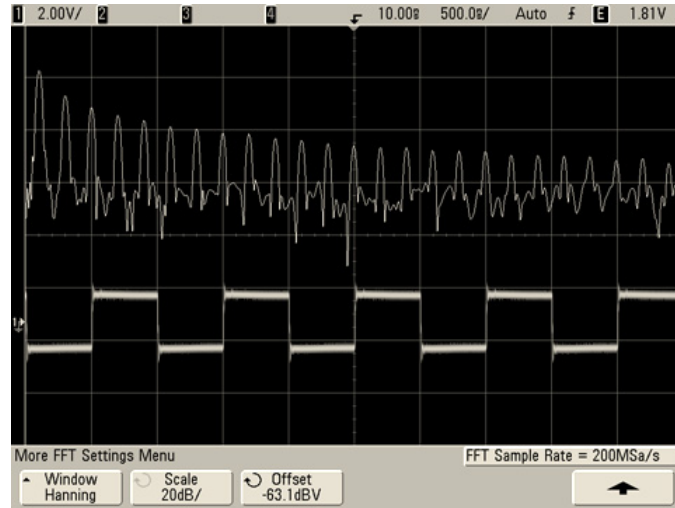


Figure 5.10: Measured time domain input signal and its spectrum in the frequency domain. Hanning window with 200 MSa/s sample rate was used to capture the input signal.



Figure 5.11: Measured time domain transmitted signal and its spectrum in the frequency domain. Hanning window with 200 MSa/s sample rate was used to capture the input signal.

180° , in steps of 30° and is shown in Fig. 5.13. In the elevation plane, ϕ was fixed at 90° and θ was varied. The axes of the transmitting and receiving coils were always maintained parallel to each other while inscribing a semi-circle around the transmitting antenna. In the azimuthal plane, θ was fixed at 90° and ϕ was varied.

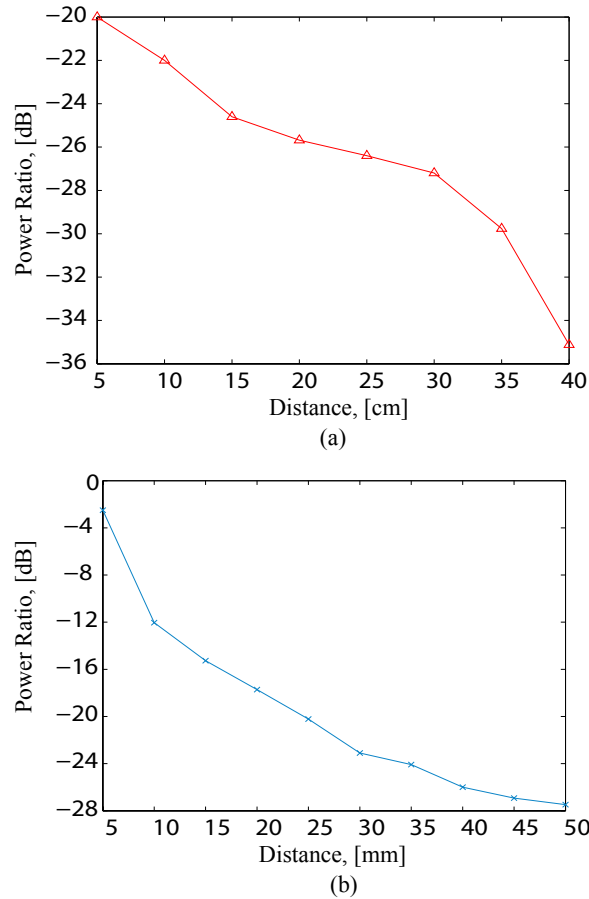


Figure 5.12: Measured relative signal strength as a function of distance for an (a) Air core solenoidal coil of 15 turns and (b) Square Planar Loop Antenna of 6 turns, with a receive antenna, which is a coil of 15 turns and radius 5 mm.

The receiving coil inscribed a semi-circle around the transmitting antenna with its axis tangential to the semi-circle. The measurements were made at axial distances of 5 cm and 10 cm in the elevation and azimuthal planes. The received signal was amplified and then captured on an oscilloscope. These measurements imply that the field is omnidirectional and depends upon the area of the transmitting coil. The signal power received can be made stronger by either increasing the voltage or the sensitivity of the receiver. These results help to conclude that solenoidal shaped antennas are an excellent choice.

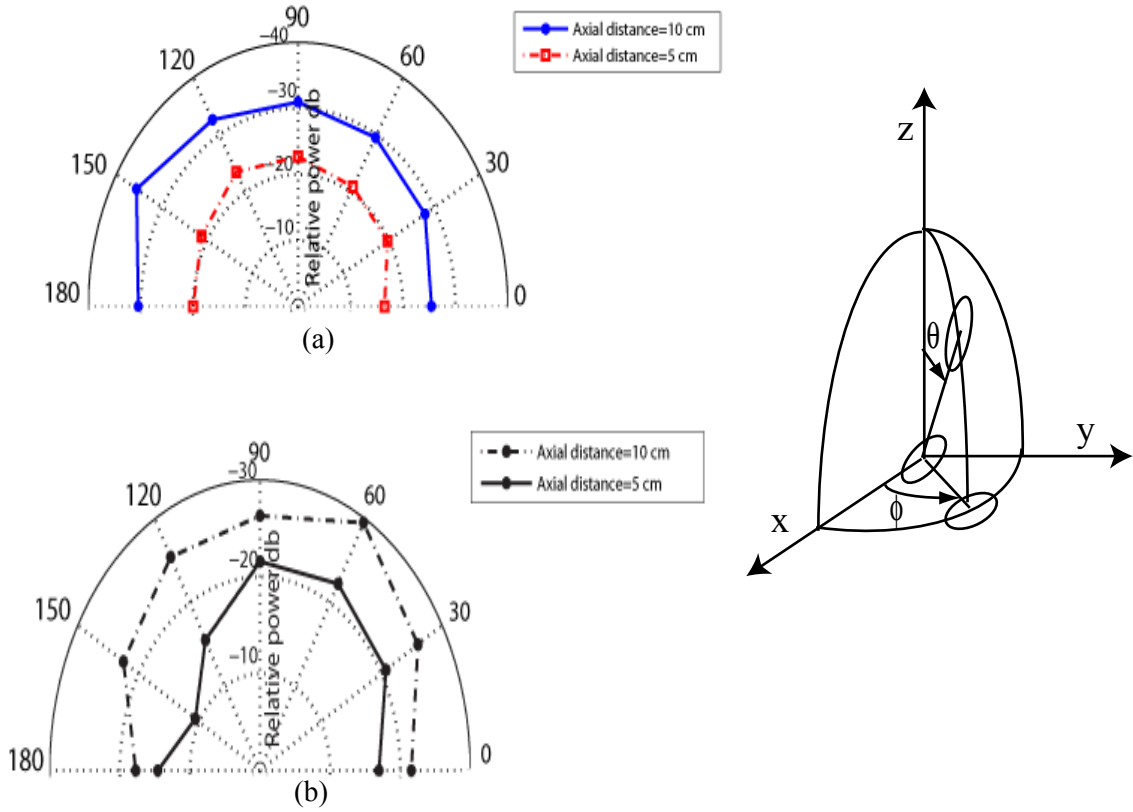


Figure 5.13: Schematic illustrating the experimental setup of the transmitting and receiving coil for measuring the received relative signal strength of the loop antenna in the elevation and azimuth plane. (a) Measured relative signal strength as a function of elevation angle θ and fixed azimuth angle ϕ . (b) Measured relative signal strength as a function of azimuth angle ϕ and fixed elevation angle θ . Measurements were taken at axial distances of 5 cm and 10 cm in both the cases.

5.4 Summary

This chapter discussed the antenna choices, namely planar loop and solenoidal loop antennas, that are available for use in implantable biomedical systems. HFSS, an electromagnetic field solver was used to analyse the electromagnetic fields around the antenna. It is based on the finite element method wherein a geometry is divided in several tetrahedra and the field is solved on its vertices. The gain pattern of the antennas was verified for their omnidirectionality and was

found that both the antennas are omnidirectional in nature. The solenoidal loop antenna had a slightly non-uniform gain pattern but the gain was larger than the gain of a planar square loop antenna. Experimental results also show that a solenoidal loop antenna appears magnetically larger and hence find suitability for use in the near-field baseband pulse radio communication presented in this work. The next chapter discusses different encoding schemes that can be employed in this particular communication scheme. A microcontroller produces the required pulses and a digital signal processor decodes the data at the receiver.

CHAPTER 6

PULSE RADIO COMMUNICATION

Contents

6.1	Introduction	111
6.2	Digital Communication	111
6.2.1	PCM Waveforms	112
6.2.2	Pulse Interval Modulation	116
6.3	Receiver Design	120
6.3.1	Digital Filter	120
6.3.2	Filter Design	122
6.4	Summary	128

6.1 Introduction

The previous chapter discussed two types of magnetic antennas, namely solenoidal and printed spiral antennas, that can be used in the near-field baseband pulse radio communication. The antennas were analysed electromagnetically to determine the radiation patterns and also the variation of the gain with distance. It was found that the solenoidal antenna is more suited for this particular application. This chapter deals with the pulse encoding schemes that is possible with the near-field baseband pulse radio communication. A conceivable implementation of a receiver algorithm is also presented in this chapter.

6.2 Digital Communication

Digital baseband signals are obtained by quantising the PAM signals into a digital word and belong to a class called pulse code modulated signals. The signal obtained from a sensor in an implantable device is sampled and quantised into a k -bit word. For baseband transmission the codeword bits will have to be transformed to pulse waveforms [43]. A digital word is impractical and has to be physically represented to be able to transmit the information through a channel. The way to achieve the above objective is to represent the digital word with electrical pulses. A representation of a digital code word and its electrical equivalent is shown in Fig. 6.1. Each codeword occupies a time slot and is a 4-bit representation of each quantised sample. In Fig. 6.1 (b), each binary one is represented by a pulse and each binary zero is simply represented by the absence of a pulse. The electrical pulses are rectangular/square in shape and can be easily generated that can be ultimately used to transmit information. Digital words can also be represented by transitions between two levels as shown in Fig. 6.1 (c). When the waveform occupies the upper positive voltage level, it represents a binary one and when it occupies the lower negative voltage level, it represents a binary zero.

The manner in which a digital word is represented leads to a form of modulation known as the pulse-code modulation (PCM) and the resulting waveform is known as a PCM waveform. An understanding of this representation is important for an attempt to transmit the pulses directly from a magnetic loop antenna. The

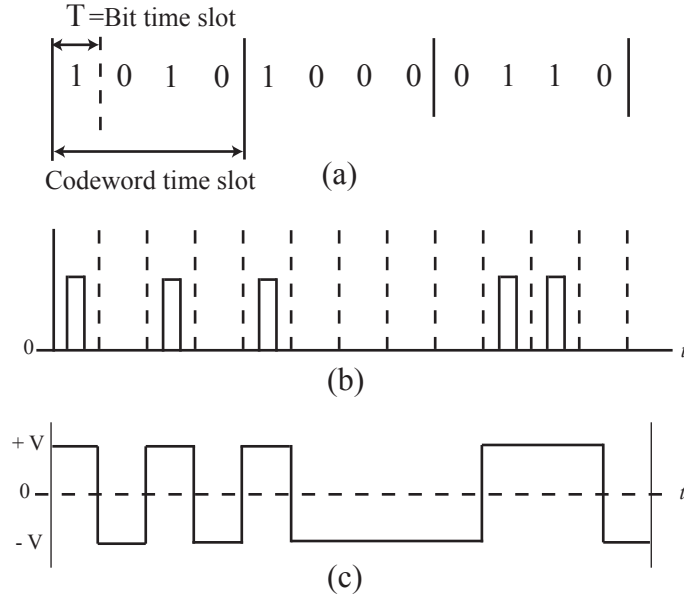


Figure 6.1: Binary Digit Waveform Representation:(a)PCM Sequence; (b)Pulse Representation of the PCM Word and (c)Pulse-Waveform.

following section will discuss the known PCM waveform types and then chooses that are relevant to the near-field baseband pulse radio communication.

6.2.1 PCM Waveforms

The PCM waveforms can be broadly classified into four types. They are:

1. Nonreturn-to-zero (NRZ)
2. Return-to-zero (RZ)
3. Phase encoded
4. Multilevel binary

The representation of the waveforms hold key for their direct emanation from the loop antenna. In a near-field baseband pulse radio communication the waveforms that are emanated should be compatible with the characteristics of the

channel. The magnetic antennas behave as pulse shaping filters and any change that affects the pulse should not make the entire communication scheme unworthy. Hence a discussion of the different PCM codes available becomes necessary.

The NRZ is the most commonly used PCM waveform. NRZ-M (M for mark) is widely used in digital logic circuits. A binary one, or mark, is represented by a change in the voltage level and the zero, or space, is represented by no change in level. This is also often referred to as differential encoding.

In RZ coding, a one is represented by the presence of a pulse and is usually half-bit wide. A zero is represented by the absence of a pulse. The bi-phase coded pulses, bi- ϕ -L (better known as Manchester coding) has its one represented by a half-bit wide pulse positioned during the first half of the bit interval and a zero being represented by a half-bit wide pulse positioned during the second half of the bit interval. With this particular scheme, there is always the presence of a pulse for either one or zero. The transition from low to high and high to low determine whether the transmitted pulse was one or zero.

Many binary waveforms use three levels, instead of two to represent the binary one and zero. Bipolar RZ and RZ-AMI belong to this group. In this particular research work, as a microcontroller generates the required data, the pulses are represented by two levels. Therefore, bipolar RZ and RZ-AMI signals are not considered for direct transmission from the magnetic antenna.

Fig. 6.2 shows the binary representation of the data sequence 10110001 in NRZ-M, RZ and Manchester format. A magnetic antenna should be able to transmit this information intelligibly. As explained in Chapter 4, the pulses will undergo distortion in a controlled manner.

Fig. 6.3 (a), (b) and (c) show the pulse shapes at the antenna terminals for NRZ, RZ and Manchester encoded pulses respectively. It is obvious that RZ and NRZ pulses suffer from the problems of synchronisation. The antenna retains the rising and falling edges from these pulses. But no information regarding the transmission of zero can be obtained at the receiver. On the other hand a Manchester encoded information can be effectively radiated from the magnetic antenna. A careful observation of the transmitted waveform reveals that once the first trailing edge is detected, any negative going spike in an one-bit interval confirms the presence of one and a positive going spike will detect the presence

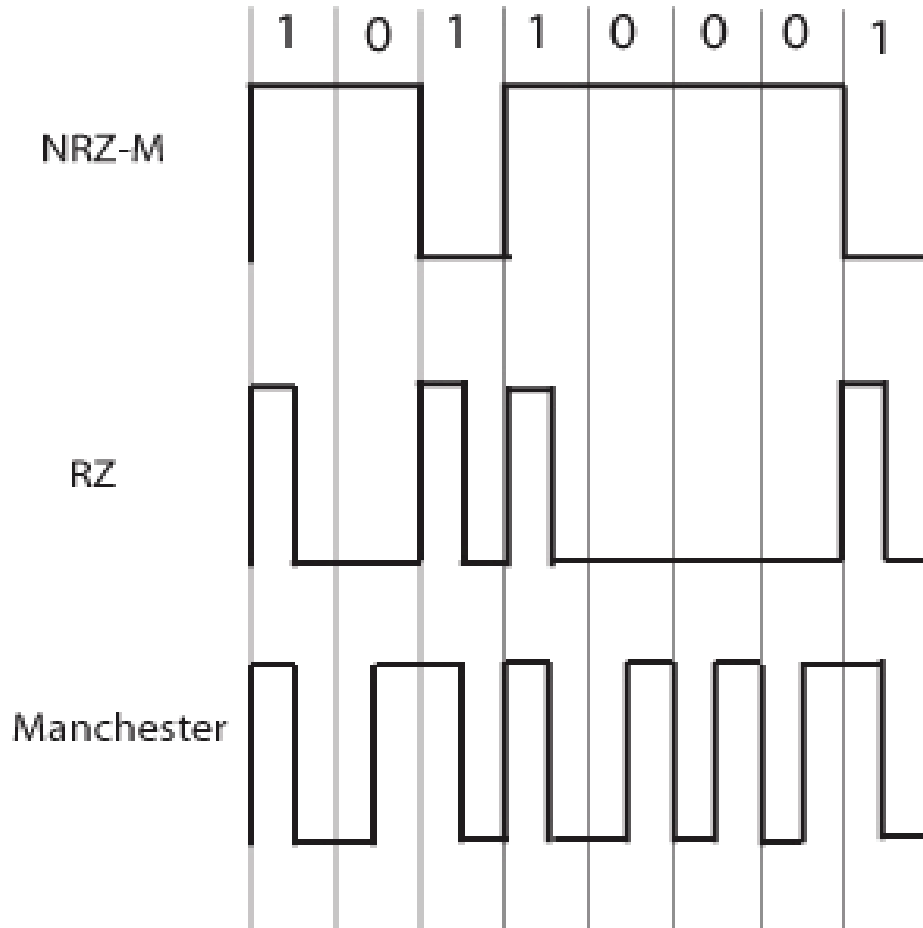
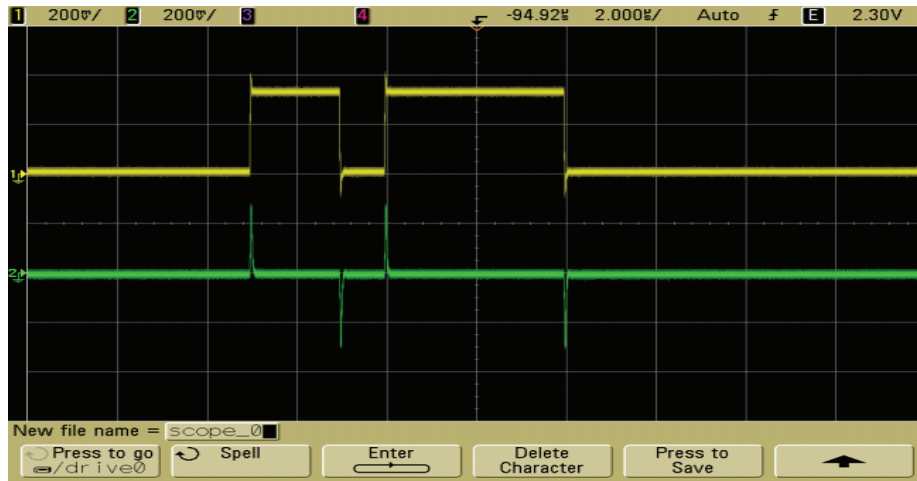


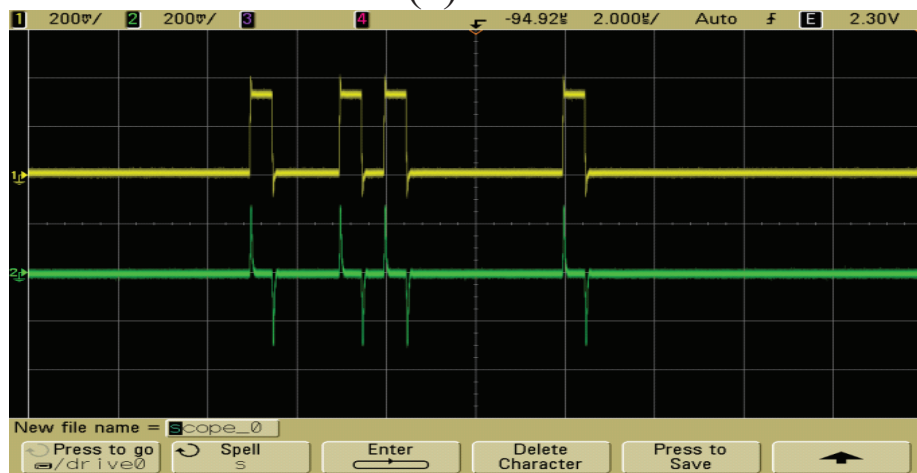
Figure 6.2: Binary Digit Waveform Representation of 10110001.

of zero in the bit pattern. Hence a sync or reference pulse can confirm the start of transmission and the trailing edge of this pulse can be taken as a reference for determining the other bit patterns.

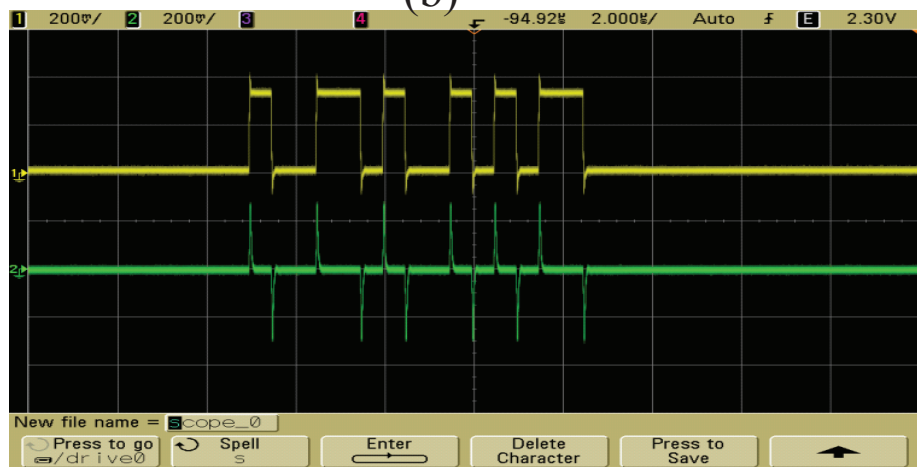
The Manchester waveform suffers from certain disadvantages. It requires twice the bandwidth required by RZ and NRZ waveforms. The microcontroller has to generate pulse for every bit irrespective of it being one or zero. The advantage that the Manchester coding offers with the ease of identification at the receiver is valuable. This arises from the inherent synchronising or clocking feature of the Manchester encoded waveform. A transition in the middle of every bit interval whether it being a one or a zero provides the clocking signal. It can be concluded



(a)



(b)



(c)

Figure 6.3: Binary Digit Waveform Representation of 10110001:(a)NRZ, (b)RZ and (c)Manchester Code.

that the Manchester coded pulses are best suited for transmission from a near-field baseband pulse antenna. The microcontroller can also be used to generate bipolar pulses to represent binary data “1” or “0”. The loop antenna can be connected between two output pins namely, out1 and out2, of the microcontroller and during the transmission of “1” the out1 is driven by a pulse and the out2 is grounded. Similarly during the transmission of “0” the out2 is driven by a pulse while out1 is grounded. The advantage of bipolar signalling is that there is no dc component and therefore the average loss of the whole transmission scheme can be reduced.

6.2.2 Pulse Interval Modulation

A near-field baseband pulse radio communication requires a fast, low power and reliable wireless modulation scheme that can be implemented with a simple, minimum and low-cost hardware. Mingsong *et al.*, have proposed a wireless modulation scheme called the pulse interval modulation (PIM) for laser communication between two communication nodes [121]. The authors claim that the pulse interval modulation effectively improves the recovery of pulses after demodulation. This is because of the improved synchronisation capabilities. The method also improves the coding efficiency and can be implemented using a microcontroller. The PIM is considered to be an improved version of PPM. A k -bit source $P = (P_1, \dots, P_k) \in \{0, 1\}^k$ is modulated with a M -ary PPM, $M = 2^k$. This yields a pulse modulated signal $A = (0, \dots, 0, 1, 0, \dots, 0) \in \{0, 1\}^M$ which will contain a one (or a pulse) in the position indicated by the binary representation of P . The PIM is shown in Fig. 6.4.

A PPM signal has a duty cycle of $1/M$. A frame in a PPM signal is divided into M slots and each slot has a width of τ . The position of a pulse in a time slot represents the corresponding symbol. The PIM involves coding the data sequence such that a symbol is represented by the time interval between the present and the previous pulse. The difference between a PPM and PIM coding is that the frame width is not constant with the latter. It varies according to the data modulated. The focus of this work is to encode a digital stream of information using pulse interval modulation. A microcontroller is used to generate the pulse stream. The

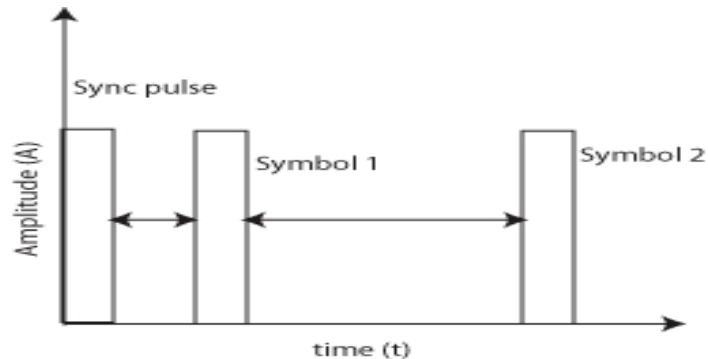


Figure 6.4: Pulse Interval Modulation.

flow chart shown in Fig. 6.5 describes the algorithm to generate the PIM pulse. The PIM encodes symbols unlike RZ, NRZ and Manchester encoding schemes. Therefore PIM increases the throughput rate of the near-field baseband wireless communication system. Throughput rate is defined as the rate at which the data can be transmitted between a transmitter and a receiver.

A sync pulse signals the start of the transmission. A PIC18F4550 microcontroller has been programmed to generate the PIM pulses. The program is written in the assembly language. The digital data is stored in the memory registers of the microcontroller. Each register is 8 bit wide and hence a symbol is made up of 8 bits of information. The microcontroller calculates the symbol value of the register and generates a pulse depending upon the delay associated with it. The timing loop is also implemented in software and this allows us to control the width of the pulse. This is essential as the pulse is going to be transmitted directly from the magnetic antenna. The shorter the pulse the higher the data rate and its decay is controlled by the lumped element values of the loop antenna. The pic18F4450 microcontroller is accompanied by MPLAB integrated development environment software that runs on a computer. It is useful for developing applications for Microchip microcontrollers and programming them too. The main components that have been used to develop codes for this particular project are:

- Project Manager

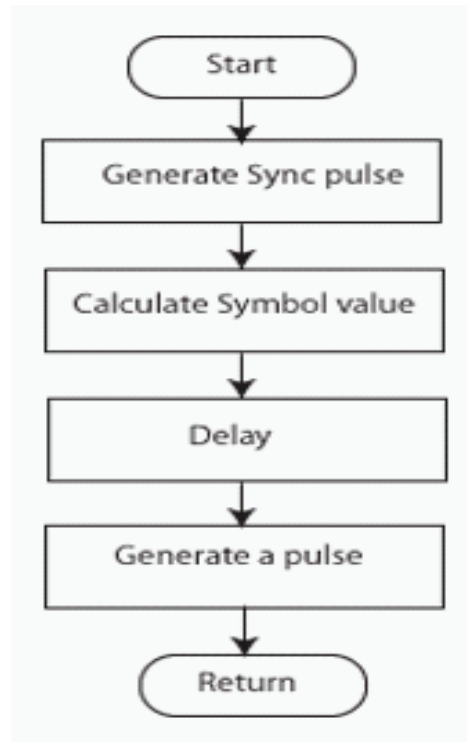


Figure 6.5: Flow Chart for implementing Pulse Interval Modulation.

- Editor
- Assembler/Linker
- Debugger

The project manager provides coordination between the integrated development environment (IDE) and the language tools. The editor is like any other text editor and it also serves as a debugger window. The assembler assembles a single file but can also be used with the linker to link separate source files, libraries and recompiled objects. The linker places the compiled code into memory areas of the target microcontroller. The debugger permits breakpoints, single stepping and watch windows.

The microcontroller was programmed to send four bytes (32 bits) of information. However it can be easily re-programmed to send any number of bytes. The code was optimised for a desirable pulse width and time-interval between

the pulses. A sync pulse was first generated that signals the start of the pulse transmission. A delay in the sync pulse is attributed to the fact that the microcontroller has to load the data into the working registers before setting its output digital port to transmit the pulse. The subsequent pulses occupy different positions in time depending upon their symbol value. The width of the pulse is 4 cycles. An instruction cycle is completed in time $t = 4/F_{\text{osc}}$, where F_{osc} is the frequency of the oscillator. It is 48 MHz for this particular case. Fig. 6.6 shows four bytes of data, namely 0x03, 0x04, 0x05 and 0x06, encoded in the PIM format. The sync pulse is the reference from which the interval between the various pulses is measured.

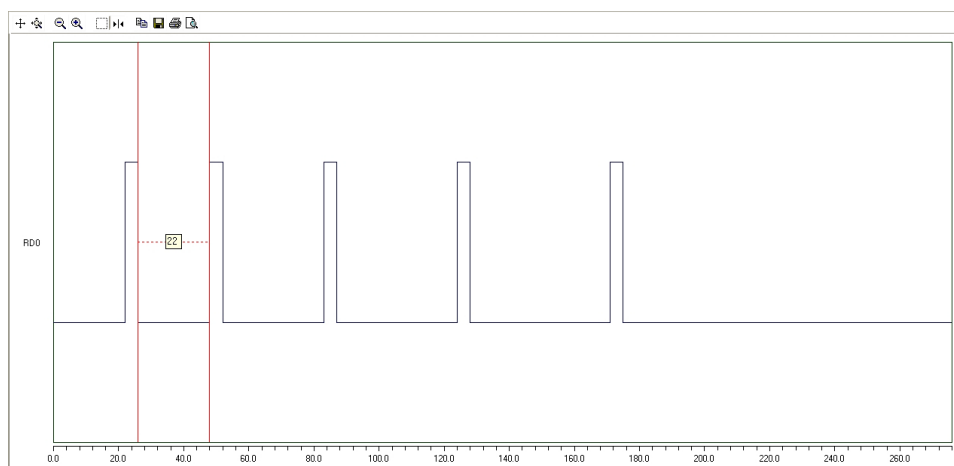


Figure 6.6: Pulse Interval Modulated Data Pattern: 0x03, 0x04, 0x05 and 0x06.

The ultimate motive of this research is to prove the practicality of being able to transmit the digital pulses efficiently from a magnetic loop antenna. The electromagnetic design of a magnetic loop antenna and the way it would alter the pulse shape was studied in detail to arrive at the conclusion that it is indeed possible to achieve a simple yet effective transmission scheme for biomedical implants. The receiving loop antenna should be able to receive very short transmitted pulses and hence its study has to be carried out in a systematic manner. Chapter 7 details the design principles that help designing the receiving loop antennas for the near-field baseband pulse radio communication. However the next section attempts to consider the processing of the received signal by designing a digital filter. It is primary in its approach and has a potential for a further research

study.

6.3 Receiver Design

The pulse transmitted by the loop antenna is received by a similar loop antenna at the receiver. An analogue comparator at the receiver will help in decoding the data bit transmitted. The comparator requires two threshold values, V_{TH} and V_{TL} , to maintain the output in a high or low state. When the input signal is greater than V_{TH} the output becomes high and when greater than V_{TL} the output becomes low. The amplitude of the received signal varies rapidly with distance and therefore specifying a fixed threshold value is not convenient. Digital signal processing will help to process the received signal and further signal processing can be done on a personal computer to decode the original symbol waveform. This necessitates the design of a digital filter that can be implemented on a digital signal processor. The analogue input signal from the magnetic loop antenna, is filtered before it is applied to the analogue-to-digital converter (ADC). An opamp provides the appropriate gain and offset to match the signal to the input range of the ADC. The output of the ADC is then processed digitally by an appropriate digital signal processor (DSP). DSPs are processors that are optimised to perform fast repetitive arithmetic, as required in digital filters or fast Fourier transforms (FFT). Here digital filtering is accomplished by using TMS320F2812 DSP from Texas instruments.

6.3.1 Digital Filter

Digital filters are neither new nor difficult. They are based on simple operations of multiplication and addition. Various methods exist to design digital filters and one common approach is to use the analogue filter approximation functions. The features that make digital filter attractive are:

1. Digital filters can be implemented with a software running on a general purpose computer. Hence easy to build and test the performance of the filter.

2. Digital filters are based solely on the arithmetic operations of addition and multiplication. Therefore they do not change with time or temperature.
3. Easy to understand and modify.

Digital filters can be restricted to two major categories: Non-recursive and recursive. A non-recursive filter generates its output by simply weighting the inputs by constants and then summing the weighted inputs. The constants are called the coefficients and they determine the filter. A design of a filter is synonymous with the computation of the values of the coefficients. The non-recursive filter can be described by the following equation:

$$y_k = c_m x_{k-m} + c_{m-1} x_{k-m+1} + \dots + c_0 x_k + \dots + c_{-m} x_{k+m} \quad (6.1)$$

$$y_k = \sum c_i x_{k-i} \quad (6.2)$$

where

$$i = -m, -m + 1, \dots, m - 1, m.$$

The above filter computes the output, y_k , from the current input, x_k , and the m inputs that preceded x_k , $x_{k-1} \dots x_{k-m}$, and the m inputs that follow x_k , $x_{k+1} \dots x_{k+m}$. The present output is thus a sum of the current input and its m preceding and succeeding inputs. The inputs do not contribute equally to the output as the contribution is controlled by the coefficient that acts as the multiplier. If the coefficient is large the particular data element can dramatically affect the output. If the coefficient is small the data element has a proportionally small effect on the filter's output.

A recursive filter is defined as a filter whose output is a function of both the inputs and past outputs. It can be defined by (6.3).

$$y_k = \sum c_i x_{k-i} + \sum d_j y_{k-j} \quad (6.3)$$

where

$$i = -m, -m + 1, \dots, m - 1, m \text{ and } j = 1, 2, \dots, n.$$

The second sum in (6.3) is called the recursive portion of the filter. The recursive coefficients are denoted as j and they are used to weigh the past outputs. When all the coefficients are zero then this becomes a non-recursive filter. Therefore non-recursive filter can be treated as a special case of a recursive filter. At the start of the computation it is assumed that the outputs for negative indices are zero before the input data starts affecting the output. That is, the inputs and outputs are assumed to be zero for negative indices. The computation of the outputs begin when the first nonzero input enters the nonrecursive portion of the filter. After that the outputs are sequentially computed and used to calculate the successive filter outputs.

6.3.2 Filter Design

A magnetic loop antenna is said to differentiate the pulse that is being transmitted from it. Hence the pulse at the receiver needs to be integrated to recover the original rectangular pulse. A perfect integrator can be represented by (6.4). The frequency response of an integrator can thus be described by (6.5).

$$y(t) = \int_{-\infty}^t x(\tau) d\tau \quad (6.4)$$

$$H_{\text{integrator}}(\omega) = \frac{1}{j\omega} \quad (6.5)$$

A differentiator produces an output that is the differential of its input as shown in (6.6). The frequency response is given by (6.7).

$$y(t) = \frac{dx(t)}{dt} \quad (6.6)$$

$$H_{\text{diff}}(\omega) = j\omega \quad (6.7)$$

It can be seen from (6.5) and (6.7) that the frequency responses are reciprocal of each other. In the s -domain $j\omega$ can be replaced by s . This discussion helps in making the conclusion that once a transfer function of an integrator is known, the transfer function of the differentiator is just the inverse and vice-versa. The

analogue transfer function of the transmitter in the s-domain, given by (4.17), differentiates the pulse applied at its terminals. Hence a reciprocal of the above transfer function will represent a filter that can integrate the pulse. The reciprocal of (4.17) is given by (6.8).

$$R(s) = \frac{s^2 + s\left(\frac{1}{RC}\right) + \left(\frac{1}{LC}\right)}{s\left(\frac{1}{RC}\right)} \quad (6.8)$$

An approximation of the above equation will lead to a digital filter. The approach taken in this work can be summarised as beginning the design with a good analogue transfer function and then approximating it with a digital filter. The bilinear transformation provides the user with a simple technique for approximating analogue filters with digital filters. The bilinear transform design technique can be summarised as below:

1. An analogue transfer function that has the desired characteristics has to be found first.
2. Sampling rate of the digital filter T , has to be selected.
3. The s in the analogue transfer function has to be substituted by (6.9).
4. Compute the z-transform by solving the transfer function after substitution.
5. Realise the digital filter from its z-transform i.e., identify the coefficients from the pole and zero locations.

$$s = \frac{2}{T} \frac{1 - z^{-1}}{1 + z^{-1}} \quad (6.9)$$

The derivatives of the outputs are fed back to form the output and hence a digital filter can be unstable. This must be avoided when using an analogue filter as a basis for digital filters. An analogue filter is said to be stable if all bounded inputs generate bounded outputs and unstable if any bounded input causes an infinite output. This bounded-input, bounded-output is really restriction on the filter's impulse response and a filter is stable if and only if its impulse response goes to zero with increasing time. If the impulse response increases with time (known as "blowing up") then the filter becomes unstable.

A filter's stability or the lack of it, can be determined by the filter's pole locations. A digital filter is stable if its pole lie inside the unit circle [122]. In other words the magnitude of the pole must be less than or equal to 1. Matlabs FDA tool can be used to design the desired digital filter. The analogue transfer function was approximated to compute the z-transform representation of the digital filter. The digital filter has two zeroes at $z=-0.11$ and $z=-0.99$, and two poles at $z=1$. The analogue signal was sampled at 2 MHz and this was selected as the pulse had a width of $1 \mu\text{s}$. Fig. 6.7 shows the pole zero plot of the digital filter designed to reconstruct the received pulse. The zeroes are marked by "O" and the poles are marked by "X".

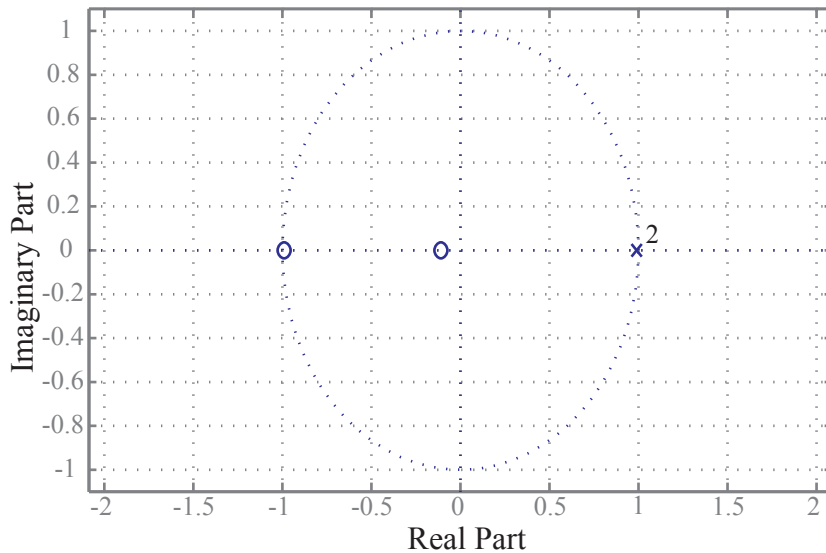


Figure 6.7: Pole Zero Plot of the Digital Filter used to reconstruct the transmitted pulse.

Fig. 6.8 represent the magnitude and phase response of the digital filter that is designed to reconstruct the very short transmitted pulse. The poles located on the real-axis make the magnitude to be larger at low frequencies and the zeroes in the left-half of the pole-zero plot are responsible for the stop band at higher frequencies. The filter basically acts as a low-pass filter and the impulse and step responses are shown in Figs. 6.9 and 6.10 respectively. The magnitude response is very similar to the response of an integrator based on Simpson's rule wherein the

magnitude decreases for increasing frequencies. Thus this work aims to achieve the filtering of the received waveform with a new approach to the filter design.

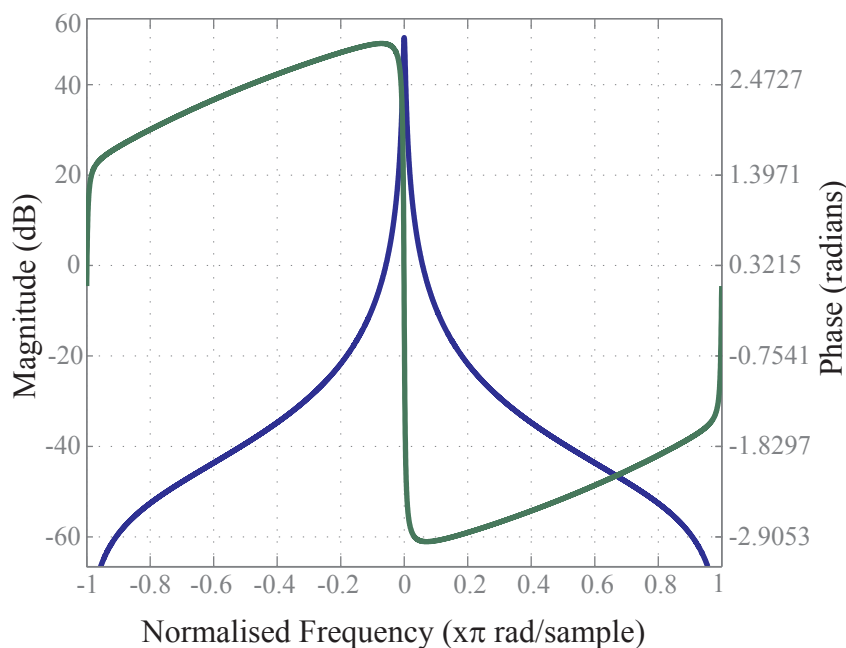


Figure 6.8: Magnitude and phase response of the digital filter, with two poles at 1; zeroes at -0.11 and -0.99 .

The coefficients of the digital filter were determined with the help of the IIR filter module of the Texas Instruments TMSF2812. A 2-bit Manchester code waveform was emanated from the loop antenna. The pulse underwent distortion and was received by a 10 turn solenoidal loop antenna. A sync pulse marks the beginning of the transmission of bits [1 1]. It was digitised by a 12-bit ADC which had a sampling frequency of 2 MHz. Fig. 6.11 shows the plot of the signal before and after reconstruction by the digital filter for which the coefficients were determined as explained in Sec. 6.3.1. It is worth noting that the filter has considerably filtered the noise and the peaks are clearly visible. The flat portions of the peak represent the integration of the received pulse by the digital filter.

A further processing of the filtered signal will help identifying the bits that are being transmitted. The Manchester coded waveform carries the clock information and this aids in identifying the bits transmitted. The advantage of the near-field

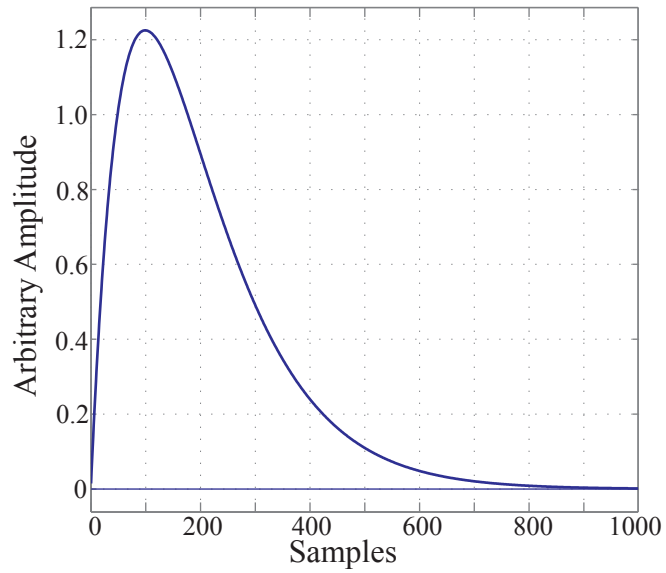


Figure 6.9: Impulse response of the digital filter.

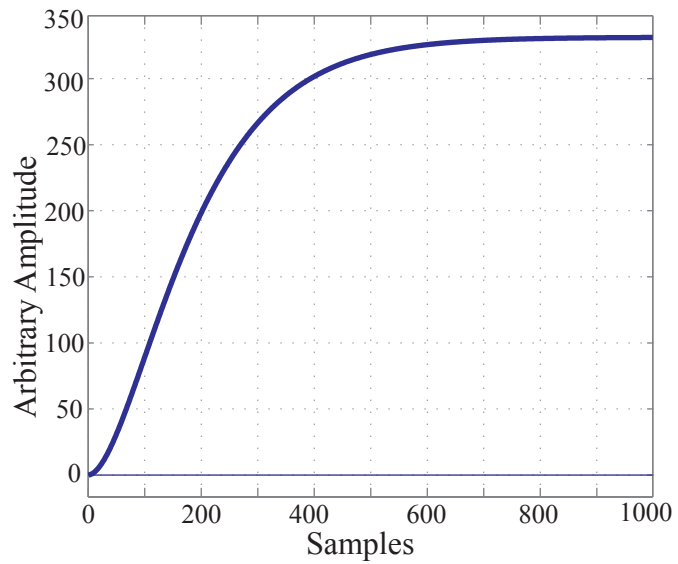


Figure 6.10: Step response of the digital filter.

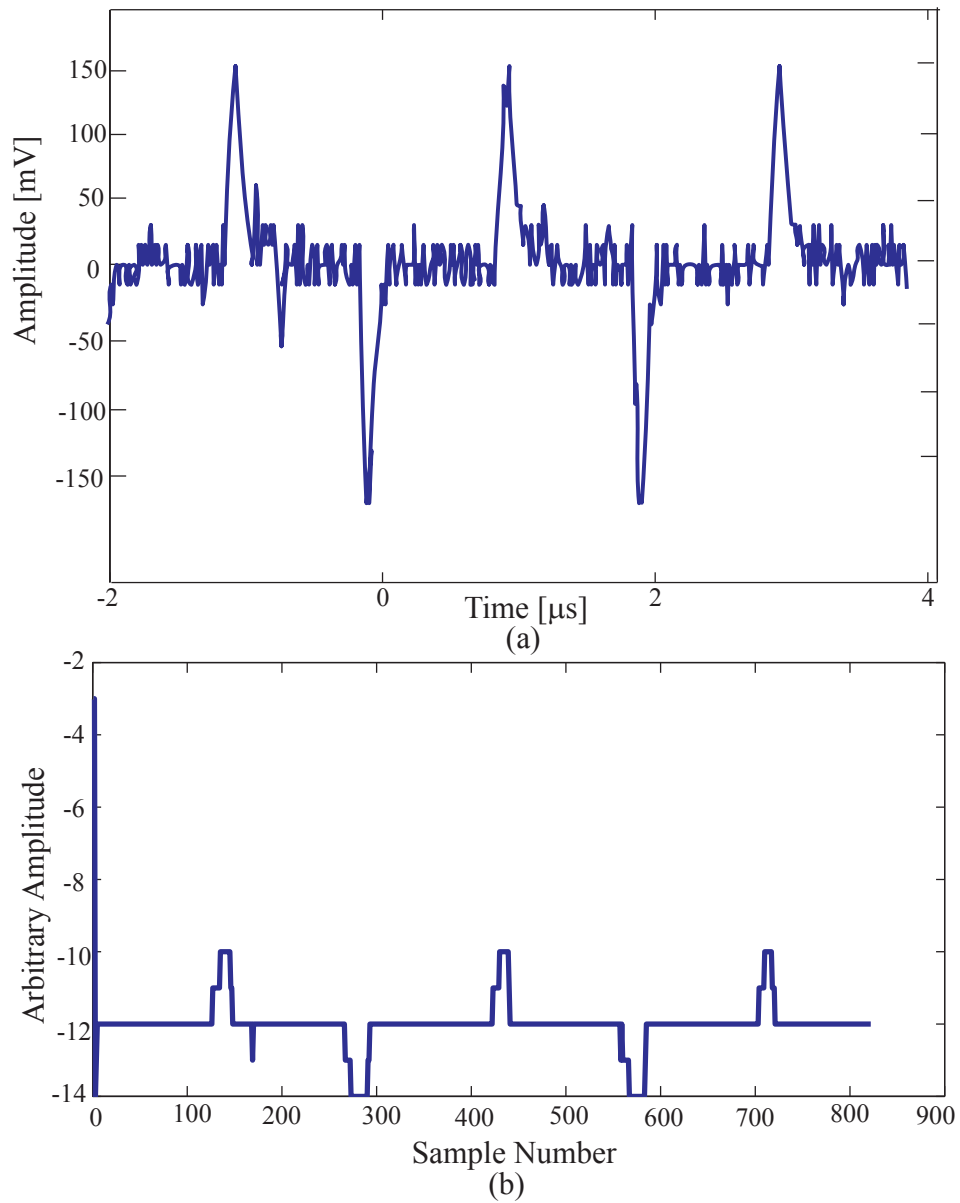


Figure 6.11: (a) Waveform received by the loop antenna that acts as input to the digital filter; and (b) Reconstructed waveform at the output of the digital filter.

baseband communication is that it retains the rising and the trailing edges of each pulse. The algorithm that has been developed looks for the sync pulse and sets a counter on the negative peak of the sync pulse. The counter counts the number of samples and checks for either a positive or negative peak, every one-bit interval. If a negative peak is detected then the algorithm concludes that the transmitted bit was a 1. If a positive peak is detected then the transmitted bit was 0. The discussion presented in this section will help in concluding that receiver algorithms can be developed for the efficient demodulation of the transmitted information. The algorithm provided satisfactory results in the current experiment which had a noise floor less than 40 mV (or an SNR of 25.46 dB). The performance of the algorithm in highly noisy environments was not tested and therefore high degree of confidence is not yet established in this regard. More robust filtering algorithms like the matched filters and transversal equalisers may be required for efficient decoding of the received pulses in more noisy environments [43]. All the codes for this chapter can be found in Appendices A, B and C.

6.4 Summary

This chapter discussed the various digital pulse coding schemes that can be applied to the near-field baseband pulse radio communication. A microcontroller was used to generate the pulse coded waveforms. Pulse interval modulation provides high throughput and can be easily implemented on a microcontroller. Digital filtering algorithms were developed for processing the received signal. It has scope for further development and only preliminary results are presented. The next chapter discusses the design of a loop antenna to receive very short pulses. It analyses different antenna loading configurations and suggests a design strategy that can be employed to receive the near-field baseband pulses.

CHAPTER 7

ANTENNA IN RECEIVING MODE

Contents

7.1	Introduction	130
7.2	Near-Field Magnetic Communication	130
7.3	Loop Antenna Equivalent Circuit	131
7.3.1	Near-field Transmission Model	134
7.3.2	System Design	139
7.3.3	Simulation Parameters	141
7.4	Experimental Results	146
7.4.1	Salt Water Experiment	149
7.5	Summary	151

7.1 Introduction

The previous chapter discussed several coding schemes for use in a near-field baseband communication system. A microcontroller was used to generate the waveforms that represent a particular coding scheme. At the receiver, a filtering algorithm was developed for the signal reconstruction and implemented on a digital signal processor. In this chapter, a detail design procedure is laid out for receiving wideband pulses emanated by a magnetic antenna. An analytical treatment, accompanied by simulation and experimental results, is carried out.

7.2 Near-Field Magnetic Communication

Near-Field pulse radio communication for implants was earlier proposed in Chapter 4. In this scheme, information encoded pulses were radiated directly from a transmitting loop antenna without any use of traditional modulation schemes. It was evident from the design technique that pulse shapes are instrumental in conveying the necessary information. An exemplary feature of sending pulses using loop antennas at the transmitter is in contrast with the wireless power-delivery systems and radio frequency identification devices (RFID's), wherein a loop antenna transmits signal on a single-frequency or over a very narrow frequency band [123]. Simultaneous exchange of power and data occur on forward and reverse links respectively. In scenarios where only data is transmitted, a loop antenna is resonated with a suitable capacitance to convey information over a very narrow bandwidth. UWB is a system that remotely bears a resemblance to the near-field pulse radio system. UWB systems send and receive pulses, but in the far-field of an antenna. Recently UWB has been gaining attention for unique system characteristics of low-power, easy transmitter implementation, etc., as explained in Chapter 2. The pulses are either Gaussian or Gaussian-like whose widths are in the sub-nanosecond range [124]. As a result of very narrow pulse widths UWB systems have a very wide operational bandwidth. Electric antennas like spiral or patch antennas are used to radiate pulses in the far-field. UWB systems are also faced with the challenge of maintaining the pulse shape at the receiving antenna. Two approaches have been generally used to tackle such a problem. One approach

is to use large size antennas and the other being the use of broadband small size antennas. However the latter suffers from the problem of poor sensitivity. It has been suggested that a magnetic loop antenna is effective in receiving narrow pulses with minimum possible distortion [125]. This suggestion might be valid for near-field inductive communication systems also, as most of the energy is stored in the magnetic fields surrounding a loop antenna. Hence, a loop antenna was decided to be used for coupling the information carried by pulses.

The remainder of this chapter discusses a design topology to link the magnetic fields around a loop antenna by using another loop antenna for a pulse-based transmission scheme. The aim is to increase the sensitivity of the loop antenna to receive the very short pulses with minimal distortion.

7.3 Loop Antenna Equivalent Circuit

A loop antenna is primarily inductive and can be modelled as a lumped network as shown in Fig. 7.1 [84]. In Chapter 4, the discussion of a loop antenna as a lumped equivalent circuit was made. The detailed analysis helped in concluding that the antenna's internal resistance and capacitance had very little effect on the input pulse shape. This did not matter much as an additional resistance and capacitance was necessary to be included in the lumped equivalent circuit to achieve the desirable pulse shape. Therefore the parasitic capacitance of the transmitting loop antenna was neglected. The stray capacitance of the receiving antenna has to be included in the analysis to see its effect on the sensitivity of the antenna. This capacitance along with any external capacitance might deteriorate the signal received and therefore an examination of the loop antenna's internal capacitance has to be carried out. Thus unlike the design of a transmitting antenna, the receiving antenna demands a different design approach.

The resistance R is a combination of the radiation resistance R_r and loss resistance R_L . R_r represents the power radiated and R_L represents the dc and ac losses in a loop antenna. The radiation resistance R_r is given by (7.1). It is very small for both the transmitting and receiving antennas. The practical approach employed to increase the radiation resistance considerably is to increase the number of turns in the coil antenna. This increases the dc resistance and

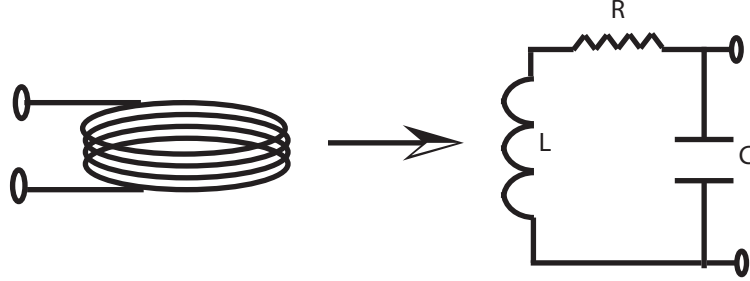


Figure 7.1: Electrical Equivalent Circuit of a Loop Antenna.

therefore it is necessary to include its effects. Here we consider two loop antenna designs: a spiral pancake coil and a solenoidal coil.

$$R_r = 20\pi^2 \left(\frac{C}{\lambda} \right)^4 N^2 \quad (7.1)$$

Firstly, the capacitance of both the spiral and solenoidal antenna will be determined. C_p represents the distributed stray capacitances of a multiturn loop antenna. Stray capacitances depend upon the type of loop antenna used. Hence different approaches to calculate stray capacitances of spiral and solenoidal shaped loop antennas. The stray capacitance C_{AB} for a solenoid can be calculated by using (7.2), (7.3) and (7.4) [126], and the individual capacitance C_{tt} is given by (7.5).

$$C_{AB}(2) = C_{tt} + \frac{C_{ts}}{2} \quad (7.2)$$

$$C_{AB}(3) = \frac{C_{tt}}{2} + \frac{C_{ts}}{2} \quad (7.3)$$

$$C_{AB}(n) = \frac{C_{AB}(n-2) \cdot C_{tt}/2}{C_{AB}(n-2) + C_{tt}/2} + \frac{C_{ts}}{2} \quad (7.4)$$

$$C_{tt} = \frac{\pi^2 D \epsilon_o}{\ln \left(p/2r + \sqrt{(p/2r)^2 - 1} \right)} \quad (7.5)$$

The overall stray capacitance C_{AB} of an air-core solenoid is calculated differently depending on the number of turns being even or odd. For a coil with even number of turns, two turns in the middle of the winding is considered. Fig. 7.2 shows the resulting capacitive network. It consists of the capacitance between two turns in parallel with a series combination of the turn-to-shield capacitance. The equivalent capacitance of the above network is given by (7.2). In case of coils with odd number of turns, the three turns in the middle of the winding are considered with an equivalent capacitance given by (7.3). This argument is extended for a coil having many turns by starting from two-turns (or three-turns) network and systematically adding one more turn at each side of the network. Thus, for a network with a larger number of turns ($n > 3$) the total stray capacitance is given by (7.4). The turn-to-turn capacitance is given by (7.5).

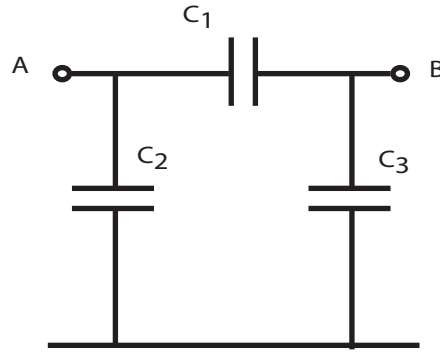


Figure 7.2: π equivalent circuit of the distributed stray capacitance of the solenoid air-core inductor.

For a spiral coil, the capacitance between two turns is modelled as closely spaced parallel cylinders, where a is the radius of the inner copper conductor, D corresponds to the total outer diameter, l_t is the total length of each turn, with b_m being the average radius between two turns. Then the total capacitance is equal to the series combination of such individual capacitances C_p given by (7.6) [127].

$$C_p = \frac{2\pi\epsilon l_t}{\cosh^{-1}\left(\frac{D^2}{2a^2} - 1\right)} \quad (7.6)$$

7.3.1 Near-field Transmission Model

The wireless baseband system can be modelled as a near-field transmission system similar to power-transfer RFID transmission systems [128, 129]. As the mutual inductance of such a system is low, it represents a poorly coupled transmission system [130]. Fig. 7.3 shows the near-field equivalent transmission model.

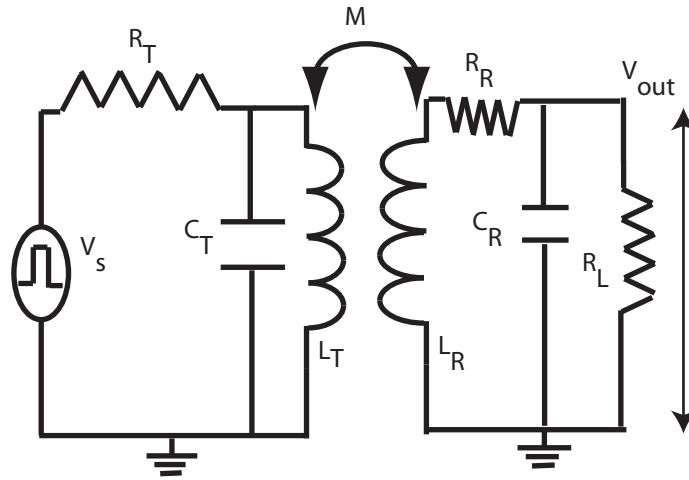


Figure 7.3: Near-Field Transmission Model.

Unlike using tuned resonant coils to maximise the current flow and increase the power transfer, typical of RFID devices, the pulses are directly applied to the carefully designed tank circuit. At the receiver, a loop antenna is used as a receiving antenna. The induced emf is then amplified and decoded to obtain the information transmitted. The emphasis is on the design of the receiving loop antennas for such pulse-based near-field transmission systems. Therefore the secondary circuit of the near-field transmission model is investigated for changes in the parameter values that constitute it. Minimising distortion of the received pulses is crucial for detection. An expression for the output voltage at the secondary will help determine the variables that affect the pulse in the time domain. The output voltage at the transmitter was derived analytically in Chapter 4 and is given again by (7.7) for immediate reference. (7.8) gives the voltage induced across the load impedance Z_L . The parallel combination of R_L and C_R is represented by Z_L . From (7.8), it can be seen that the received pulse is affected by

changes in the load impedance Z_L . In other words, R_L and C_R play a vital role in maintaining the integrity of the received pulse. It is assumed that the receiver is placed at a distance greater than the loop dimensions to ensure to meet the conditions of poor coupling.

$$V_{LP}(t) = \frac{V_S \zeta}{\sqrt{\zeta^2 - 1}} (e^{s_1 t} - e^{s_2 t}) \quad (7.7)$$

where ζ is the damping ratio.

$$V_{out} = \frac{V_s M}{L_T Z_L - L_R R_T} \left(e^{-\frac{t R_T}{L_T}} - e^{-\frac{t Z_L}{L_R}} \right) \quad (7.8)$$

The near-field transmission model can be considered as a transformer and its voltage transfer function can be obtained. The field associated with a simple air core transformer is shown in Fig. 7.4 [11]. The fields are highly concentrated and linear within the winding as these fields are produced by summation of the individual fields from each wire. Outside the winding the field is weak and divergent. The stored energy density is high within the winding and considerable energy is also stored in the weaker field outside the winding because the volume extends to infinity. Following the changes to the equivalent reactance on the primary (L_T, C_T) and the secondary (L_R, C_R), the derivation is similar to the voltage transfer function obtained for a linear transformer [131]. The radiation resistance (R_R) is small and hence neglected. Summing the voltages for closed paths on both sides of the transformer gives us (7.9) and (7.10).

$$\left(R_T + \frac{j\omega L_T}{1 - \omega^2 L_T C_T} \right) I_T + j\omega M I_R = V_S \quad (7.9)$$

$$j\omega M I_T + \left(R_L + \frac{j\omega L_R}{1 - \omega^2 L_R C_R} \right) I_R = 0 \quad (7.10)$$

The notations can be simplified by defining the self and mutual impedances. The self-impedances of the primary and secondary sides are

$$Z_{11} = R_T + \frac{j\omega L_T}{1 - \omega^2 L_T C_T} \quad (7.11)$$

and

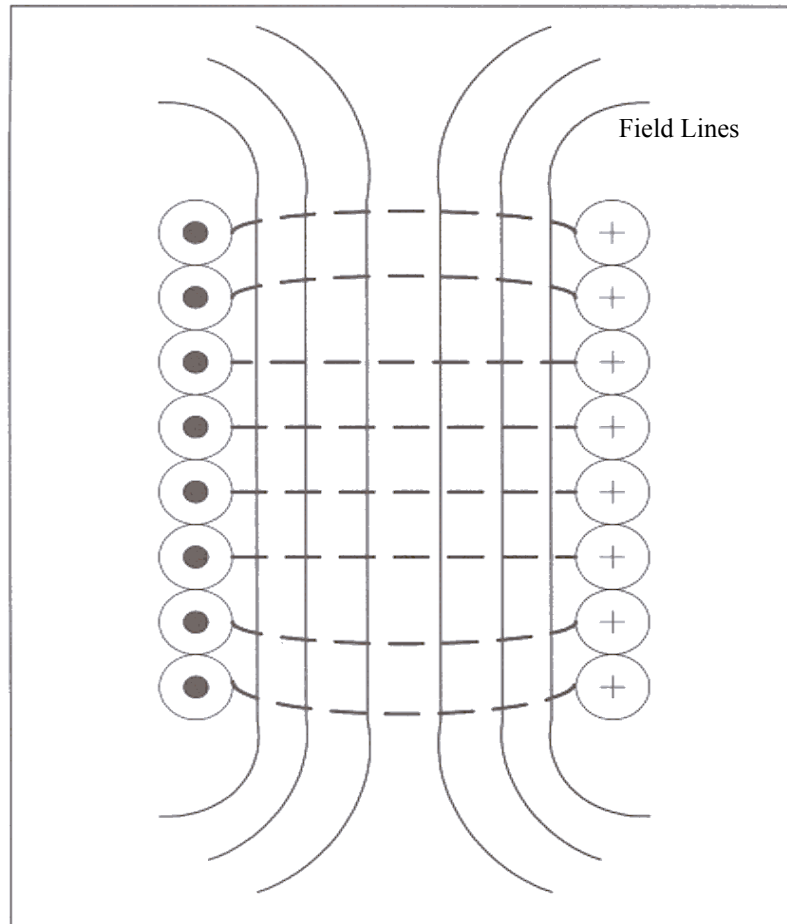


Figure 7.4: Air-Core Transformer [11].

$$Z_{22} = \frac{j\omega L_R}{1 - \omega^2 L_R C_R} \quad (7.12)$$

respectively, and the mutual impedances are

$$Z_{12} = Z_{21} = M \quad (7.13)$$

The voltage transfer function in the frequency domain can thus be obtained as:

$$\frac{V_S}{V_{out}} = \frac{Z_{21}R_L}{Z_{11}(Z_{22} + R_L) - Z_{12}Z_{21}} \quad (7.14)$$

The above equation shows that the voltage at the secondary terminals can be made larger or smaller than the voltage at the primary terminals. There is also no dc path between the two antennas and therefore any attempt to transmit dc will result in heating losses at the primary.

The mutual inductance between the two loop antennas depend upon their geometry and separation distance [12]. Fig. 7.5 show two coils of radii a and A . Their lengths x and l are taken as equal to the number of turns times the pitch of the windings. Therefore the winding densities n_1 and n_2 are, respectively, $n_1 = \frac{N_1}{x}$ and $n_2 = \frac{N_2}{l}$.

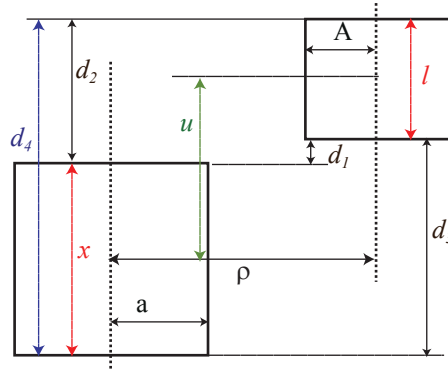


Figure 7.5: Two coils of radii a and A separated by an axial distance of ρ . The various distances that are calculated are also shown [12].

Let ρ = distance between the axes, and four distances d_n between the ends of the coil are calculated as below:

$$d_1 = u - \left(\frac{x+l}{2} \right) \quad (7.15)$$

$$d_2 = u + \left(\frac{l-x}{2} \right) \quad (7.16)$$

$$d_3 = u + \left(\frac{x-l}{2} \right) \quad (7.17)$$

$$d_4 = u + \left(\frac{x+l}{2} \right) \quad (7.18)$$

in which u =axial distance between the centers of the coils. From these distances, the four radii vectors $r_n = \sqrt{\rho^2 + d_n^2}$ and the four cosines $\mu_n = \frac{d_n}{r_n}$ are calculated. Finally the mutual inductance is given by

$$M = 0.001\pi^2 a^2 A^2 n_1 n_2 \left[\frac{X_1}{r_1} - \frac{X_2}{r_2} - \frac{X_3}{r_3} + \frac{X_4}{r_4} \right] \mu H \quad (7.19)$$

in which

$$X_n = \left[1 - \frac{1}{4} K_1 \frac{A^2}{r_n^2} P_2(\mu_n) + \frac{1}{8} K_2 \frac{A^4}{r_n^4} P_4(\mu_n) - \frac{5}{64} K_3 \frac{A^6}{r_n^6} P_6(\mu_n) + \dots \right] \quad (7.20)$$

The constants K_1, K_2, K_3 and K_4 are functions of $\alpha^2 = a^2/A^2$ and may be calculated from the formulas

$$K_1 = 1 + \alpha^2 \quad (7.21)$$

$$K_2 = 1 + 3\alpha^2 + \alpha^4 \quad (7.22)$$

$$K_3 = 1 + 6\alpha^2 + 6\alpha^4 + \alpha^6 \quad (7.23)$$

$$K_4 = 1 + 10\alpha^2 + 20\alpha^4 + 10\alpha^6 + \alpha^8 \quad (7.24)$$

The harmonics $P_{2n}(\mu_n)$ may be interpolated from the auxiliary table and the convergence of (7.20) is better the smaller the values of $(A/r_n)^2$ and each r_n must be greater than $(A+a)$. Table 7.1 shows the magnitude of the mutual inductance calculated for solenoidal loop antennas of equal lengths ($x=l=1$ cm) and equal radii ($a=A=0.5$ cm) with varying ρ . As expected when the distance between the axes increases the mutual inductance decreases.

The variation of the mutual inductance with varying axial distance between the centers of the loop antennas (u) is calculated for a fixed ρ as shown in

ρ (cm)	Mutual Inductance (nH)
2	5.896
3	1.809
4	0.770
5	0.396

Table 7.1: Mutual inductance for two equal solenoidal loop antennas with increasing distance between their axes.

Table 7.2. It can be seen that the mutual inductance is more sensitive to variations in ρ than u .

u (cm)	Mutual Inductance (nH)
1	1.882
2	1.182
3	0.860

Table 7.2: Mutual inductance for two equal solenoidal loop antennas with increasing distance between the centers of the antennas at a fixed distance between them ($\rho=2$ cm).

7.3.2 System Design

The inductance, capacitance and resistance depend upon the shape and size of the loop antenna. These parameters will affect the sensitivity of the loop antenna and therefore the acceptable electrical values of the antennas have to be determined. The solenoidal and spiral shaped antennas are considered for this particular analysis. A larger area of the receiving loop antenna will help in coupling maximum field around it. This translates to bigger value of inductance in the secondary circuit of the near-field transmission model. The inductance of the solenoidal coil and the spiral pancake coil is given by (7.25) and (7.26) respectively. The internal capacitance varies accordingly. Figs. 7.6 and 7.7 show the calculated capacitance of an n turn solenoidal loop antenna and a spiral antenna. As the number of turns increases the capacitance decreases and this effect is similar for both antenna shapes. Figs. 7.8 and 7.9 show the calculated capacitance of a 10 turn solenoidal and spiral shaped antennas for varying radius. In general it can

be deduced from the graphs that the capacitance of a spiral coil is larger than the capacitance of a solenoidal coil. It can now be summarised that the loop antenna can be made sensitive by either increasing the number of turns or its area. The internal capacitance decreases as the number of turns increases and increases as the radius of the loop antenna increases.

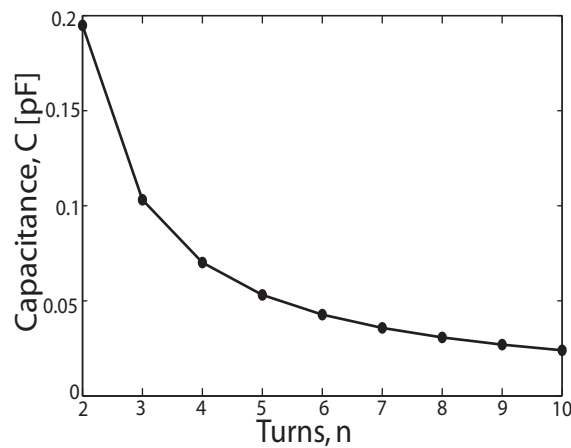


Figure 7.6: Calculated Stray Capacitances of a Solenoidal Coil as a function of the number of turns.

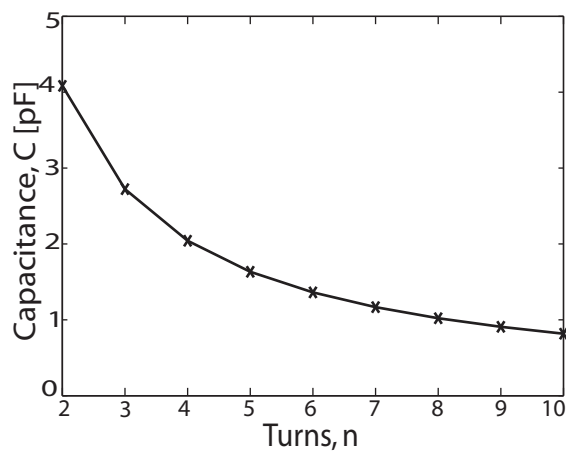


Figure 7.7: Calculated Stray Capacitances of a Spiral Coil as a function of the number of turns.

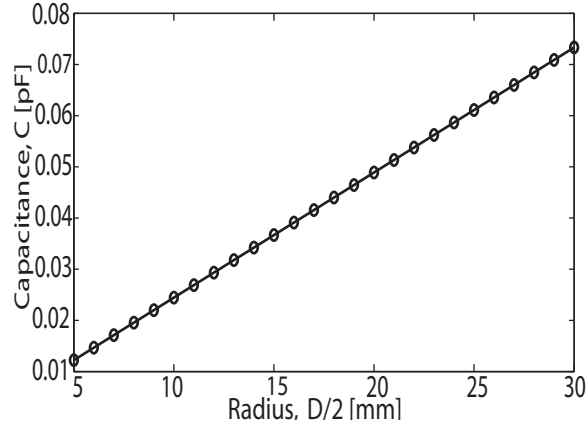


Figure 7.8: Calculated Stray Capacitances of a 10-Turn Solenoidal Coil as a function of the Coil Radius.

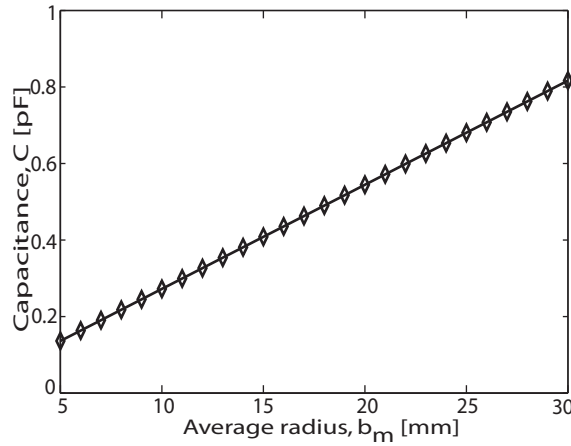


Figure 7.9: Calculated Stray Capacitances of a 10-Turn Spiral Coil as a function of the Average Coil Radius.

7.3.3 Simulation Parameters

ADS software is used to observe the changes in the pulse shape with the resistive and capacitive loading. In the first instance it is assumed that no load is connected to the secondary and hence R_L neglected. The skin effect resistance and proximity resistance are also neglected since they are usually small. The DC resistance is given by (7.27). a is the wire radius, ρ is the resistivity and b_i is the radius of the i^{th} ring. It follows from Biot-Savart's law [132] that the induced voltage given by

the rate of change of flux can be maximised by using a loop of larger area at the receiver. To see the effect of increasing the loop area that in turn increases the inductance, a simulation model is set up with parameters as shown in Table 7.3. At the receiver, dc resistance is theoretically calculated to be between 0.1Ω and 0.3Ω .

$$L_{solenoid} = \frac{\mu_0 \mu_r N^2 A}{l} \quad (7.25)$$

$$L_{spiral} = \frac{r^2 N^2}{8r + 11d} \quad (7.26)$$

where

L_{spiral} =inductance (μH)

r =mean radius of the coil (inches)

N =number of turns

d =depth of the coil (outer radius-inner radius) (inches)

$$R_{DC} = \frac{2\rho}{a^2} \sum_{i=1}^N b_i \quad (7.27)$$

Variables	Values
L_T	$0.5\mu\text{H}$
C_T	1nF
R_T	10Ω
Transmitted pulse width	140ns

Table 7.3: Simulation parameters.

As suggested by (7.8), the amplitude of the received signal is directly proportional to the mutual inductance between the two coils used for communication. The mutual inductance (M) given by (7.28) was proposed by Nuemann which gives the relation between flux linkages of two coils (ϕ_{12}) and the current (i) flowing in the transmitting coil. Faraday derived the relation between flux linkages associated with any two coils. The flux linkage is directly proportional to the current flowing in the transmitter coil and also the geometrical shape and size of the transceiver coils. It is inversely proportional to the distance (r) between

the two transceiver coils. By substituting (7.29) in (7.28), it can be seen that the mutual inductance is only dependent on the geometry of the two coils and distance between them. For simulations, it is assumed that the mutual inductance is 25 nH . The larger the mutual inductance the greater the amplitude of the received signal.

$$M = \frac{\phi_{12}}{i} \quad (7.28)$$

$$\phi_{12} = \frac{\mu_o i}{4\pi} \int_1 \int_2 \frac{dl_1 \cdot dl_2}{r} \quad (7.29)$$

With the values of M and R_R determined, the effects of inductance and stray capacitance on the pulse shape can be modelled. The stray capacitance is generally small and therefore in simulations, it is varied between 0.01 pF and 0.2 pF . Fig. 7.10 shows that the pulse shape changes significantly and the amplitude decreases sharply for larger values of inductance.

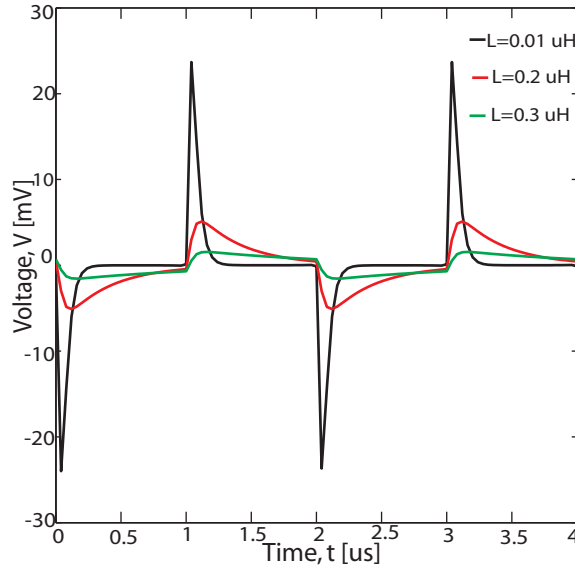


Figure 7.10: Simulation Results of an Inductor.

It can be deduced from the simulation results that the pulse shape is still detectable for inductance values of nearly half of the transmitting loop antenna's

inductance. But in practice, this value of inductance of the receiving loop antenna corresponds to a radiating element of size less than that of the transmitting loop antenna. An unloaded antenna hence poses a limit on the size of the receiving loop which is undesirable, as larger the area of the receiving loop antenna, the stronger the magnetic field linked to it. Hence the volume occupied around the transmitter has to be significantly larger. Ideally a receiving loop has to be as large as possible. In the second set of simulations the effect of loading the receiving loop antenna is investigated. The aim is to achieve a loop of larger area without distorting the shape of the received pulse. The amplitude of the pulse should also be large enough to have a better signal-to-noise ratio. The antenna terminated by resistance and capacitance is examined by increasing the resistance to about $1\text{ k}\Omega$ and the capacitance varied between 0.1 pF and 10 pF . It was observed that the shape of the pulse was preserved for larger values of loop inductance and increasing the capacitance had little or no effect on the shape of the pulse. The amplitude variations were also less significant. This suggests that addition of a large resistance (about $1\text{ k}\Omega$) significantly improves the sensitivity of a loop antenna. But if the resistance is increased beyond $1\text{ k}\Omega$, then the pulse received is considerably distorted, even with the slightest variations in capacitance or inductance of the loop antenna. This condition can be envisaged when amplifiers are used to amplify the pulse received at the receiver. Therefore in the third set of simulations, the effect of terminating a loop antenna with high resistance in the order of hundreds of $\text{k}\Omega$ is determined. The simulation was set up for a resistance of $100\text{ k}\Omega$ and a loop inductance of $1.5\text{ }\mu\text{H}$. Fig. 7.11 shows the simulation results for various capacitance values. The capacitance is a total combination of the stray and input capacitances of the amplifier.

It is evident that as the capacitance increases the oscillations set in and the shape of the pulse is severely distorted. The pulse retains its shape and also has sharp peaks to enable efficient detection for capacitances between 1 pF and 10 pF . But for capacitances larger than 10 pF , the lower frequency components are not attenuated considerably that leads to ringing.

The above discussion leads to the following conclusions:

1. The parasitic capacitance has no effect when the antenna is unloaded. The inductance is crucial to the changes in the shape of the received pulse.

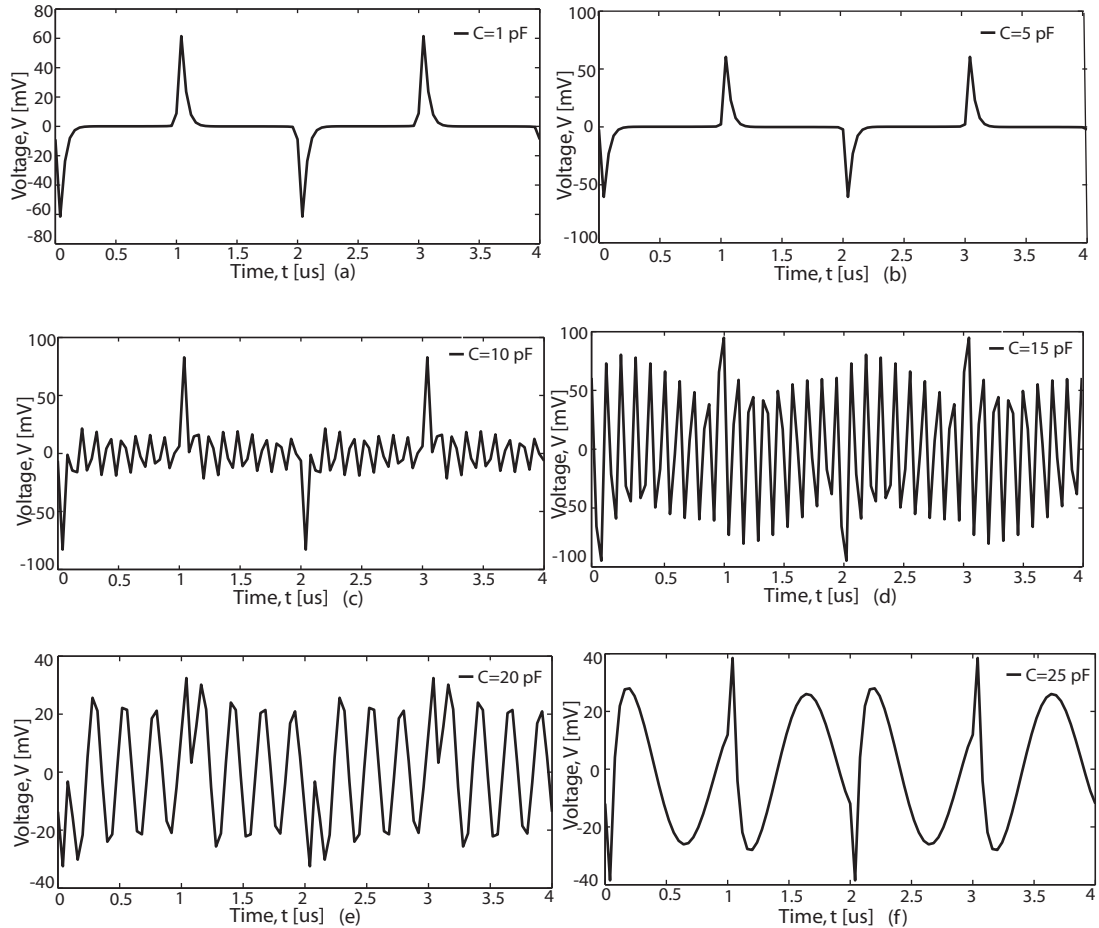


Figure 7.11: Simulation Results of an Inductor with different loading configurations.

2. Loading a loop antenna increases its sensitivity and pulses can be received without much distortion.
3. A resistive loading of about a $k\Omega$ makes it possible to employ loops with larger inductance to receive short duration pulses. The parasitic capacitance has little or no effect on the pulse shape.
4. Parasitic capacitances influence the pulse shape when the resistive load is of the order of hundreds of $k\Omega$.

7.4 Experimental Results

The transmitter consisted of a loop antenna that was wound in the form a solenoid. It had 9 turns and a pitch of 1 *mm*. The wire was made of copper and had a cross-sectional area of $0.397 \mu\text{m}^2$. To experimentally determine the optimal shape for pulse reception, two coils were used. One in the shape of a solenoid and the other in the shape of a spiral. The radius of the wire was same as that of the wire used for the transmitting loop antenna. The solenoid coil had 10 turns, a pitch of 1 *mm* and a radius of 5 *mm*. While the spiral had 7 turns, an inner radius of 1.5 and outer radius of 2 *cm*. A dual display LCR meter B371 was used to measure the inductance. It was found that the solenoid had an inductance of $0.3 \mu\text{H}$ and the spiral's inductance was $2 \mu\text{H}$. The receiving antenna was followed by an amplifier AD8011A. It had an input resistance of $450 \text{ k}\Omega$ and a capacitance of 4 *pF*.

The pulse pattern to be transmitted is shown in Fig. 7.12. Each pulse has a width of $0.5 \mu\text{s}$. Fig. 7.13 shows the amplified waveform that is received by a solenoidal loop antenna. The amplifier had a gain of 100.

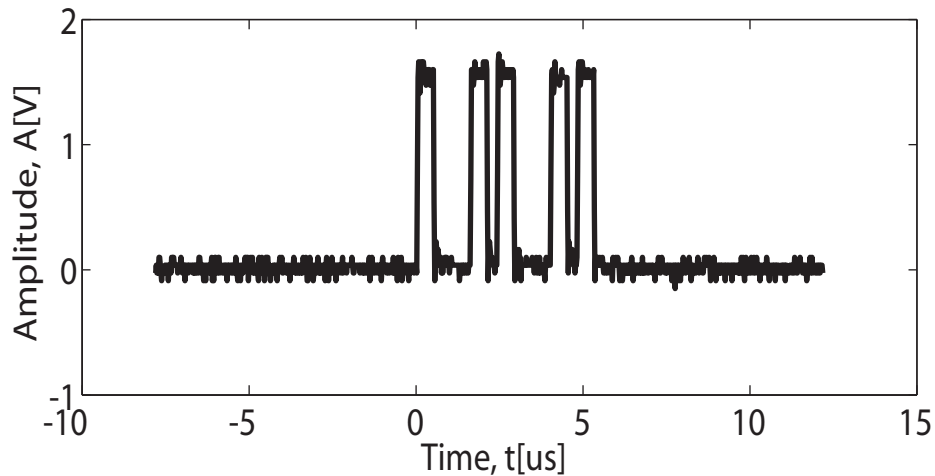


Figure 7.12: Transmitted information bits.

It can be seen that the pulse received has sharp rising and falling edges. This can be detected and the pulse pattern can be efficiently decoded. The receiving antenna had similar number of turns to the transmitting loop antenna indicating

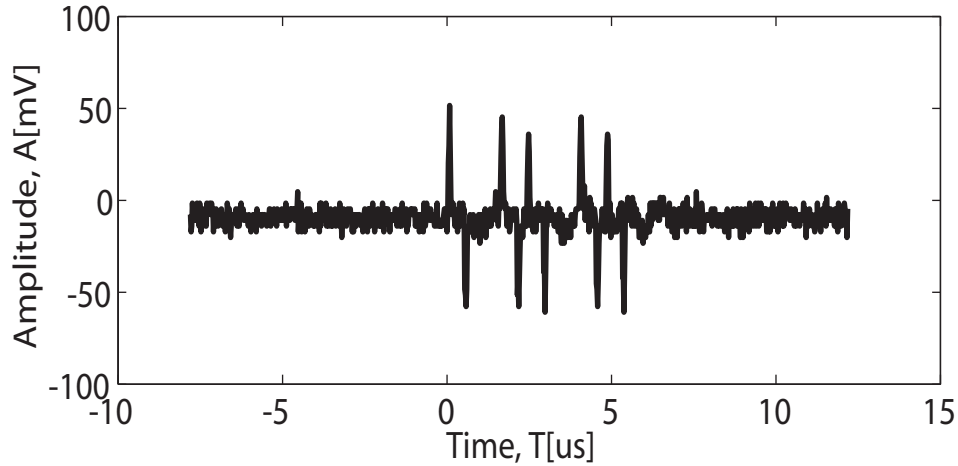


Figure 7.13: Captured waveform by a 10-turn solenoidal loop antenna at a distance of about 9 cm. The rising and falling edges are clearly visible that makes identification of the bits transmitted.

that if the load resistance is very high then the pulse received can be easily detected. However the range of operation was limited to 9 cm. Fig. 7.14 shows the waveform received by a spiral antenna. A careful observation of the captured waveform reveals that the trailing edges do not settle as fast as the edges of the received waveform of a solenoidal antenna. The range is about 15 cm. As the peaks are still visible, the symbol can be efficiently decoded.

A plot of signal-to-noise ratio (SNR) against distance for the two types of antennas is shown in Fig. 7.15. The spiral loop has a better SNR than the solenoidal loop antenna and has a better range.

The spiral loop antenna is much bigger than the solenoidal loop antenna contributing to a larger inductance and capacitance. By subjecting the antenna to a resistive loading a bigger loop antenna can thus be used with significant improvement in its range of operation.

Linear circuit network theory helps us in understanding the behaviour of the spiral and solenoidal loop antennas [131]. To receive a pulse of very short duration, a combination of the inductance, resistance and capacitance at the receiver should be such that the damping ratio should be between 0 and 1. The damping ratio is said to be underdamped and in this particular case it is the large load

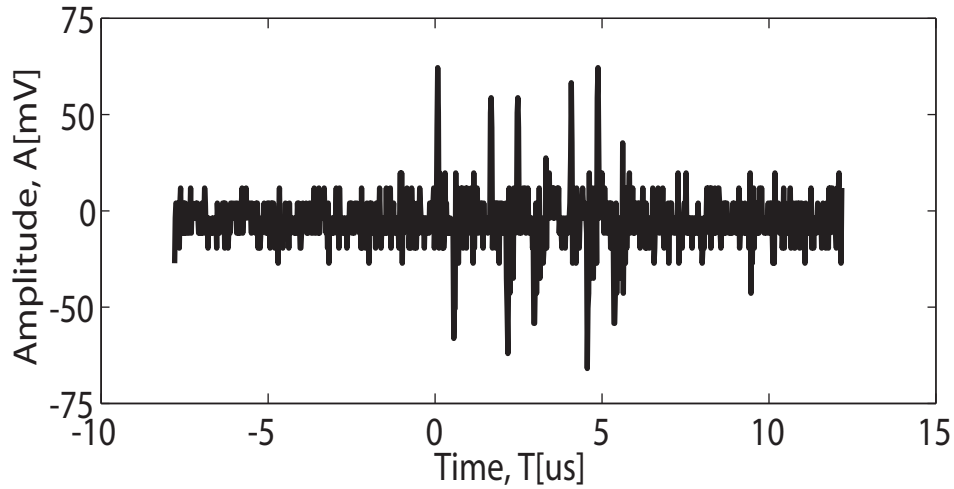


Figure 7.14: Captured waveform by a 7-turn spiral loop antenna at a distance of about 15 cm. Although the rising and falling edges are clearly visible, the antenna is liable to ringing taking more time for transients to attain a steady-state. The bits can still be efficiently detected.

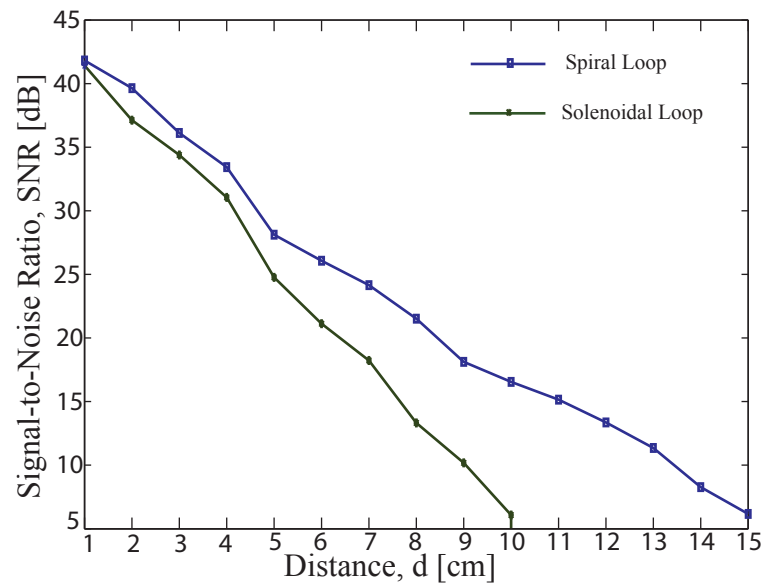


Figure 7.15: SNR against distance for the solenoidal and spiral loop antenna.

resistance that makes the secondary circuit underdamped.

7.4.1 Salt Water Experiment

An experiment was setup to observe the effects of the conducting medium on the performance of the near-field baseband communication system. Human body is a highly conducting lossy medium. A salt solution of different levels of concentration was used to mimic the lossy medium inside a human body. The transmitting loop antenna was similar to the loop antenna as described in Sec. 7.4. It was enclosed in a box that measured $(10 \times 4 \times 7)$ cm. The box was sealed by silicone rubber and made completely water-proof. The orientation of the transmitting loop antenna was unknown as the box was opaque. The solubility of salt in water is 36 g per 100 ml of water at room temperature [133]. A 2 litre saturated salt solution was prepared by dissolving 720 g of salt in 2000 ml of water and the concentration of the prepared solution was calculated to be 6.15 M. This 100% saturated salt solution was diluted to 20%, 40%, 60% and 80% concentrations and the conductivity of these different concentrations was measured by a conductivity meter. Table 7.4 gives the measured conductivity. A physiological solution has a concentration of 0.15 M which is less than the concentrations of the salt solution prepared and therefore a transmitter that can operate effectively in the above circumstances will perform well in normal physiological solutions too [134]. Note that the conductivity in Table 7.4 is for DC measurements and hence the values are lower than those shown for human tissue at higher frequencies in Tables 3.1, 3.2 and 3.3 [135].

Salt Solution Concentration	Conductivity \mathcal{U}/m at DC
20%	0.08
40%	0.118
60%	0.14
80%	0.18
100%	0.22

Table 7.4: Various Concentrations of Salt Solution and its respective Conductivity.

The table suggests that the conductivity increases with the salt concentration. The transmitting antenna enclosed in a box was immersed in a cylindrical container containing the salt solution. The container had a diameter of 15 cm and a

depth of 15.5 cm. It could hold upto 2 litres of solution. The receiving antenna was similar to the spiral antenna that was discussed in Sec. 7.4. The receiver was placed along the periphery of the container and moved both vertically and horizontally in straight lines. This was repeated all round the container. Fig. 7.16 shows the kind of waveform received at every location around the periphery of the cylindrical container.

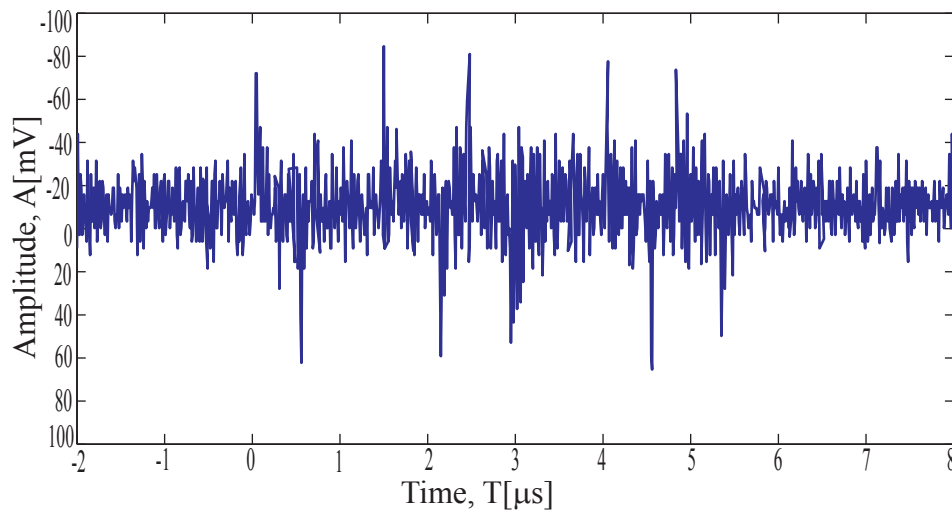


Figure 7.16: Captured waveform by a 7-turn spiral loop antenna at a distance of about 15 cm. The rising and falling edges are clearly visible that makes identification of the bits transmitted. The transmitter was inside a beaker containing salt solution.

There was hardly any noticeable change with either the pulse shape or the amplitude for varying salt concentrations in the solution. The difference between the waveforms received by the spiral antenna in air (shown in Fig. 7.14) and in the solution is that in the latter there is too much noise present in the waveform. Nevertheless the peaks were still clearly visible and hence waveforms could be decoded. The results presented in this section help in concluding that the near-field baseband wireless communication scheme looks promising for use in biomedical implantable systems.

7.5 Summary

In this chapter, a detailed discussion of designing an antenna suitable for receiving near-field baseband pulses is presented. The aim was to increase the sensitivity of the loop antenna and this was achieved by subjecting the antenna to resistive and capacitive loading. The near-field baseband communication system was tested for operation in highly conducting salt solution and it emerged from the results that this system has a huge potential for implementation in pill-shaped biomedical devices. In the next and final chapter, a summary of the conclusions from the research will be provided along with some suggestions for future work.

CHAPTER 8

CONCLUSION

Contents

8.1	Introduction	153
8.2	Final Analysis	153
8.2.1	Low-Frequency Magnetic Fields	153
8.2.2	Overdamped Circuit Configuration	155
8.2.3	Magnetic Antenna	157
8.2.4	Coding Schemes-Amplitude Modulation	158
8.2.5	Receiving Antenna Design	159
8.3	Future Work	160
8.3.1	Pulse Shape Analysis	160
8.3.2	UWB Antennas	162
8.4	Summary	162

8.1 Introduction

The previous chapter demonstrated the efficacy of employing near-field baseband communication system for use in biomedical implants. It also laid out the design principles for an antenna to receive pulses of very short duration. The shape of the pulse is crucial for its detection and therefore a different approach to the antenna design was necessary. The objective was achieved by resistive and capacitive loading of the receiving antenna. This chapter provides a reasoning for the research findings presented in this work and offers some useful suggestions for future work.

8.2 Final Analysis

The present work concentrated on developing a novel near-field baseband communication system for use in pill-shaped ingestible devices. The aim was to achieve a reliable communication link between an implantable transmitter and a receiver, external to the human body via magnetic fields. Miniaturisation of the implantable antenna, minimising the number of blocks in the transmitter and thereby reducing the power consumption were of particular importance. A final investigation is now carried out to review some of the major contributions of this research work.

8.2.1 Low-Frequency Magnetic Fields

As pointed out earlier, reducing the number of blocks in the transceiver was one of the main objectives to be realised in this research. The approach taken to solve this problem was to use low-frequency pulses for the exchange of data between the transmitter and the receiver, whilst not using traditional modulation schemes to imprint information upon a high frequency carrier. A pulse is characterised by its amplitude, width and shape. It is also made up of several harmonic frequencies. The solution intended is to use antennas as pulse shaping filters to directly emanate the pulses and also maintain the integrity of a pulse.

A pulse has an infinite bandwidth and the antenna can only work efficiently

within a certain range of the frequency spectrum. Therefore the bandwidth of operation has to be determined in the frequency domain. The time domain response of the antenna is critical too, as any changes to the pulse in the frequency domain will severely affect the pulse in the time domain. The rising and falling edges of the pulse will help decoding the symbol being transmitted. The transmission is therefore a waveform transmission, wherein the antennas have to preserve the shape of the pulse being transmitted.

Antennas come in basically two forms:(a) Electric and (b)Magnetic. The suitability of either of the two antennas was investigated in Chapter 3. The electric antenna was found to be capacitive and hence inconvenient for use to wirelessly exchange information between the transmitter and receiver. The magnetic antennas were found to be ideal for use in implants as they coupled information through magnetic fields and also behaved as perfect pulse shaping filters to make the near-field wideband baseband communication a possible option. Communication via magnetic fields is of great significance to human body communication because of the fact that magnetic fields are less attenuated by biological tissues. As the pulses were also of low frequency they will be effectively radiated by the magnetic (loop) antennas through a highly conductive and lossy medium, like a human body. The use of a magnetic antenna has disadvantages too. The circumstance at very low frequencies, referred to as quasi-stationary case, can be represented by equations (8.1), (8.2) and (8.3).

$$E_{\phi} = \frac{I_m l \sin \theta}{4\pi r^2} \quad (8.1)$$

$$H_r = \frac{I_m l \cos \theta}{2\pi \eta k r^3} \quad (8.2)$$

$$H_{\theta} = \frac{k I_m l \sin \theta}{4\pi \eta k r^3} \quad (8.3)$$

The above equations give the magnitude of the fields surrounding a loop antenna at low (or dc) frequencies. It can be seen that the magnetic fields decay rapidly with distance. Since the fields vary as $1/r^2$ or $1/r^3$, they are effectively confined to the vicinity of the loop antenna. Magnetic fields do not have sources

or sinks and their magnitude is directly proportional to the current flowing in the antenna element. The range of operation has been cause for major concern with such low-frequency near-field baseband communication system. An appreciable range of about 15-20 cm has been achieved with an application of 3 V at the antenna terminals. This is negligible compared to the ranges achieved with the ultra wide-band antennas that are of the size comparable with the ones used in this work. It has to be borne in mind that the ultra wideband antennas have been so far used in applications operating in free space.

8.2.2 Overdamped Circuit Configuration

The need to send pulses without any modulation demanded an entirely new approach to antenna design. The antenna was perceived to be a filter that could be realised by a passive network of resistors, inductors and capacitors. The electrical equivalence corresponds to the physical dimensions of the loop antenna. In order to increase the rate at which the magnetic energy is building in a loop antenna, additional resistance and capacitance is included in the circuit. The passive network was analysed for variations in reactances with frequency and the effect that it has on the pulse in the time domain. It was found in Chapter 4 that the antenna must have a wide magnitude response and a linear phase response to perfectly shape the pulse that is being radiated. The pulse was severely distorted when the antenna was underdamped. The part of the frequency spectrum that conforms to the inductive behaviour of the loop antenna has to be identified that will facilitate the design of such antennas for the near-field baseband communication for implantable sensors. Parameters such as Q-factor, damping coefficient α and damping ratio ζ characterise a passive network of elements. All these are related with each other and therefore it was decided to work with ζ . Moreover a circuit is termed underdamped, critically damped or overdamped depending upon the value of ζ being less than 1, 1 or greater than 1 respectively. In this particular case the circuit has to be overdamped suggesting the value of ζ to be always greater than 1. A relation between the pulse and the antenna spectra was derived in terms of the resonant frequency of the antenna, pulse width and the damping ratio ζ . This is given by (8.4).

$$f_o t_p \geq 2\zeta \quad (8.4)$$

One of the main criteria to be satisfied in customising the antenna to behave as a wide-band magnetic antenna is to make the antenna overdamped. This will require an addition of a resistance to the antenna's lumped equivalent circuit which contributes to the losses due to heating. The loop antenna has certain inductance associated with it and more the inductance stronger is the magnetic field associated with it. The width of the transmitted pulse is proportional to the loop antenna's inductance and hence short pulses having widths in nanosecond range are difficult to be radiated with controlled distortion. This is because the pulse takes more time to decay and therefore slows the rate at which the magnetic energy builds up in the loop antenna. A possible solution is to increase the resistance but then the losses due to resistive heating will increase too. The capacitance although decreases the decay rate of the pulse by about 30% and thereby increases the rate at which the transmitter can operate, it nevertheless is an additional component in the communication block. The size of the loop antennas considered for usage in implants have considerable magnetic energy and will complement the near-field baseband pulse radio communication making it a viable candidate for use in biomedical ingestible devices. The design process for the pulse radio communication can be summarised as below:

1. The size of the implant is constrained in size and hence a suitable solenoidal shaped antenna must be selected for use in such implants. This involves determining the number of turns, radius of the loop antenna and its length.
2. The capacitance and the external resistance must be selected such that ζ must be greater than or equal to 1 and the selected value for the resistance must be as low as possible.
3. With the width of the data pulse known, it must be ensured that (8.4) is satisfied.

8.2.3 Magnetic Antenna

A loop antenna is regarded as the best choice for application in near-field pulse radio communication. It comes in varying shapes and sizes. The electromagnetic design aspects of such an antenna were discussed in Chapter 5. HFSS, a commercial software package was employed to know the nature of the fields surrounding the magnetic antenna. The antenna was found to be omnidirectional which is a very desirable feature for implantable antennas. Two variants, namely solenoidal loop antenna and printed square loop antenna, were analysed for their performance as magnetic antennas. Both the antennas were omnidirectional but it was found that the solenoidal antenna had a greater range of operation. The gain of the solenoidal loop antenna was larger than a printed loop antenna. It was evident that the radiating structure had to occupy considerable volume to be able to couple magnetic fields with a similar receiving loop antenna. The solenoidal loop antenna appears as a much larger magnetic structure than a printed loop antenna. The disadvantage of such a voluminous antenna is that it poses a maximum restraint on the size of a pill-shaped ingestible device. It can be asserted that near-field magnetic antennas have to be of a considerable size to achieve an appreciable range between the transmitting and receiving loop antennas. A reliable communication link can be achieved.

The magnetic antenna makes the near-field baseband pulse radio communication a simple and attractive option for biomedical implants. The key to its success is the location of the transmitter and the receiver in the near-field where the magnetic fields are predominant and are offered a low reluctance path in a highly conductive medium like the human body. This was experimentally verified by placing the transmitter in salt solution of different concentrations and observing the coupled information at the receiver. It was found that information was effectively received at the receiving antenna. The conductivity of the solution had little or no effect on the signal strength. A magnetic antenna suffers from a major drawback and that is its operation is confined to the reactive and radiating near-field region surrounding it. An electric antenna on the other hand when made to resonate at high frequencies can offer us several advantages in terms of a reduction in its size and an increase in the operational range. However the

transmitter has to operate at very high frequencies and will increase the absorption of the radiated fields by the tissues in the human body. The operation of a near-field baseband magnetic antenna is only possible at low frequencies and any attempt to improve its range has to compromise with an increase in its size too.

8.2.4 Coding Schemes-Amplitude Modulation

Pulses representing a digital information are central to the near-field baseband communication system. The coding schemes readily available to represent the pulses are: (a)Return-to-zero (RZ), (b)Non-return-to-zero (NRZ), (c)Manchester Encoding. The NRZ coding scheme is not suitable for this particular communication scheme as the pulse undergoes “no transition” for similar bits. Manchester Encoding requires the data generator to produce the high and low states for every bit in the symbol and this helps in detecting the individual pulses at the receiver effectively. The only possible concern is the data rate which is limited by the bandwidth of the Manchester encoded pulses. Pulse-position modulation is suggested to be the most proficient scheme for use in near-field baseband pulse radio communication. Eight bits of information is encoded in a single pulse and its position in time determines its symbolic value. It is highly band-width efficient and can be readily integrated with implantable CMOS technology for the development of very small ingestible devices.

All the pulse modulation schemes are just an improvement over the bandwidth requirement for transmitting pulses from the loop antenna directly, without a need for oscillators and mixers. In a nutshell, the near-field baseband pulse communication is similar to the amplitude modulation. This statement holds true as it is evident that the rising and falling edges are key to the presence of a pulse. This also has to be a salient feature of the received pulses as any failure in detecting these peaks will result in the entire communication become worthless. The main disadvantage of a communication scheme which is similar to amplitude modulation is that it is sensitive to noise signals and has a low range of operation. This is coupled with the fact that the baseband pulse communication makes use of low frequency magnetic fields between two loop antennas, one at the transmitter and the other at the receiver. The receiving antenna has to be

very sensitive to receive these very short pulses without distortion. Hence the design of a near-field receiving antenna poses a major challenge and a slightly new approach is employed in this work for attaining the best possible results.

8.2.5 Receiving Antenna Design

Different loading configurations of the receiving antenna were explored as the pulses to be received were very short and have to be minimally distorted for any detection to be made at the receiver. The shape of the pulse being received was important for the detection of the symbol being transmitted. The rising and falling edges of the pulse help in detecting a particular bit and any change in the shape of the received pulse will severely hamper the decoding mechanism. Hence a careful study of the changes to the pulse shape with the geometry of the receiving antenna was imperative. The two geometrical shapes that were analysed include a spiral and solenoidal antenna. The resistance, inductance and capacitance of the antenna influence the pulse shape at the receiver. It was important to consider the effect of each of these parameters in order to propose a solution that will help achieve the objective of receiving very short baseband pulses with minimal distortion.

The study reveals that an unloaded loop antenna has very little resistance and the capacitance has no influence on the shape of the pulse received. Any change in the inductance will result in drastic changes to the received pulse and the pulse becomes unidentifiable as the inductance increases. In other words a smaller receiving antenna should be used to fulfil the above criteria. This is a hindrance as a smaller magnetic antenna will couple with only few magnetic lines of force and therefore results in smaller amplitude of the pulse. The range of operation is also less. It was found that resistive loading of the loop antenna increases its sensitivity to receive the pulses with minimal distortion. Large spiral loops could also be employed that was not possible with the unloaded loop antenna configuration. When the resistive loading was of the order of a $k\Omega$ the parasitic capacitance had no effect on the pulse shape. Any increase in the resistance (hundreds of $k\Omega$) will be characterised by changes in the pulse shape for small variations in the capacitance.

8.3 Future Work

The focus of this research work was to see the feasibility of using low frequency near-field baseband pulses for communication in implantable biomedical systems. A novel idea of transmitting information encoded pulses directly by a suitable magnetic antenna was demonstrated. As a consequence of the efforts of this work several key areas of additional research have been identified that could help further develop and improve the technology.

8.3.1 Pulse Shape Analysis

The pulse shape that was used in this piece of work is rectangular. Several pulse shapes are found in literature, some of which are spectrally inefficient [79, 81] and others are frequency tolerant [136]. A discussion on pulse shapes holds key for implementation of UWB antennas in biomedical implants. UWB devices have rarely been used for wireless sensor communication within the human body. It is one of the recent technologies that has a huge potential for making big in the field of biomedical communication engineering.

The choice of a pulse shape for UWB implementation dictates the hardware power consumption and complexity. David D. Wentzloff has suggested three metrics to compare the performance of various pulse shapes to determine relative performances in terms of bit error rate (BER) [124]. They are:(a)Spectral efficiency, (b)Out-of-band emissions and (c)time-bandwidth product.

The spectral efficiency of a pulse determines the loss registered by the unoccupied -10 dB bandwidth in the channel spectrum of the receiver. A receiver is assigned an average power limit and a -10 dB channel bandwidth. This is because a system performance depends upon the received signal energy and not on the shape of the pulse. The spectral efficiency is given by:

$$\eta_{ch} = \frac{E_{ch}}{P_{EIRP}BW_{-10dB}} \quad (8.5)$$

where E_{ch} is the pulse energy within the -10 dB channel bandwidth, P_{EIRP} is the maximum average power spectral density in W/MHz and BW_{-10dB} is the -10 dB bandwidth in MHz. The spectral efficiency qualifies how well a pulse

spectrum utilises the available bandwidth.

The out-of-band emissions determine the ratio of a pulse's energy outside the -10 dB channel to the energy within the -10 dB channel. It is given by:

$$\eta_{out} = \frac{(E_{tot} - E_{ch})}{E_{ch}} \quad (8.6)$$

The time-bandwidth product quantifies the localisation of a pulse in both time and frequency domains. The lower this number, the more localised a pulse is in both time and frequency. The time-bandwidth product is given by:

$$B_{tw} = D.d \quad (8.7)$$

where

$$D^2 = \frac{1}{2\pi E} \int_{-\infty}^{\infty} \omega^2 |F(\omega)|^2 d\omega \quad (8.8)$$

and

$$d^2 = \frac{1}{E} \int_{-\infty}^{\infty} t^2 |f(t)|^2 dt. \quad (8.9)$$

$F(\omega)$ is the Fourier transform of the pulse and $f(t)$ is the representation of the pulse in the time domain [137]. E is the energy of the pulse and is given by:

$$E = \int_{-\infty}^{\infty} |f(t)|^2 dt = \frac{1}{2\pi} \int_{-\infty}^{\infty} |F(\omega)|^2 d\omega. \quad (8.10)$$

A comparison of four different pulse shapes based on the performance metrics is given in Table 8.1. The sinc pulse has the highest spectral efficiency but requires the a complex transmitter to generate which is certainly not desirable for biomedical implants.

Pulse Shape	Spectral Efficiency	Out-of-Band Emissions	Time-BW Product
Sinc	100%	0%	∞
Square	60%	12.8%	∞
2^{nd} order filtered	59.2%	2.8%	0.55
Gaussian	56.5%	3.3%	0.50

Table 8.1: Pulse Shape Metrics.

The square pulse is the simplest to generate and it was used in this present work. The width of the pulse was in microseconds and not in the nanoseconds range. However it is clear from the table that the square pulse results in the highest out-of-band emissions. The adjacent channel interference is high for a square pulse. The Gaussian pulse has the lowest time-bandwidth product and hence it is more localised in both time and frequency. The more interesting aspect is that with the filtering of a square pulse, the 2nd order filtered pulse will perform similar to a Gaussian pulse.

8.3.2 UWB Antennas

UWB antennas can be used to emanate nanosecond RF pulses effectively. An UWB antenna has to operate over a bandwidth of 7.5 GHz and while doing so must also ensure that the pulse is not distorted to a great degree. The UWB antennas are omnidirectional thus delivering the freedom in the location of a transmitter and receiver. The losses have to be minimised to increase the radiation efficiency. This certainly improves the operational range and encourage the use of UWB antennas in biomedical ingestible devices. Several physically compact and low profile antennas can be explored [138]. These antennas can then be tested for *in-situ* operation and their performances can be compared with the low frequency near-field baseband pulse radio communication.

8.4 Summary

This research has suggested a novel method of communication that involves the use of information encoded pulses in the near-field region of an antenna. The technique is very simple that makes it attractive for integration with lab-in-a-pill technology. An ingenious way of designing and characterising the magnetic antennas has been suggested. This is applicable for the near-field baseband pulse radio communication which has a great potential for achieving communication between a biomedical implant and an external receiver.

APPENDIX A

The following program finds the negative and positive peaks of the received pulse:

```

%Leading edge detection for the receiver
%i=index for the memory location
%a=value to be stored used for comparing to arrive at a threshold value
%f=flag to synchronise
%n=counter and used to determine the bit or half-bit period
%t=temporary threshold value to be compared
%q=array for storing the answer
%input=500kHz and hence 1 bit period=1us, which is equivalent to 140 samples
%decision to be made for an interval of 2-bit period after synchronisation(1-bit period)
clear
fid=fopen('output.dat');
data=fgetl(fid);
b=fscanf(fid,'%f');
figure(1)
plot(b);
n=0;      %initial value of counter
f=0;      %initial value of flag
s=1;      %index for accessing the memory location
p=0;
for i=1:2
q(i)=0;
end
q=q';
for i=1:6
a=b(i);
end
i=7;
while (f==0)
t=a-b(i);

```

```

n=n+1;
i=i+1;
if t≤-2      %check for positive peak
n=0;
end
if t≥=2      %check for negative peak
if n≥140
q(s)=1;
s=s+1;
n=0;        %counter reset
f=1;       %flag set to come out of the loop
end
end
end
while (p< 1)
t=a-b(i);
n=n+1;     %increment the counter
i=i+1;
if t≤-2    %check for positive peak and also for the bit interval
if n≥280  %check if the counter is greater than the 2-bit period, if yes
perform the following
q(s)=0;
s=s+1;
n=0;
p=p+1;
end
end
if t≥2    %check for the negative peak and also for the bit interval
if n≥280  %check if the counter is greater than the 2-bit period, if yes
perform the following
q(s)=1;
s=s+1;
n=0;

```

```
p=p+1;
end
end
end
%Generation of the data bits corresponding to the decoded signal waveform
c=1;      %pointer to the decoded data array q
s=s-1;    %decrement the pointer to q to the exact number of data elements
r=1;
while (s≠0)
if q(c)==1
for i=1:140
f(r)=1;
r=r+1;
end
for i=141:280
f(r)=0;
r=r+1;
end
c=c+1;
s=s-1;
end
if q(c)==0
for i=1:140
f(r)=0;
r=r+1;
end
for i=141:280;
f(r)=1;
r=r+1;
end
c=c+1;
s=s-1;
end
end
```

```
c=c-1  
end  
f=f';  
figure(2)  
plot(f)
```

APPENDIX B

The following program computes the pulse interval modulated data bit pattern:

```

include p18F4550.inc
define polynomlow b'00000101'      ; Low byte of polynomial
define polynomhigh b'10000000'     ; High byte of polynomial
define polynomlength 0x10          ; 16-bit polynomial length
define datalength 0x04             ; Data length in bytes
udata 0x80
counter1   res   1                  ;slot counter (numbered from 1 to 256)
counter3   res   1
org 0x0000
goto begin
org 0x5000
;this block loads 3 bytes of data in successive memory locations
begin   LFSR 0, 3ABh
        movlw 0x03
        movwf POSTINC0
        movlw 0x04
        movwf POSTINC0
        movlw 0x05
        movwf POSTINC0
        movlw 0x06
        movwf POSTINC0
        movwf counter1
        movlw 0x04
        movwf counter3
LFSR 0, 3ABH
;this block clears port D and sets the location 0 to be the output
Main   clrf PORTD
        clrf LATD
        movlw 0x00
        movwf TRISD
        bcf STATUS,C

```

```
        bsf PORTD,0
        nop
        nop
        nop
        bcf PORTD,0
start   movf POSTINC0,w
        movwf counter1
        movlw 0x00
        xorwf counter1,w
        bz ton0
routine movlw 0x01
        xorwf counter1,w
        bz ton
        decf counter1
        goto routine
ton0    bsf PORTD,0
        nop
        nop
        nop
        bcf PORTD,0
        goto poston
ton     bsf PORTD,0
        nop
        nop
        nop
        bcf PORTD,0
poston  decf counter3
        bnz start
end
```

This code generates the Manchester coded waveforms of the input data pattern:

```

include p18F4550.inc
define polynomlow b'00000101'      ; Low byte of polynomial
define polynomhigh b'10000000'     ; High byte of polynomial
define polynomlength 0x10          ; 16-bit polynomial length
define datalength 0x04             ; Data length in bytes
udata 0x80
high  res  1      ; shift register 1
low   res  1      ; shift register 2
bits  res  1      ; number of data bits
databytes  res  1 ; number of bytes of data
temp  res  1      ; temporary register
COUNT  res  1
MANCHESTER  res  1
TIME     res  1
        org 0x0000
goto    begin
        org 0x5000
begin   movlw  0x6000      ; set pointer to begin of data block
        movwf FSR0
        movlw 0xAA
        movwf INDF0
        incf FSR0,f
        movlw 0x10
        movwf INDF0
        incf FSR0,f
        movlw 0x02
        movwf INDF0
        movlw 0x6000      ; set pointer to first data location
        movwf FSR0       ; initialize FSR register
;Manchester Code
Main   incf FSR0,f

```

```
        movf high,w
        movwf INDF0
        incf FSR0,f
        movf low,w
Start   clrf  WREG           ;clear W register
        movwf PORTC       ;clear PORTC
        movwf TRISC       ;config PORTC as outputs
        movlw 0x04
        movwf TIME
        movlw 0x6000
        movwf FSR0
        movf INDF0,w
        movwf MANCHESTER
Init    movlw 0x07
        movwf COUNT
Sub     rlf  MANCHESTER
        bc  Led1
        bcf PORTC,0
        goto Delay1
s1      bsf PORTC,0
        goto Delay2
s2      decf COUNT
        bz  terminal
        goto Sub
Led1    bsf PORTC,0
        goto Delay1
        bcf PORTC,0
        goto Delay2
        decf COUNT
        bz  Start
        goto Sub
Delay1  Nop
        Nop
```

```

                                Nop
                                Nop
                                Nop
                                Nop
goto                               s1
Delay2                             Nop
goto                               s2
terminal                           incf FSR0,f
                                movf INDF0,w
                                decf TIME
                                bz stop
goto                               Init
stop                               goto stop
end
```

APPENDIX C

```

*****/
include "Device.h"
include "filter.h"
include "iir.h"
/*****
* Function: main() *
  * Description: main routine for the IIR16 application. *
  * DSP: TMS320F2812 *
  * Include files: none *
  * Function Prototype: void main(void) *
  * Usage: main(); *
  * Input Parameters: none *
  * Return Value: none *
  * Notes: none *
*****/
void main(void)
/**** Initialization ****/
InitSysCtrl(); // Initialize the CPU (FILE: SysCtrl.c)
InitGpio(); // Initialize the shared GPIO pins (FILE: Gpio.c)
InitPieVectTable(); // Initialize the PIE Vectors (FILE: PieVect.c)
InitPieCtrl(); // Enable the PIE (FILE: PieCtrl.c)
InitEv(); // Initialize the Event Managers (FILE: Ev.c)
InitAdc(); // Initialize the ADC (FILE: Adc.c)
/**** Get the IIR16 loop going ****/
InitGptimer2(sampleperiod); // Initialize timer2 (FILE: IIR16.c)
/**** Enable global interrupts and the realtime debugger interrupt ****/
asm(" PUSH IER"); // copy the IER to the DBGIER
asm(" POP DBGIER");
asm(" CLRC INTM, DBGM"); // enable global and debugger realtime inter-
rupts
/**** Main loop ****/
while(1) // endless loop, wait for interrupt
asm(" NOP");

```

```

// end main()
/** end of file *****/
This routine computes the digital filter output from the ADC input samples:
include "Device.h"
include "filter.h"
include "iir.h"
/* Create an Instance of IIR5BIQD16 module and place the object in "iirfilt"
section */
pragma DATASECTION(iir, "iirfilt");
IIR5BIQ16 iir=IIR5BIQ16DEFAULTS;
/* =====
Modify the delay buffer size to comensurate with the no of biquads in the
filter
Size of the Delay buffer=2*nbiq
=====
/* Define the Delay buffer for the cascaded 1 biquad IIR filter and place it in
"iirfilt" section */
pragma DATASECTION(dbuffer,"iirfilt");
int dbuffer[2*IIR16LPFNBIQ];
/* =====
Modify the array size and symbolic constant to suit your filter requiremnt.
Size of the coefficient array=5*nbiq
=====
/* Define the Delay buffer for the cascaded 1 biquad IIR filter and place it in
"iirfilt" section */
const int coeff[5*IIR16LPFNBIQ]=IIR16LPFCOEFF;
/* Filter Input and Output Variables */
int xn,yn;
void IIRFILTER()
/* IIR Filter Initialisation */
iir.dbufferptr=dbuffer;
iir.coeffptr=(int *)coeff;
iir.qfmat=IIR16LPFQFMAT;

```

```

iir.nbiq=IIR16LPFNBIQ;
iir.isf=IIR16LPFISF;
iir.init(&iir);
/* End: IIRFILTER() */
/*_____
Nothing running in the background at present
_____*/

void interrupt isr()
xn=AdcRegs.ADCRESULT0 << 1; // read ADC result, I1Q15
iir.input=xn;
iir.calc(&iir);
yn=iir.output;
void InitGptimer2(Uint16 period)
EvaRegs.T2CON.all = 0x0000; //disable timer
EvaRegs.T2CNT = 0x0000; //clear timer counter
EvaRegs.T2PR = period; //set timer period
EvaRegs.T2CMPR = 0x0006; //set compare for ADC trigger
EvaRegs.GPTCONA.all = (EvaRegs.GPTCONA.all — 0x0620) & 0x0FF3;
/* x = don't change
bit 15 0: reserved
bit 14 0: T2STAT, read-only
bit 13 0: T1STAT, read-only
bit 12 0: T2CTRIPE, 0=disable timer2 compare trip
bit 11 x: T1CTRIPE, 0=disable timer1 compare trip
bit 10-9 11: T2TOADC, 11 = timer2 compare flag starts ADC
bit 8-7 xx: T1TOADC
bit 6 x: TCOMPOE, 0 = Hi-z all timer compare outputs
bit 5 1: T2COMPOE, 0 = timer2 compare HI-z'd
bit 4 x: T1COMPOE, 0 = timer1 compare HI-z'd
bit 3-2 00: T2PIN, 00 = forced low
bit 1-0 xx: T1PIN
*/
EvaRegs.T2CON.all = 0xD782; //enable timer

```

```
/* bit 15-14 11: 11=do not stop on emulator suspend
bit 13 0: reserved
bit 12-11 10: 10 = continuous-up count mode
bit 10-8 000: 000 = x/1 prescaler
bit 7 1: T2SWT1, 1 = use GPTimer1 TENABLE bit
bit 6 0: TENABLE, 1 = enable timer
bit 5-4 00: 00 = HSPCLK is clock source
bit 3-2 00: 00 = reload compare reg on underflow
bit 1 1: 0 = enable timer compare
bit 0 0: SELT1PR, 0 = use own period register /
//end InitGptimer2()
```

REFERENCES

- [1] N. F. Güler and E. D. Übeyli, "Theory and Applications of Biotelemetry," *Journal of Medical Systems*, vol. 26, no. 2, pp. 159–178, Apr. 2002.
- [2] A. J. Kurtenbach and A. E. Dracy, "The design and application of an FM/AM temperature telemetering system for intact, unrestrained ruminants," *IEEE Trans. Biomed. Eng.*, vol. 12, no. 3 and 4, pp. 187–190, Oct. 1965.
- [3] C. F. Andren, M. A. Fadali, V. L. Gott, and S. R. Topaz, "The skin tunnel transformer: A new system that permits both high efficiency transfer of power and telemetry of data through the intact skin," *IEEE Trans. Biomed. Eng.*, vol. 15, no. 4, pp. 278–280, Oct. 1968.
- [4] W. H. Ko, J. Hyneczek, and J. Homa, "Single frequency RF powered ECG telemetry system," *IEEE Trans. Biomed. Eng.*, vol. 26, no. 2, pp. 278–280, Feb. 1979.
- [5] B. C. Towe, "Passive telemetry by frequency keying," *IEEE Trans. Biomed. Eng.*, vol. 33, no. 10, pp. 905–909, Oct. 1986.
- [6] M. Nardin and K. Najafi, "A multichannel neuromuscular microstimulator with bi-directional telemetry," *Proceedings of the 8th International Conference on Solid-State Sensors and Actuators, and Eurosensors(Stockholm, Sweden)*, pp. 59–62, June 1995.

- [7] A. P. Chandrakasan, N. Verma, and D. C. Daly, "Ultralow-Power Electronics for Biomedical Applications," *Annual Review of Biomedical Engineering*, pp. 247–274, Aug. 2008.
- [8] C. A. Balanis, *Antenna Theory: Analysis and Design*, 3rd ed. Wiley Interscience, John Wiley and Sons, 2005.
- [9] A. J. Johansson, "Wireless communication with medical implants: Antennas and propagation," Ph.D. dissertation, Univ. of Lund, Sweden, June 2004. [Online]. Available: <http://www.tde.lth.se/home/ajn/publications/PhD%20Thesis%20AJJ.pdf>
- [10] R. S. Popovic, P. M. Drljaca, and P. Kejik, "CMOS magnetic sensors with integrated ferromagnetic parts," *Sensors and Actuators A: Physical*, vol. 129, no. 1-2, pp. 94–99, 2006.
- [11] L. H. Dixon. (2001) Introduction and basic magnetics. [Online]. Available: <http://focus.ti.com/docs/training/catalog/events/event.jhtml?sku=SEM401014>
- [12] F. W. Grover, *Inductance calculations*. Dover publications, New York, 1962.
- [13] G. S. Smith, "The proximity effect in systems of parallel conductors," *J. Appl. Phys.*, vol. 43, no. 5, pp. 2196–2203, May 1972.
- [14] J. D. Meindl, "Biomedical implantable microelectronics," *Science*, vol. 210, pp. 263–267, Oct. 1980.
- [15] L. Wang, E. A. Johannessen, P. Hammond, L. Cui, S. W. J. Reid, J. M. Cooper, and D. R. S. Cumming, "A programmable microsystem using System-on-chip for real time biotelemetry," *IEEE Trans. Biomed. Eng.*, vol. 52, no. 7, pp. 1251–1260, 2005.
- [16] Y. K. Chen and S. Y. Kung, "Trend and challenge on System-on-a-Chip designs," *Journal of signal processing systems*, vol. 53, pp. 217–229, Nov. 2008.

- [17] F. Nebeker, “Golden accomplishments in biomedical engineering,” *IEEE Trans. Biomed. Eng.*, vol. BME-21, pp. 17–47, June 2002.
- [18] R. A. M. Receveur, F. W. Lindemans, and N. F. de Rooij, “Microsystem technologies for implantable applications,” *Journal of Micromechanics and Microengineering*, vol. 17, pp. R50–R80, Apr. 2007.
- [19] J. Mouine, K. A. Ammar, and Z. Chtourou, “A completely programmable and very flexible implantable pain controller,” *Proceedings of the 22nd Annual EMBS International Conference (Chicago IL., USA)*, pp. 603–622, 2000.
- [20] K. Najafi and M. Ghovanloo, “A Multichannel Monolithic Wireless Microstimulator,” *Proceedings of the 26th Annual EMBS International Conference (San Francisco, CA, USA)*, pp. 4197–4200, Sept. 2004.
- [21] K. Arabi and M. Sawan, “Implantable multiprogrammable microstimulator dedicated to bladder control,” *Medical and Biological Engineering and Computing*, vol. 34, no. 1, pp. 9–12, Jan. 1996.
- [22] J. D. Meindl and A. J. Ford, “Implantable telemetry in biomedical research,” *IEEE Trans. Biomed. Eng.*, vol. BME-31, no. 12, pp. 817–823, Dec. 1984.
- [23] T. Mussivand, A. Hum, K. S. Holmes, and W. J. Keon, “Wireless monitoring and control for implantable rotary blood pumps,” *Artif. Organs*, vol. 21, no. 7, pp. 661–664, 1997.
- [24] I. Guler and S. Kara, “A low-cost biotelemetry system for long time monitoring of physiological data,” *J. Med. Syst.*, vol. 20, no. 3, pp. 151–156, 1996.
- [25] C. K. Kasten. (2007, Oct.) Telemetry is coming of age. [Online]. Available: <http://www.raven1.net/telem1.htm>
- [26] L. Cromwell, F. J. Weibell, and E. A. Pfeiffer, *Biomedical Instrumentation and Measurements*. Prentice-Hall, 1980.

- [27] C. Enokawa, Y. Yonezawa, H. Maki, and M. Aritomo, “A microcontroller-based implantable telemetry system for sympathetic nerve activity and ECG measurement,” *Proceedings of the 19th International Conference - IEEE/EMBS (Chicago, Illinois, USA)*, vol. 5, pp. 2232–2234, Oct. 1997.
- [28] J. A. V. Arx and K. Najafi, “A wireless single-chip telemetry-powered neural stimulation system,” pp. 214–215, Feb. 1999.
- [29] B. Jacobson, “Endoradiosonde techniques- A survey,” *Medical and Biological Engineering and Computing*, vol. 1, no. 2, pp. 165–180, Apr. 1963.
- [30] D. G. Thompson, D. L. Wingate, L. Archer, M. J. Benson, W. J. Green, and R. J. Hardy, “Normal patterns of human upper small bowel motor activity recorded by prolonged radiotelemetry,” *Gut*, vol. 21, no. 6, pp. 500–6, June 1980.
- [31] R. S. Mackay, *Biomedical Telemetry*. IEEE Press, 1992.
- [32] P. Valdastri, A. Menciassi, A. Arena, C. Caccamo, and P. Dario, “An implantable telemetry platform system for in vivo monitoring of physiological parameters,” *IEEE Trans. on Information Technology in Biomedicine*, vol. 8, no. 3, pp. 271–278, Sept. 2004.
- [33] E. A. Johannessen, L. Wang, W. C., D. R. S. Cumming, and J. M. Cooper, “Biocompatibility of a lab-in-a-pill sensor in artificial gastrointestinal environments,” *IEEE Trans. Biomed. Eng.*, vol. 53, no. 11, pp. 2333 – 2340, 2006.
- [34] L. Wang, T. D. Drysdale, and D. R. S. Cumming, “*In Situ* Characterization of Two Wireless Transmission Schemes for Ingestible Capsules,” *IEEE Transactions on Biomedical Engineering*, vol. 54, no. 11, pp. 2020–2027, Nov. 2007.
- [35] M. K. Fouri, O. Marinov, P. Quevedo, N. Faramarzpour, S. Shirani, L. W.-C. Liu, Q. Fang, and M. J. Deen, “Toward a miniaturized wireless fluorescence-based diagnostic imaging system,” *IEEE J. Selected Topics in Quantum Electronics*, vol. 14, no. 1, pp. 226–234, 2008.

- [36] X. Chen, X. Zhang, L. Zhang, N. Qi, H. Jiang, and Z. wang, “A Wireless Capsule Endoscopic System with a Low-Power Controlling and Processing ASIC,” in *IEEE Asian Solid-State Circuits Conference*, Fukuoka, Japan, Nov. 2008.
- [37] M. M. Marchal and M. T. Marchal, “French patent,” Patent 1.200.043, 1956.
- [38] H. E. Haynes and W. A. L., “The pill that talks,” *RCA Engineer*, vol. 5, pp. 52–54, 1960.
- [39] W. Welkowitz, S. Deutsch, and M. Akay, *Biomedical Instruments Theory and Design*. Academic Press, 1976.
- [40] B. Ziaie, M. D. Nardin, A. R. Coghlan, and K. Najafi, “A single-channel implantable microstimulator for functional neuromuscular stimulation,” *IEEE Trans. Biomed. Eng.*, vol. 44, no. 10, pp. 909–920, 1997.
- [41] L. Wang, *Research on dynamic monitoring techniques and data processing methods of upper digestive tract pH and simultaneously recorded ECG*. Biomedical Engineering Ph. D. dissertation, Xi’an Jiaotong University, Xi’an, China, 2000.
- [42] R. S. Mackay, “Radio telemetering from within the body,” *Science*, vol. 134, pp. 1196–1202, 1961.
- [43] B. Sklar, *Digital Communications-Fundamentals and Applications*. Prentice-Hall, 2001.
- [44] S. Haykin, *Communication Systems*. Wiley, 1978.
- [45] A. V. Oppenheim, A. S. Willsky, and S. H. Nawab, *Signals and Systems*. Prentice-Hall, 1983.
- [46] J. T. Farrar, V. K. Zworykin, and J. Baum, “Pressure-sensitive Telemetering Capsule for Study of Gastrointestinal Motility,” *Science*, vol. 126, no. 3280, pp. 975–976, Nov. 1957.

- [47] R. S. Mackay and B. Jacobson, "Endoradiosonde," *Nature*, vol. 179, no. 4572, pp. 1239–1240, June 1957.
- [48] W. O. Essler and G. E. Folk, "The determination of 24-hour physiological rhythms of unrestrained animals by radio telemetry," *Nature*, vol. 190, pp. 90–91, 1961.
- [49] G. L. Shook and G. E. F. Jr, "Body moisture and the operating life of implantable heart rate transmitters," *IEEE Trans. Biomed. Eng.*, vol. 12, pp. 44–46, 1965.
- [50] A. E. Dracy, W. O. essler, and J. R. Jahn, "Recording intrareticular temperatures by radiosonde equipment," *Journal of Dairy Science*, vol. 56, pp. 241–242, Mar. 1963.
- [51] A. E. Dracy and A. J. Kurtenbach, "Radio telemetry-a tool for studying bloat," *South Dakota Farm and Home Research*, vol. 15, pp. 15–17, 1964.
- [52] J. S. Barlow, "A simple time-division multiplexing system for low-frequency bioelectric signals," *IEEE Trans. Biomed. Eng.*, vol. 13, no. 4, pp. 195–199, Oct. 1966.
- [53] E. M. Lonsdale, J. W. Steadman, and W. L. Pancoe, "A telemetering system for securing data on the motility of internal organs," *IEEE Trans. Biomed. Eng.*, vol. 13, no. 3, pp. 153–159, July 1966.
- [54] H. Fischler, N. Peled, and S. Yerushalmi, "FM/FM mulitplex radio-telemetry system for handling biological data," *IEEE Trans. Biomed. Eng.*, vol. 14, no. 1, pp. 30–39, Jan. 1967.
- [55] R. B. R. II and W. H. Ko, "A six channel physiological telemetry system," *IEEE Trans. Biomed. Eng.*, vol. 14, no. 1, pp. 40–46, Jan. 1967.
- [56] J. R. Zweizig, R. T. kado, J. Hanley, and W. R. Adey, "The design and use of an FM/AM radiotelemetry system for multichannel recording of biological data," *IEEE Trans. Biomed. Eng.*, vol. 14, no. 4, pp. 230–238, Oct. 1967.

- [57] W. H. Ko, "Design of radio frequency powered coils for implant instruments," *Med. Biol. Eng. Comput.*, vol. 15, pp. 634–640, 1977.
- [58] Z. Tang, B. Smith, J. H. Schild, and P. H. Peckham, "Data transmission from an implantable biotelemetry by load-shift keying using circuit configuration modulator," *IEEE Trans. Biomed. Eng.*, vol. 42, no. 5, pp. 524–528, May 1995.
- [59] Q. Huang and M. Oberle, "A 0.5mW passive telemetry IC for biomedical applications," *IEEE journal of Solid-State Circuits*, vol. 33, no. 7, pp. 937–946, July 1998.
- [60] M. Clements, K. Vichienchom, W. Liu, C. Hughes, E. McGuken, C. DeMarco, and J. Mueller, "An implantable power and data receiver and neurostimulus chip for a retinal prosthesis system," *Proceedings of IEEE International symposium on Circuits and Systems*, vol. 1, pp. I194–I197, 1999.
- [61] H. J. Park, H. W. Nam, B. S. Song, J. L. Choi, H. C. Choi, J. C. Park, M. N. Kim, J. T. Lee, and J. H. Cho, "Design of bi-directional and multi-channel miniaturized telemetry module for wireless endoscopy," *Proceedings of the 2nd annual International IEEE-EMBS special topic conference on Microtechnologies in Medicine and Biology*, pp. 273–276, May 2002.
- [62] T. B. Tang, E. A. Johannessen, L. Wang, A. Astaras, M. Ahmadian, A. F. Murray, J. M. Cooper, S. P. Beaumont, B. W. Flynn, and D. R. S. Cumming, "Toward a miniature wireless integrated multisensor microsystem for industrial and biomedical applications," *IEEE Sensors Journal*, vol. 2, no. 6, pp. 628–635, Dec. 2002.
- [63] P. Valdastri, S. Rossi, A. Menciassi, V. Lionetti, F. Bernini, F. A. Recchia, and P. Dario, "An implantable ZigBee ready telemetric platform for in vivo monitoring of physiological parameters," *Sensors Actuators A:Phys*, vol. 142, no. 1, pp. 369–378, Mar. 1995.
- [64] P. Valdastri, A. Menciassi, and P. Dario, "Transmission power requirements for novel zigbee implants in the gastrointestinal tract," *IEEE Trans. Biomed. Eng.*, vol. 55, no. 6, pp. 1705–1710, June 2008.

- [65] ICNIRP Guidelines, “Guidelines for limiting exposure to time-varying electric, magnetic and electromagnetic fields (up to 300 GHz,” *Health Physics*, vol. 74, pp. 494–522, Apr. 1998.
- [66] C. L. Bennett and G. F. Ross, “Time-domain Electromagnetics and its applications,” *Proceedings of the IEEE*, vol. 66, no. 3, pp. 299–318, Mar. 1978.
- [67] T. W. Barrett, “History of Ultrawideband (UWB) Radar and Communications: Pioneers and Innovators,” in *Proc. Progress in Electromagnetics Symposium (PIERS) 2000*, Cambridge, MA, July 2000.
- [68] —, “History of Ultrawideband Communications and Radar: Part I, UWB Communications,” *Microwave Journal*, pp. 22–56, Jan. 2001.
- [69] —, “History of Ultrawideband Communications and Radar: Part II, UWB Radar and Sensors,” *Microwave Journal*, pp. 22–46, Feb. 2001.
- [70] H. M. Rein, “Subnanosecond Pulse Generator with Variable Pulsewidth Using Avalanche Transistors,” *IEEE Electronics Letters*, vol. 11, no. 1, pp. 21–23, Jan. 1975.
- [71] R. Tielert, “Subnanosecond-Pulse Generator Employing 2-Stage Pulse Step Sharpener,” *IEEE Electronics Letters*, vol. 12, no. 3, pp. 54–84, Feb. 1976.
- [72] H. Kim, D. Park, and Y. Joo, “Design of CMOS Scholtz’s Monocycle Pulse Generator,” in *IEEE Conference on Ultra Wideband Systems and Technologies*, Reston, VA, Nov. 2003.
- [73] K. Marsden, H. J. Lee, D. S. Ha, and H. S. Lee, “Low Power CMOS Re-programmable Pulse Generator for UWB Systems,” in *IEEE Conference on Ultra Wideband Systems and Technologies*, Reston, VA, Nov. 2003, pp. 443–447.
- [74] R. L. Pickholtz, D. L. Schilling, and L. B. Milstein, “Theory of spread spectrum communications- A tutorial,” *IEEE Transactions on Communications*, vol. 30, no. 5, pp. 855–884, May 1982.

- [75] F. Lee and A. Chandrakasan, "A 2.5nJ/b 0.65V 3-to-5GHz subbanded UWB receiver in 90nm CMOS," in *IEEE Int. Solid-State Circ. Conf.*, 2007, pp. 116–117.
- [76] T. Buchegger, G. Ossberger, E. Hochmair, U. Folger, A. Reiszahn, and A. Springer, "An ultra low power transcutaneous impulse radio link for cochlea implants," in *Int. workshop on UWB systems*, 2004, pp. 356–360.
- [77] J. Wang and D. Su, "Design of an Ultra Wideband System for in-body Wireless Communications," in *Asia-Pac. Microwave Conf. Proc.*, 2006, pp. 565–568.
- [78] C. T. Charles, "Wireless Data Links for Biomedical Implants: Current Research and Future Directions," in *IEEE Biomedical Circuits and Systems Conference*, Montreal, Canada, Nov. 2007, pp. 13–16.
- [79] J. F. M. Gerrits and J. R. Farserotu, "Wavelet generation circuit for UWB impulse radio applications," *Electronics Letters*, vol. 38, no. 25, pp. 1737–1738, Dec. 2002.
- [80] B. Jung, Y.-H. Tseng, J. Harvey, and R. Harjani, "Pulse generator design for UWB IR communication systems," in *IEEE International Symposium on Circuits and Systems*, vol. 5, May 2005, pp. 4381–4384.
- [81] Y. Zheng, H. Dong, and Y. P. Xu, "A novel CMOS/BiCMOS UWB pulse generator and modulator," in *IEEE International Microwave Symposium*, vol. 2, June 2004, pp. 1269–1272.
- [82] K. W. Wong, S. R. karri, and Y. Zheng, "Low-power full-band UWB active pulse shaping circuit using 0.18 μ m CMOS technology," in *IEEE Radio Frequency Integrated Circuits Symposium*, vol. 2, June 2006, pp. 510–513.
- [83] Biotelemetry: Antenna Tips. [Online]. Available: <http://www.biotelem.org/antenna.htm>
- [84] C. A. Balanis, *Antenna Theory*. John Wiley and Sons, 1982.
- [85] J. D. Kraus, *Antennas*. McGraw-Hill, 1988.

- [86] L. C. Chirwa, P. A. Hammond, S. Roy, and D. R. S. Cumming, "Electromagnetic radiation from ingested sources in the human intestine between 150 MHz and 1.2 GHz," *IEEE Trans. Biomed. Eng.*, vol. 50, no. 4, pp. 484–492, 2003.
- [87] W. G. Scanlon and N. E. Evans, "Radiowave propagation from a tissue implanted source at 418 MHz and 916.5 MHz," *IEEE Trans. Biomed. Eng.*, vol. 47, pp. 527–534, Apr. 2000.
- [88] R. H. Walden, "Analog-to-Digital Converter Survey and Analysis," *IEEE Journal on Selected Areas in Communications*, vol. 17, no. 4, pp. 539–550, Apr. 1999.
- [89] M. van Elzakker, E. Tuijl, P. Geraedts, D. Schinkel, Klumperink, and B. Nauta, "A 1.9 μ W 4.4fJ/conversion-step, 10 bit, 1MS/s charge redistribution ADC," *Proceedings of the IEEE International Solid-State Circuits Conference (ISSCC)*, (San Francisco, CA, USA), pp. 3–7, Feb. 2008.
- [90] S. J. Song, N. Cho, and H. J. Yoo, "A 0.2-mW 2-Mb/s Digital Transceiver Based on Wideband Signaling for Human Body Communications," *IEEE Journal of Solid-State Circuits*, vol. 42, no. 9, pp. 2021–2033, Sept. 2007.
- [91] M. Ghovanloo and K. Najafi, "A wideband frequency-shift keying wireless link for inductively powered biomedical implants," *IEEE Transactions on Circuits and Systems—Part I: Fundamental Theory and Applications*, vol. 51, no. 12, pp. 2374–2383, Dec. 2004.
- [92] L. C. Chirwa, P. A. Hammond, S. Roy, and D. R. S. Cumming, "Towards a miniature integrated multisensor microsystem for industrial and biomedical applications," *IEEE Transactions on Biomedical Engineering*, vol. 50, no. 4, pp. 484–492, Apr. 2003.
- [93] M. Ahmadian, B. W. Flynn, A. F. Murray, and D. R. S. Cumming, "Miniature transmitter for implantable microsystems," *Proc. 25th IEEE-EMBC(Cancun, Mexico)*, vol. 4.

- [94] J. Riistama, J. Väisänen, S. Heinisuo, H. Harjunpää, S. Arra, K. Kokko, M. Mäntylä, J. Kaihilahti, P. Heino, M. Kellomäki, O. Vainio, J. Vanhala, J. Leikkala, and J. Hyttinen, “Wireless and Inductively Powered Implant for Measuring Electrocardiogram,” *Med. Bio. Eng. Comput.*, vol. 45, no. 12, pp. 1163–1174, Dec. 2007.
- [95] T. G. Tang, Q. M. Tieng, and M. W. Gunn, “Equivalent Circuit of a Dipole Antenna Using Frequency-Independent Lumped Elements,” *IEEE Transactions on Antennas and Propagation*, vol. 41, no. 1, pp. 100–103, Jan. 1993.
- [96] E. C. Jordan and K. C. Balmain, *Electromagnetic Waves and Radiating Systems*. Englewood Cliffs, N.J. Prentice-Hall, 1968.
- [97] C. Gabriel, “Compilation of the dielectric properties of body tissues at rf and microwave frequencies,” technical report AL/OE-TR-1996-0037, Brooks Air Force.
- [98] P. Köpf-Maier, *Atlas of human anatomy*, 5th ed. Karger, 2000.
- [99] L. C. Chirwa, P. A. Hammond, S. Roy, and D. R. S. Cumming, “Radiation from Ingested Wireless Devices in Biomedical Telemetry Bands,” *Electronics Letters*, vol. 39, no. 2, pp. 178–179, Jan. 2003.
- [100] C. J. Chu, “Physical limitations of omnidirectional antennas,” *J. Appl. Phys.*, vol. 19, pp. 1163–1175, Dec. 1948.
- [101] G. W. Streable and L. W. Pearson, “A numerical study on realizable broadband and equivalent admittances for dipole and loop antennas,” *IEEE Transactions on Antennas and Propagation*, vol. 29, no. 5, pp. 707–717, Sept. 1981.
- [102] S. A. Schelkunoff and H. T. Friis, *Antennas-Theory and Practice*. New York:Wiley, 1952.
- [103] D. C. Yates, A. S. Holmes, and A. J. Burdett, “Optimal Transmission Frequency for Ultralow-Power Short-Range Radio Links,” *IEEE Transactions*

- on Circuits and Systems—Part I: Fundamental Theory and Applications*, vol. 51, no. 7, pp. 1405–1413, July 2004.
- [104] J. D. Kraus and K. R. Carver, *Electromagnetics*, 2nd ed. McGraw-Hill, 1981.
- [105] S. Ramo, J. R. Whinnery, and T. V. Duzer, *Fields and Waves in Communication Electronics*. Wiley, 1994.
- [106] D. C. Yates, “Ultra-low power short-range radio links for size constrained wireless sensors,” Ph.D. dissertation, Imperial College London, London, May 2004.
- [107] E. H. Newman, P. Nohely, and C. H. Walter, “Two Methods for the Measurement of Antenna Efficiency,” *IEEE Transactions on Circuits and Systems—Part I: Fundamental Theory and Applications*, vol. AP-23, no. 4, pp. 457–461, July 1975.
- [108] G. S. Smith, “Radiation Efficiency of electrically Small Antennas,” *IEEE Transactions on Antennas and Propagation*, vol. AP-20, no. 5, pp. 656–657, 1972.
- [109] R. C. Johnson, *Antenna Engineering Handbook*, 3rd ed. McGraw-Hill, 1993.
- [110] M. Z. Win and R. A. Scholtz, “Impulse radio:How it works,” *IEEE Communications Letters*, vol. 2, no. 2, pp. 36–38, 1998.
- [111] ———, “Ultra-wide bandwidth time-hopping spread spectrum impulse radio for wireless multiple-access communications,” *IEEE Transactions on Communications*, vol. 48, no. 4, pp. 679–691, Apr. 2000.
- [112] J. H. Reed, *An introduction to ultra wideband communication systems*. Prentice Hall, 2005.
- [113] R. J. Fontana, “Recent system applications of short-pulse ultrawideband (UWB) technology,” *IEEE Transactions on Microwave Theory and Techniques*, vol. 52, no. 4, pp. 2087–2104, 2004.

- [114] D. C. Yates and A. S. Holmes, "Loop antenna design for ultra low power transmitters," *Proceedings of IEEE workshop on Antenna Technology: Small antennas and novel metamaterials (San Francisco, CA, USA)*, pp. 287–290, Mar. 2005.
- [115] K. Fotopoulou and B. W. Flynn, "Optimum Antenna Coil Structure for Inductive Powering of Passive RFID Tags," in *IEEE International Conference on RFID*, Gaylord Texan Resort, Grapevine, TX, USA, Mar. 2007, pp. 71–77.
- [116] S. C. Q. Chen and V. Thomas, "Optimization of inductive rfid technology," in *Proc. IEEE International Symposium on Electronics and the Environment*, Denver, CO, USA, 2001, pp. 82–87.
- [117] H. A. Wheeler, "Small antennas," *IEEE Transactions on Antennas and Propagation*, vol. 23, no. 4, pp. 462–469, 1975.
- [118] S. S. Mohan, M. del Mar Hershenson, S. P. Boyd, and T. H. Lee, "Simple Accurate Expressions for Planar Spiral Inductances," *IEEE Journal of Solid-State Circuits*, vol. 34, no. 10, pp. 1419–1424, Oct. 1999.
- [119] H. A. Wheeler, "Simple inductance formulas for radio coils," in *Proc. IRE*, vol. 16, no. 10, Oct. 1928, pp. 1398–1400.
- [120] M. Hershenson, S. S. Mohan, S. P. Boyd, and T. H. Lee, "Optimization of inductor circuits via geometric programming," in *Design Automation Conf.*, New Orleans, LA, USA, June 1999, pp. 994–998.
- [121] M. Chen, T. Zhou, and F. Ao, "The Study of Pulse Interval Modulation in Wireless Laser Communication System," in *International Conference on Communication Technology 2006*, Nov. 2006, pp. 1–4.
- [122] C. S. Williams, *Designing Digital Filters*. Prentice-Hall, 1986.
- [123] R. Want, "An introduction to RFID technology," *IEEE Pervasive Comput.*, vol. 5, no. 1, pp. 25–33, 2006.

- [124] D. D. Wentzloff, "Pulse-based ultra-wideband transmitters for digital communication," Ph.D. dissertation, Massachusetts Institute of Technology, USA, June 2007.
- [125] G. P. Pochanin, P. V. Kholod, and T. N. Ogurtsova, "The UWB receiving loop antenna," in *International Conference on Antenna theory and Techniques*, Sevastopol, Ukraine, 2003, pp. 546–548.
- [126] G. Grandi, M. K. Kazimierczuk, A. Massarini, and U. Reggiani, "Stray capacitances of single-layer solenoid air-core inductors," *IEEE Transactions on Industry Applications*, vol. 35, no. 5, pp. 1162–1168, 1999.
- [127] R. Rodriguez, J. M. Dishman, F. T. Dickens, and E. W. Whelan, "Modeling of two-dimensional spiral inductors," *IEEE Transactions on Components, Hybrids and Manufacturing Technology*, vol. 3, no. 4, pp. 535–541, Dec. 1980.
- [128] D. C. Galbraith, M. Soma, and R. L. White, "A wide-band efficient inductive transdermal power and data link with coupling insensitive gain," *IEEE Transactions on Bio-Medical Engineering*, vol. 34, pp. 265–275, Apr. 1987.
- [129] K. Finkenzeller, *RFID Handbook*. Chichester, UK: Wiley, Apr. 2001.
- [130] B. Ziaie, K. Najafi, and D. J. Anderson, "A low-power miniature transmitter using a low-loss silicon platform for biotelemetry," in *Proc. IEEE 19th Int. Conf. engineering in Medicine and Biology Soc.*, vol. 5, 1997, pp. 2221–2224.
- [131] D. R. Cunningham and J. A. Stuller, *Circuit Analysis*. Houghton Mifflin, 1995.
- [132] G. Lancaster, *Introduction to Fields and Circuits*. New York:Oxford Univ. Press, 1992.
- [133] J. Burgess, *Metal ions in solution*. Ellis Horwood, New York, 1978.
- [134] K. Yokoyama, T. Ogawa, A. Fujita, K. Asaoka, and J. Sakai, "Fracture of Ni-Ti superelastic alloy under sustained tensile load in physiological saline

- solution containing hydrogen peroxide,” *Journal of biomedical materials research, Part A*, vol. 82A, no. 3, pp. 558–567, 2006.
- [135] S. Gabriel, R. W. Lau, and C. Gabriel, “The dielectric properties of biological tissues: II. Measurements in the frequency range 10 Hz to 20 GHz,” *Phys. Med. Biol.*, vol. 41, pp. 2251–2269, 1996.
- [136] Y. H. Choi, “Gated UWB pulse signal generation,” *IEEE Conference on Ultrawideband Systems and Technologies*, pp. 122–124, May 2004.
- [137] L. J. V. Vliet. (2002) Time-frequency bandwidth product of a gaussian. [Online]. Available: <http://www.qi.tnw.tudelft.nl/lucas>
- [138] J. Powell, “Antenna design for ultra wideband radio,” Master’s thesis, Massachusetts Institute of Technology, USA, May 2004.